



**DEVELOPMENT OF AERO MORPHING REINFORCED COMPOSITE
MATERIALS EMBEDDED WITH NiTi ALLOYS**

by

MBULELO PATRICK DLISANI

**Thesis submitted in partial fulfilment of the requirements for the
degree**

Master of Technology: Mechanical Engineering

in the Faculty of Mechanical Engineering

at the Cape Peninsula University of Technology

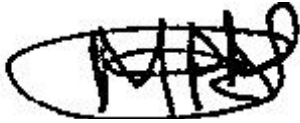
Supervisor: Oscar Philander
Co-supervisor: G. Oliver

Bellville

Date submitted: 13 October 2011

DECLARATION

I, Mbulelo Patrick Dlisani, declare that the contents of this thesis represent my own unaided work, and that the thesis has not previously been submitted for academic examination towards any qualification. Furthermore, it represents my own opinions and not necessarily those of the Cape Peninsula University of Technology.



13 October 2011

Signed

Date

ABSTRACT

This study deals with the development of aero morphing reinforced composite materials embedded with NiTi alloys. It is shown that the composite materials can be manufactured using resin infusion process to produce better mechanical properties such as tensile strength and material stiffness. These composite materials are modelled experimentally using temperature and time parameters. The object of the modelling is to determine the effect of process temperature on the smart material alloy (SMA). As a result, a composite structural designer would now possess an added dimension in optimising material design.

In addition, the study is conducted to analyse the structural behaviour of composite materials when embedded and when not embedded with NiTi alloys. The analysis is constrained to the evaluation of material tensile strength and stiffness upon performance of composite structures. A macro mechanical approach is employed to perform the analysis in specimens with different fibre orientation [0°, 45° and 90°]. The estimation of tensile strength and stiffness parameters is based on the characteristics obtained from a macro mechanical approach. The orientation which possesses the best material properties is selected to embed NiTi alloys.

The experimental results of unembedded specimens are validated with the application of micromechanics equations and an Ansys software finite element modelling tool. There is fair agreement between the finite element simulation of macro mechanical test of the specimens and the measured experimental results. Although the macro mechanical approach is found to be successful, it is imperative to characterise the material interface strength of embedded specimens using a pull out test.

The pullout test showed to some great extent the properties of reinforced composite embedded with NiTi alloys. Material interface strength was investigated using three different surface treatments such as hand sanding, corroded and untreated wires. The quality of interface strength was characterised using apparent interfacial shear strength. The data obtained, is made available for the first time and it can be utilised for future investigations of the behaviour of reinforced structures embedded with NiTi alloys.

The mechanical behaviour of unembedded SMA wires is provided to qualitatively confirm the loading behaviour of the material at ambient and elevated temperatures. The significance in looking at the mechanical behaviour of SMA wires is the introduction of the recovery stresses due to their possession of shape memory effect. It is known that the shape memory effect begins either by application of load where large strains are generated or upon the application of heat where the original geometrical shape of the structure is recovered.

The material properties of reinforced composites embedded with NiTi alloy were investigated and these materials were found to be better in terms of material stiffness as compared to virgin specimen without SMA. In contrast, the virgin specimen without SMA was found to be better in terms of tensile strength. This is attributed to the size of SMA, location and the amount embedded into the specimen. It was noted that when the NiTi alloy is actuated, the compressive strains begin to decrease, i.e. the compressive strain field into the composite material is greatly affected by temperature changes arising by the NiTi alloy activation. Increasing the amount of embedded wires resulted in geometric failure of the composite specimen in a compressive manner. This failure mechanism of the specimen in compression at elevated temperatures is known as warpage.

ACKNOWLEDGEMENTS

I wish to thank:

- my supervisor, Prof Philander, for his guidance, encouragement and support;
- my co-supervisor, Prof Oliver, for his support as well as guidance;
- my co-supervisor, Prof Gryzagoridis, for his support as well as guidance;
- the staff in the Faculty of Mechanical and Mechatronics at the Cape Peninsula University of Technology for their support and encouragement;
- the librarians at the Cape Peninsula University of Technology Library for their assistance;
- the financial assistance of CPUT towards this research is acknowledged;
- my parents, for their love and support.

TABLE OF CONTENTS

Declaration	ii
Abstract	iii
Acknowledgements	iv
Glossary	xii

CHAPTER ONE: INTRODUCTION

1.1	Problem statement	1
1.2	Aims of the study	2
1.2.1	The specific aims of the study	2
1.3	Hypothesis of the study	2
1.4	Background and review of the related literature	2
1.4.1	Fundamentals of material constituents	2
1.4.2	Manufacturing methodology	3
1.4.3	Manufacturing alternatives	4
1.4.3.1	Resin transfer moulding (RTM)	4
1.4.3.2	Prepegs	5
1.4.3.3	Vacuum bagging process	5
1.4.3.4	Resin infusion process	5
1.4.4	Composite tensile test	7
1.4.5	Composite laminates	8
1.4.5.1	The behaviour of the composite laminates	9
1.4.5.2	Types of composite laminates	9
1.4.6	History of NiTi shape memory alloys	10
1.4.7	Martensite and austenite phases	13
1.4.8	Shape memory effects on shape memory alloys	14
1.4.8.1	One-shape memory	14
1.4.8.2	Two-way shape memory	14
1.4.9	Shape memory effect (SME)	18
1.4.10	Interfacial bond strength test	20

CHAPTER TWO: RESIN INFUSION TECHNIQUE IN MANUFACTURING FLAT COMPOSITE MATERIAL.

2.1	Introduction	24
2.2	Manufacturing the composites	25
2.3	Description of Resin Infusion Process (RIP)	25
2.4	Fabrication phase	26
2.5	Tooling	26
2.6	Resin infusion process	27
2.7	Curing process phases	34
2.8	Elimination of sacrificial mat	37
2.9	Results	38
2.10	Summary	39
2.11	Conclusions	40

CHAPTER THREE: DETERMINE THE PROPERTIES OF FIBRE COMPOSITES LAMINATES WITHOUT NiTi SMAs

3.1	Introduction	41
3.2	Problem statement	41
3.3.	Sampling and testing of specimens	41
3.4	Experimental procedure	43
3.4.1	Tensile test of UD composite specimen	43
3.4.2	Fibre orientation	46
3.5	Experimental results	47
3.5.1	Tensile properties of an e-glass / epoxy material with fibre plies orientated at 0°	47
3.5.2	Axial tensile tests of UD e-glass / epoxy with fibre plies oriented at 45° (Diagonal)	49
3.5.3	Axial tensile tests of UD e-glass / epoxy with fibre plies oriented at 90° (Perpendicular to the longitudinal axis)	50
3.5.4	Morphology of failure of UD e-glass / epoxy reinforced composite specimens oriented at 0°, 45° and 90°.	51
3.5.5	Engineering material coefficient of variation analysis	54
3.6	Discussion of the results	55
3.7	Conclusions and Recommendations	55
3.8	Comments	56

CHAPTER FOUR: PREDICTING MATERIAL PROPERTIES USING MICROMECHANICS EQUATIONS AND AN ANSYS SOFTWARE MODEL

4.1	Introduction	57
4.2	Problem statement	57
4.3	Unidirectional composite laminate	58
4.3.1	Prediction of axial stiffness of UD composite	59
4.3.2	Prediction of transverse stiffness of UD composite	59
4.3.3	Prediction of major poisson's ratio of UD composite	60
4.3.4	Prediction of shear modulus of UD composite	60
4.4	Computing the contribution of material parameters of the constituents to the composite moduli	61
4.5	Comparison of the theoretical predictions to experimental composite moduli measurements	61
4.6	Finite element simulations	62
4.7	Tensile tests [0°] ₁₀ specimen results	63
4.8	Conclusions	67

CHAPTER FIVE: CHARACTERISING MATERIAL INTERFACE STRENGTH USING THE PULLOUT TEST

5.1	Introduction	68
5.2	Selected Materials	69
5.3	Specimen preparation	70
5.4	Effect of surface treatments	72
5.5	Experimental procedure for the pullout tests	74
5.6	Experimental results	74
5.6.1	Hand sanded specimens	75
5.6.2	Corroded specimen	75
5.6.3	Untreated specimen	76
5.7	Discussion of the results	76
5.8	Conclusions	79
5.9	Recommendations	79

CHAPTER SIX: THE MECHANICAL BEHAVIOUR OF SMA WIRES

6.1	Introduction	80
6.2	SMA selection	80
6.3	Experimental procedure	81
6.4	Characteristics of the NiTi SMA specimens at ambient temperature	82
6.5	Characterisation of the NiTi SMA specimens at elevated temperature (115°C)	84
6.6	Conclusions	90
6.7	Recommendations	90

CHAPTER SEVEN: INVESTIGATING AND DETERMINING THE MATERIAL PROPERTIES OF REINFORCED COMPOSITES EMBEDDED WITH NiTi SMAs

7.1	Introduction	91
7.2	Experimental procedure	91
7.2.1	Testing of 1 embedded NiTi wire in the unidirectional (UD) reinforced e-glass / epoxy composite	94
7.2.2	Testing of 2 embedded NiTi wires in the e-glass / epoxy composite	96
7.2.3	Testing of 3 embedded NiTi wires in the e-glass / epoxy composite	97
7.2.4	Discussion on stress vs. strain graphs	98
7.2.5	Results on ultimate tensile material strength and longitudinal stiffness	99
7.3	Heating of embedded pre-strained NiTi wires	102
7.3.1	Experimental setup for heating an embedded pre-strained NiTi wires	102
7.3.2	Experimental Procedure	103
7.3.3	Results of embedded pre-strained NiTi wires	104
7.3.3.1	Testing of 1, 2 and 3 pre-strained embedded NiTi wires	104
7.4	Conclusions	110
7.5	Recommendations	111

REFERENCES

112

LIST OF FIGURES

Figure 1.1: Headgear and J-hooks for connections into patient's mouth	11
Figure 1.2: Golf clubs (driver, putter & iron)	11
Figure 1.3: Thumb stent in artery	12
Figure 1.4: Boeing 787	12
Figure 1.5:	13
Figure 1.6: Illustration of 1-way shape memory effect	15
Figure 1.7: Illustration of 2-way shape memory effect	15
Figure 1.8: Austenite BCC, twinned and detwinned martensite structures.	18
Figure 1.9: A pull out test schematic of tested specimens	22
Figure 2.1: Preparation of the molding tool	28
Figure 2.2: Application of the heat using heat gun	29
Figure 2.3: Placing 300 x 250 mm carbon fiber and e-glass plies onto the mould	29
Figure 2.4: Release film layout	30
Figure 2.5: Laying peel ply	30
Figure 2.6: Laying resin distribution fabric	31
Figure 2.7: Laying breather or absorption fabric	32
Figure 2.8: Insert spiral wrap at inlet and outlet side of the mould	32
Figure 2.9: Apply vacuum bag using tacky tape	33
Figure 2.10: Resin infusion using vacuum pump	34
Figure 2.11: Four step cure cycle	36
Figure 2.12: Flow speed of unidirectional (UD) material mat	37
Figure 2.13: Set up with one and two glass moulds	38
Figure 3.1: E-glass fibre reinforced / epoxy AR 600 tabs	42
Figure 3.2: Diamond cutting blades	42
Figure 3.3: Specimens as finally prepared with "tabs"	44
Figure 3.4: Specimens initially tested	44
Figure 3.5: A quarter bridge strain gauge connection	45
Figure 3.6: Tensile specimen secured in the machine's jaws	45
Figure 3.7: Dimensions and geometrical shape of Tensile test specimens	46
Figure 3.8: Force vs. elongation for the 0° fibres oriented specimens	48
Figure 3.9: Stress-strain graph for the 0° fibre oriented specimen	49
Figure 3.10: Force vs. Extension for the oriented fibres specimens [45°]10s	50
Figure 3.11: Force vs. Extension for the 90° fibre oriented specimens	51
Figure 3.12: [0°] tensile test specimen failure	52
Figure 3.13: Failure surface under tensile load for the UD Eg/ep [90°]	53
Figure 3.14: [45°] tensile test specimen failure	53
Figure 3.15: [90°] tensile test specimen failure	54
Figure 4.1: Finite element mesh and boundary load application for the [0°] specimen.	63
Figure 4.2: Simulated contours of nodal displacement u_x for the [0°] specimen.	64
Figure 4.3: Simulated contours of nodal strains for the [0°] specimen.	65

Figure 4.4: Simulated contours of tensile stress σ_1 for the $[0^\circ]$ specimen.	65
Figure 4.5: Simulated contours of transverse stress for the $[0^\circ]$ specimen.	66
Figure 5.1: A pullout test schematic of test specimens	71
Figure 5.2: Masking tape application	71
Figure 5.3: Vacuum application	72
Figure 5.4: Typical force - extension curves for tested specimens	74
Figure 5.5: Difference in initial debond stress of various surface treatment cases	77
Figure 5.6: Difference in final debond stress of various surface treatment cases	77
Figure 5.7: Apparent IFSS plotted as a function of embedded length	78
Figure 6.1: NiTi SMA attached to the crosshead of the tensile testing machine	81
Figure 6.2: Martensite load – extension curve showing loading profile	82
Figure 6.3: Equipment employed when electrically activating the NiTi SMA through resistive heating	85
Figure 6.4: Martensite force – extension graph demonstrating loading behaviour	85
Figure 6.5: Stress-strain relation	86
Figure 6.6: Temperature profiles of NiTi SMA wire during heating	88
Figure 6.7: Force – Temperature graph	88
Figure 6.8: Stress – Temperature graph	89
Figure 6.9: Temperature – strain graph	89
Figure 7.1: Embedded un-strained and pre-strained NiTi alloys	92
Figure 7.2: Experimental set up	92
Figure 7.3: Strain gauge sensors attached to the experimental specimens	93
Figure 7.4: Experimental specimens tested using Hansfield tensile testing machine	94
Figure 7.5: A typical load vs. extension curves for (embedded NiTi SMA wires) composite specimens	95
Figure 7.6: Tensile failure mode of the specimens with 1 embedded NiTi alloy wire	96
Figure 7.7: Tensile failure mode of 2 embedded NiTi wires in the composite specimen	96
Figure 7.8: Tensile failure mode of 3 embedded NiTi wires in the composite specimen	97
Figure 7.9: A typical tensile stress – strain curves for (1, 2 and 3 embedded NiTi SMA wires) for composite specimen	98
Figure 7.10: Effects of embedding different number of NiTi SMA wires on the ultimate tensile strength and longitudinal stiffness of epoxy /E-glass fibre / NiTi composite	101
Figure 7.11: An experimental setup for heating an embedded pre strained NiTi alloy wires	102
Figure 7.12: Testing of 1 pre-strained embedded NiTi wire	104
Figure 7.13: Strain vs. time graph for all SMA 1, 2 & 3	105
Figure 7.14: Temperature vs. time graph for SMA 1, 2 & 3	105
Figure 7.15: Testing of 2 pre-strained embedded NiTi wires	107
Figure 7.16: Testing of 3 pre-strained embedded NiTi wires	108

LIST OF TABLES

Table 1.1: Some alloys exhibiting shape memory effect	17
Table 2.1: Fabrication materials and consumables	27
Table 3.1: Statistics for Engineering Materials Constants	47
Table 4.1: Material constituent's data and computed moduli	61
Table 4.2: Comparison of the mechanical properties for composite laminates	62
Table 5.1: NiTi SMA material data	69
Table 6.1: Properties of SMA 0 and SMA 1 at ambient temperature (Gauge length = 150)	84
Table 6.2: Properties of SMA 1 at elevated temperature (Gauge length = 150 mm)	87
Table 7.1: Ultimate tensile strength and longitudinal stiffness of reinforced composite embedded with NiTi SMAs	99

APPENDICES

Appendix A: Calculations of e-glass fibre content	116
Appendix B: Results of polynomial regression analysis	116

GLOSSARY

Terms/Acronyms/Abbreviations	Definition/Explanation
SMA	Smart material alloys
MT	Martensitic transformation
CPUT	Cape Peninsula University of Technology
NiTi	Nickel Titanium
FRC	Fibre-reinforced composite
etc	Et cetera
UAV	Unmanned
RTM	Resin transfer moulding
RIP	Resin infusion process
GRP	Glass reinforced plastic
BCC	Body-centred cubic
SRPO	Single rod pullout
UD	Unidirectional
Cc	Close corporation
ASTM	American standards for testing and materials
V	Volume
W	Weight
CV	Coefficient of variation
Ep	Epoxy
Eg	E glass
UV	Ultra violet
wrt	with respect to
IFSS	Apparent interfacial shear strength
IEM	Instruments for Engineering Measurement
UTS	Ultimate tensile strength
TDL	Tiny Data Logger
s.a.	Sine anno

CHAPTER 1

INTRODUCTION

1.1 Problem statement

Increasing demand on the performance of engineering materials requires them to exhibit high stiffness and strength properties. The concept of developing reinforced composites with embedded wire made of Smart Material Alloys (SMAs) emerged in the late 1980s and pooled interest in the research for the last two decades. Buket et al. (2001) mentioned that the development of aero morphing reinforced composites consisting of SMAs is achieved by fabricating a reinforced fabric and SMA elements into matrix materials such as polymers, metals and ceramics. The SMAs can either be in the form of wires, ribbons or particles. The physical properties of the matrix materials are either improved by the SMA elements or by actively controlling the progress of the martensitic transformation (MT) in the SMA elements. Buket et al. (2001) further mentioned that internal compressive stresses are created in the surrounding matrix when the embedded and prestrained SMA elements are exposed to different environmental conditions. These compressive stresses give added strength and better stiffness properties to the composite. It is also understood that the generation of internal stresses would externally change the geometrical shape of the composite.

Current research efforts have already shown the feasibility and application of some proposed concepts in engineering fields. Yet, workable prototypes of engineering applications of SMA hybrid composites have not been developed. This research focuses on embedding NiTi alloys in the wire form in fibre reinforced polymers and particularly on material destined to build a UAV at Cape Peninsula University of Technology (CPUT).

1.2 Aims of the Study

The purpose of the present study is to develop an aero morphing reinforced composite material, consisting of e-glass fibres, epoxy resin AR 600 and NiTi alloy.

1.2.1 The specific aims of the study are:

- 1.2.1.1** To master the Composites Manufacturing Procedure of Resin Infusion for flat surfaces.
- 1.2.1.2** To investigate the properties of fibre reinforced composites without NiTi SMAs upon performance of a composite structure.
- 1.2.1.3** To investigate the properties of fibre reinforced composites containing NiTi SMAs upon performance of a composite structure.

1.3 Hypothesis of the study

The hypothesis of the study is that in a fibre-reinforced composite (FRC) material embedding NiTi alloys could change the mechanical properties of the composite. Thus the laminate developed, from the combined materials, would be structurally stiffer and better in strength.

1.4 Background and review of the related literature

1.4.1 Fundamentals of material constituents

The use of e-glass fibre reinforced composites has found an attractive and wide application in the field of automobile, aerospace, military, civil and commercial industries. Their applications are qualified due to their light, low-cost, high specific strength and low weight to length ratio.

According to experts in NetComposite.com, the fundamental role of e-glass fibre reinforcements is that of increasing the mechanical properties of the neat resin system. In this work, epoxy resin such

as AR 600 mixed with a hardener AH 2338 at a weight ratio of 100:30 would be used as a matrix of choice. Yet, these composites have often exhibited different mechanical properties when manufactured and tested at different geographical locations. Therefore, in order to know the mechanical properties, a basic tensile testing of the composite samples is required to be conducted. Testing under different conditions had been expedited by several researchers such as (Abraham et al., 1998; Van Paepegem et al., 2005; Gommers et al., 1998; Fereshteh-Saniee et al., 2005) to determine mechanical properties of the glass / epoxy composite at low strain rates and with specimens having different fibre orientation.

During curing or polymerisation the composite's physical structure changes as a result of the curing cycle. The curing cycle depends on the part size and thickness, method of heat application and end properties required. These curing conditions often improve the interfacial adhesion between the e-glass fibre and matrix, hence, possibly better mechanical properties.

1.4.2 Manufacturing methodology

This part of the research explains the benefits of selecting the resin infusion process as the manufacturing method of choice over other known methodologies. A comparison based on literature review was drawn and a suitable method was adopted for the development of these reinforced composite materials. A manufacturing procedure and process model of the material laminate is presented by means of experiments. The process model was achieved by means of a temperature-time graph that was obtained. The data were analysed in order to determine the effect of process temperature on the SMAs. Thereafter an experimental investigation on the mechanical properties of the structure was conducted and compared to the known data of other processes presented in the relevant literature.

1.4.3 Manufacturing Alternatives

1.4.3.1 Resin transfer moulding (RTM)

This is a process of using a two sided mould that forms both surfaces of a laminate. The lower side of the mould is made rigid while the upper side is either a rigid or a flexible mould. The two sides fit together to form a mould cavity. The salient feature of resin transfer moulding is that the reinforcement materials are placed into the cavity. Resin transfer moulding includes numerous forms which differ in the mechanics of how the resin is introduced to the reinforcement in the mould cavity. These moulding varieties may be made up using vacuum infusion or vacuum assisted resin transfer moulding. Janke et al. (2004) highlighted that the process could be performed in either ambient or elevated temperatures.

According to Pai (2007), the manner of manufacturing composites, especially resin matrix composites, could depend very much on the particular combination of materials in question, on the scale and geometry of the structure to be manufactured. Large and relatively complex open structural laminate shapes are easily constructed by resin transfer moulding using vacuum to consolidate a stack of impregnated fabric against two sided mould. Resin transfer moulding would be carried out carefully to produce internal association of fibres in different layers, with expulsion of air and excess resin. The curing of the composite laminates would be performed once these conditions are met. The load bearing characteristics of laminates would differ according to the following parameters such as orientation of the fibres, overlapping or defective layers, resin content and curing cycle. The limitations of resin transfer moulding are as follows:

- Expensive tooling.
- Problems in manufacturing large parts over 4 m in length.

1.4.3.2 Prepegs

Prepegs have shown advantageous in the manufacturing of advanced composite products with increase in fibre content. The limitation in the application of this technology is based on the tendency of the material to be more expensive as well as the requirement for expensive tooling such as an oven or autoclave for curing.

1.4.3.3 Vacuum bagging process

Resin matrix composites are made largely by the vacuum bagging moulding method in which the fibres and matrix have been pre-mixed and vacuum bagged. The major disadvantage with such a process is that the resin may cure before vacuum process is applied especially in complex shaped geometries of the laminate.

1.4.3.4 Resin infusion process

Vacuum bagging is taken over by the resin infusion process (RIP) in which the system is vacuum bagged and later the resin is introduced at constant pressure and temperature (under vacuum conditions). In the system, reinforced fabric is placed on a mould and a vacuum bag is sealed over the mould using tacky tape. A vacuum is drawn and subsequently the resin is supplied into the mould by means of a vacuum which is maintained until the laminate is cured. The process eliminates curing of resin before time. It further reduces resin rich pockets which may cause weakness spots in the structure. In addition, harmful gas emissions are removed, thus increasing the environmental safety. The process has also gained an advantage of distributing the resin much easier.

For flat shaped aeronautical and similar structures, a resin infusion manufacturing process would be applied. Indeed, the construction of the stacked flat laminates is carried out by a mould of rigid and flexible sides. This permits for the selection of the mould that processes the laminate very rapidly, accurately, and with minimum waste of raw materials. The manufacturing method would produce laminates of greater strength and design flexibility in comparison to the traditional methods such as hand lay-up, wet lay-up (etc).

Composites would definitely exhibit variation of mechanical properties when they are produced under uncontrolled conditions. According to Pai (2007), the variation of material properties produced by hand lay-up methods is more noticeable than that of composites made by mechanized processes. Researchers such as Abraham et al. (1998) and Avila et al. (2003) were among those who conducted a comparative study on the material properties of e-glass fibre / epoxy using different manufacturing processes. Wet lay-up with autoclave consolidation and RTM were employed by Abraham et al. (1998) to determine physical properties of glass fibre epoxy. It was found that composites produced using wet lay-up with autoclave consolidation performed much better than RTM. This was further affirmed by Avila et al. (2003) when a statistical study was conducted on hand lay-up manufacturing process with cure on air, under compression and assisted by vacuum. It was found that cure under compression out performed both process in terms of strength and stiffness. Curing assisted by vacuum was second best.

The specific nature and severity of the defects found in any manufactured laminate would be a feature of the manufacturing process. Laminates produced with defects are likely to reduce the strength of the material below the required component design stress and these defects are likely to manifest when the laminate is under loading. As a result these may act as sites for initiation of cracks which may result in catastrophic damage. Parlinska* et al. (2000) highlighted that a proper manufacturing procedure has to be performed before conducting tests to determine the properties of the composites.

1.4.4 Composite tensile test

The second main objective of the research focused on investigating the properties of fibre reinforced composites upon performance of composite structures. These properties were limited to the tensile material strength and stiffness of the laminate being tested. The test was performed using the macro-mechanical approach. The uniaxial tensile test was performed in specimens with different fibre orientation. The characteristics obtained were used to estimate the tensile strength and stiffness of the composites. The test was limited to static behaviour and ambient conditions, and the failure behaviour of the composite specimens was observed and recorded. The test comprised of obtaining force-displacement graphs under uniaxial loading using a Hounsefield tensile testing machine. The force-displacement graphs for all specified orientations were analysed accordingly. The discussion and conclusion on the effect of the test is presented. The simple tensile test was chosen because it conforms to easy processing and simple analysis of the test results. The stiffness and strength of the composite was obtained in order to do a comparative analysis with laminates that would be embedded with SMAs.

Saad A. Mustasher (s.a.) characterised the glass fibre epoxy composite laminate using uniaxial tensile test. In his work, it was highlighted that the maximum tensile load for glass fibre epoxy composite improved in the case of 0° fibre orientation angle to that of 90° fibre orientation angle. Yet the shear response showed a nonlinear behaviour for the fibre orientation angle of 45° . Gommers et al. (1998) employed a similar tensile test technique for knitted fabric reinforced composites and it was shown that the stiffness and strength in tensile and in shear depend on the fibre orientations, the fibre content and the yarn density. Researchers such as Avila et al. (2005), Deng et al. (1998), Gomes et al. (2007) and Buket et al. (2001) were among those who employed this tensile test technique.

1.4.5 Composite laminates

In this case, the composite is made up of two material constituents such as epoxy and e-glass as reinforcing material. The e-glass reinforcement is embedded in epoxy resin to produce superior elastic properties above those of the constituents, specifically high strength and high stiffness. These properties are desired because the intention is to compare them with composite laminates embedded with NiTi alloys. In order to achieve that, properties of the virgin specimen need to be determined.

1.4.5.1 The behaviour of the composite laminates

The composite laminate is assumed to be a homogeneous material with orthotropic material properties. Therefore, the assumption is intended to develop the stress-strain relations in order to know the composite laminate response. In addition, the laminate is assumed to be a plane stress problem. This means that principal stresses ($\sigma_{1,2}$) and shear stress (τ_{12}) parameters lie in the principal material coordinate system. This further means that principal stress (σ_3) and shear stresses (τ_{23}) and (τ_{13}) act perpendicular to the principal material coordinate system, and are set to a value of zero. The material parameters established using empirical methods (tensile testing, etc.) are modelled using the plane stress method and micro-mechanics techniques. These material parameters would assist in determining the response of composite laminate under the influence of the applied loads (in plane loads).

1.4.5.2 Types of composite laminates

Composite laminates are classed into the following types:

- **Multiphase type**
The multiphase type is made up of two or more constituents. However at present, consideration is on those composite laminates containing only two constituents such as e-glass fibre and epoxy resin. The e-glass fibre is known as reinforcing constituent and is embedded in an epoxy resin constituent to form e-glass/epoxy composite lamina.
- **Laminated type**
The laminated composite is made up of two or more lamina bonded together using different fabrication processes such as resin infusion process (RIP), resin transfer moulding (RTM), autoclave, etc. Reinforced composites are some of many examples of composite laminates.

1.4.6 History of NiTi Shape Memory Alloy

NiTi is a shape memory alloy which has the ability to recover extensive amounts of deformation when subjected to a temperature change (<http://en.Wikipedia.org/wiki/nitinol>). The recovery of deformation is due to a phase transformation from martensite to austenite. Under normal conditions, the transformation temperature occurs around 60 °C. Its trade name is known as Nitinol which stands for Nickel Titanium Naval Ordinance Laboratory. The remarkable properties of the material were discovered in 1965 by Beuhler along with Wang. Its composition varies but normally is composed of approximately 55% Nickel by weight and 45% titanium. Any variation in composition significantly contributes to the change in the transition temperature of the alloy.

Above its transformation temperature, Nitinol is super elastic, has the ability to withstand a large amount of deformation when a load is applied and return to its original shape when the load is removed. Below its transformation temperature, NiTi displays the shape memory effect. When it is deformed it will remain in that shape until heated above its transformation temperature, at which time it will return to its original shape. NiTi alloys have found wide applications in the field of couplings, biomedical and medical, toys, actuators, heat engines, sensors, cryogenically activated die and bubble memory sockets as well as lifting devices. Figures 1.1 to 1.4 provide an illustration of NiTi applications in various engineering fields.

The NiTi alloy is chosen because of its good electrical and mechanical properties, long fatigue life, high corrosion resistance, large pseudo-elastic hysteresis and its ability to recover 5% strain as well as 345 kPa restoration stress with many cycles. This type of alloy is available in three forms such as wire, rod and bar stock, and thin film.



Figure 1.1: Headgear and J-hooks for connections into patient's mouth
(<http://en.Wikipedia.org/wiki/nitinol>)



Figure 1.2: Golf clubs (driver, putter & iron)
(<http://en.Wikipedia.org/wiki/nitinol>)

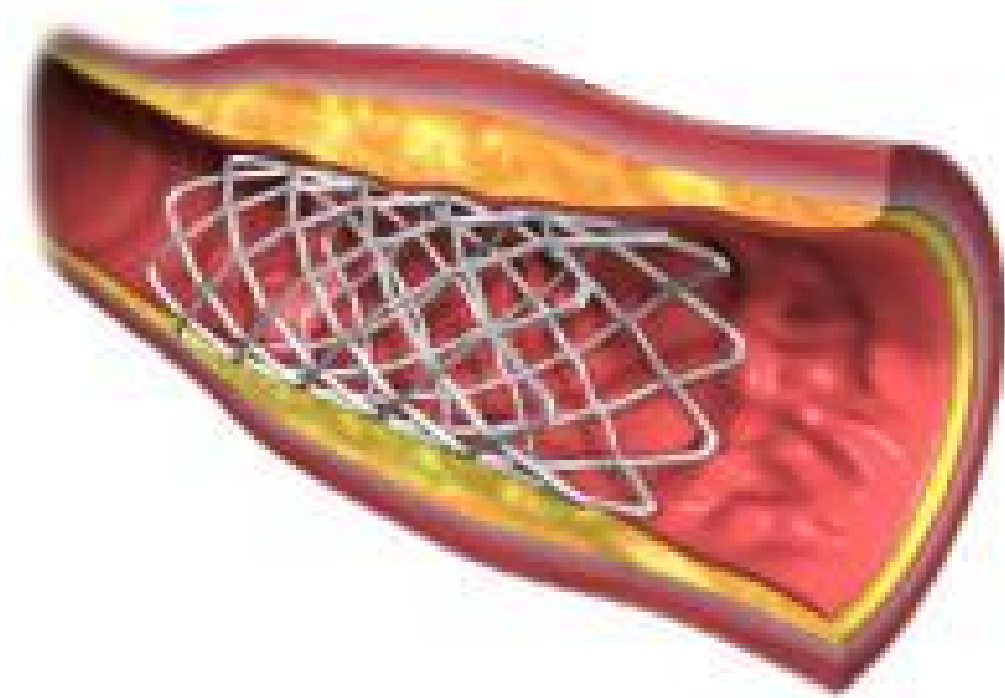


Figure 1.3: Thumb stent in artery
(<http://en.Wikipedia.org/wiki/nitinol>)



Figure1.4: Boeing 787 – Tail fin (Rudder), the wings and the nose
(<http://en.Wikipedia.org/wiki/nitinol>)

1.4.7 Martensite and Austenite Phases

The temperature (M_f) is defined as the temperature at which the transition to martensite is completed during cooling. During heating austenite start (A_s) and austenite finish (A_f) are defined as the temperatures at which the transformation from Martensite to Austenite begins and ends. One of the limitations in the use of the shape memory effect is the shift of the characteristic transformation temperatures (functional fatigue) due to their relation with a change of micro structural and functional properties of the material. The change from the martensite phase to the austenite phase is a function of temperature and stress. The change of phases is therefore independent of time since there is no diffusion involved. Even though there is no diffusion involved the process is reversible between the two phases. The variation between the heating and cooling changes gives rise to the shape of the curve hence the dependence on the material properties of the SMA such as alloying. See figure 1.5.

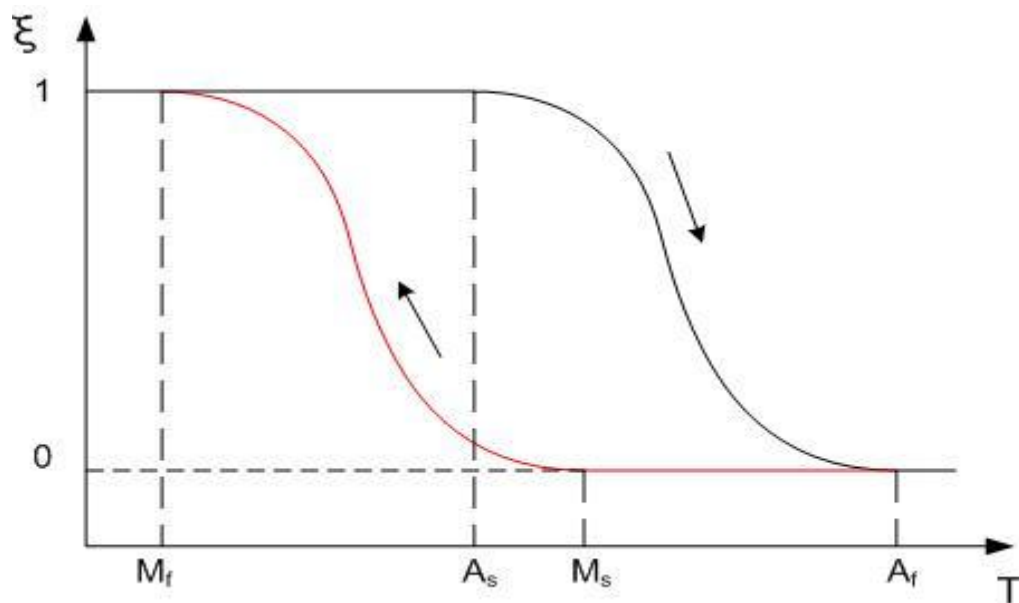


Figure 1.5: Transformation temperature profile (Janke et al. (2005))

1.4.8 Shape memory effects on shape memory alloys

It was found by most researchers that there were two memory effects in shape memory alloys. These were as follows:

1.4.8.1 One-way shape memory

When a shape memory alloy is conditioned below the austenite start temperature (A_s)(cold state), the element can be formed by bending or stretching into a variety of shapes. The element keeps the shape until it is heated above the transition temperature. During heating, the shape changes back to its original form regardless of the shape it was when conditions were cold. When the element cools again it keeps the hot shape until deformed again. According to Janke et al. (2005), this is also defined as pseudo-plastic deformations. See figure 1.6 from (<http://en.Wikipedia.org/wiki/nitinol>). Another phenomenon of one-way shape memory is pseudo-elasticity (also known as super-elasticity) in which the phase transformation from austenite to martensite takes place by raising the external stress and keeping the temperature constant. The alloy transforms again to the austenitic state by just relieving the stress.

1.4.8.2 Two-way shape memory

A material that demonstrates a shape memory effect during both heating and cooling is known as two-way shape memory. See figure 1.7. However, this can also be achieved without the application of external force. If a shape memory alloy is heated up to very high temperatures (above the one applied for training), the shape memory alloy may lose the two way memory effect. This process is known as “amnesia”.

- a. Starting from martensite.
- b. For one-way effect, reversible deformation is added or for the two-way, irreversible deformation is added.
- c. The element is heated.
- d. The element is cooled again.

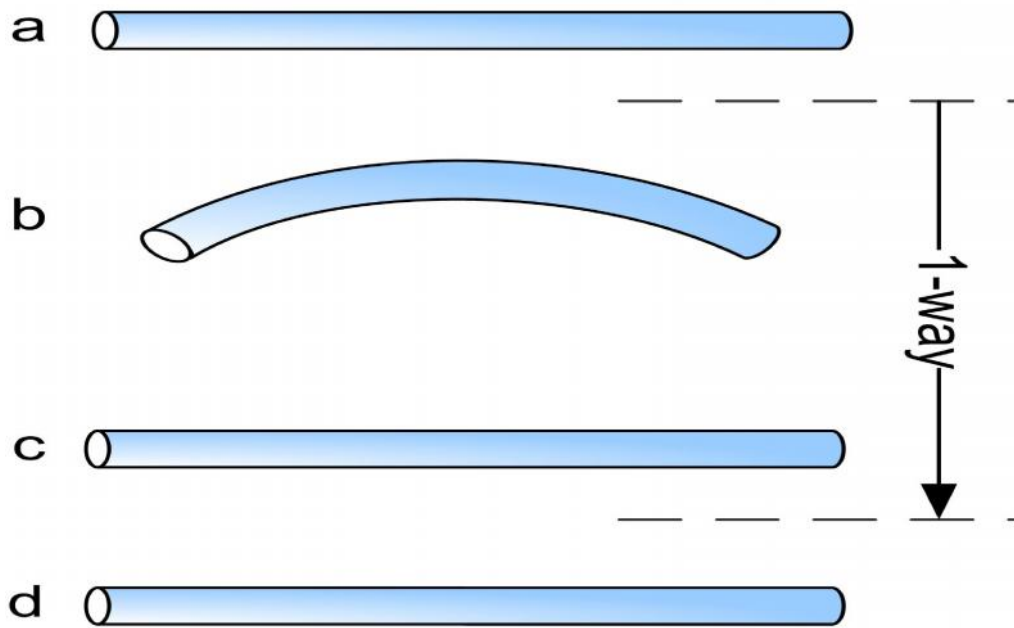


Figure 1.6: Illustration of 1-way shape memory effect

(<http://en.Wikipedia.org/wiki/nitinol>)

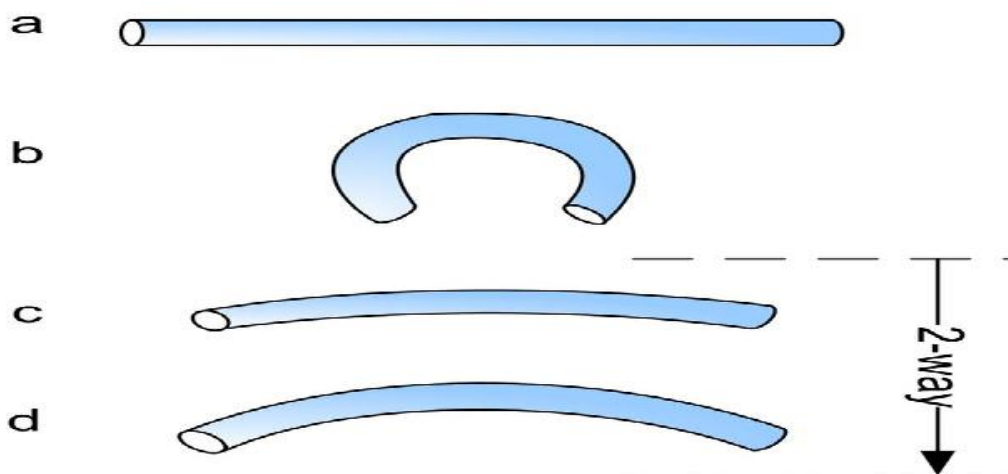


Figure 1.7: Illustration of 2-way shape memory effect

(<http://en.Wikipedia.org/wiki/nitinol>)

The embeddement of smart material alloys into reinforced composite structures is of particular interest because it raises the question of the effect it may have on the material properties of the composite laminate. Again the focus is specifically on tensile strength and tensile stiffness of the embedded laminate. Sitter et al. (2000) describes the incorporation of SMAs as a phenomenon that may either improve the physical properties of the composite laminate or may even actively modify the controlling progress of the SMA elements during the martensitic phase (Sitter and Stalmans 2000). They further pointed out that the SMA elements have the ability to generate internal compressive stresses in the surrounding matrix when the embedded and prestrained SMA elements are heated. These compressive stresses could strengthen the composite, improve the damping properties or even change the natural vibration frequencies together with the external shape variations.

SMAs have more than one crystal structure (polymorphism) which depends on both temperature and external stress (Janke et al. (2005)). The temperature transformations allow for the reversible switching between the temperature phases in SMAs as well as suitability of applications in advanced, smart or adaptive engineering structures. The group of SMAs presented in table 1.1 serve to illustrate the composition and transformation of the atoms.

Table 1.1: Some alloys exhibiting shape memory effect

Alloy	Composition [atomic %]	Transformation
Cu-Al-Ni	28-29Al, 3.0-4.5 Ni	TE=Thermoelastic
Cu-Sn	15 Sn	TE
Cu-Zn (brass)	38.5-41.5 Zn	TE
Cu-Zn-X	(X=Si, Al, Ga, Sn) few %X	TE
Fe-Cr-Ni-Mn-Si	9 Cr, 5Ni, 14 Mn, 6 Si	Non-TE
Fe-Mn-Si	28-33 Mn, 4-6 Si	Non-TE
Fe-Ni-c	31 Ni, 0.4 C	Non-TE
Fe-Ni-Co-Ti	33 Ni, 10 Co, 4 Ti	TE
	31 Ni, 10 Co, 3 Ti	Non-TE
Fe-Ni-Nb	31 Ni, 7 Nb	Non-TE
Mn-Cu	5-35 Cu	
Ni-Al	36-38 Al	TE
Ni-Ti	49-51 Ni	TE
Ni-Ti-Cu	8-20 Cu	TE

The NiTi alloys are applied in the laminate to prevent structural fatigue. Structural fatigue is simply the accumulation of micro-structural defects in addition to formation of growth of surface cracks until the material finally ruptured / fractured (Janke et al. (2005)). The fatigue resistance of the structure is influenced by factors such as temperature, type of loading, alloy composition, specimen size, micro-structure and surface quality. Embedding the NiTi alloys might bring an increase in mechanical strength of the composite laminate which perhaps results in higher fatigue resistance of the material.

1.4.9 Shape memory effect (SME)

SME as reported by Pai (2007) is described as the ability of a material to remember a predefined shape after deformation, with an increase in temperature. A process of annealing is conducted to allow the SMA NiTi to possess SME. The NiTi specimens are cut to size and then put in the oven at 230°C for a period of 10 hours. Thereafter, the specimens are cooled in room temperature environment. Although shape memory alloys display more than two phases, in this work, austenite and martensite phases are considered due to their capabilities to exist in higher temperature and lower temperature phases. Their phase characteristics provide NiTi alloys with the ability to perform shape memory recovery after deformation. Austenite phase has a very strong and stable crystalline structure that is made up of body-centred cubic (BCC) lattice presented in figure 1.8. In the BCC structure, Ti atoms exist at the vertex of the cube and Ni atoms exist at the centre.

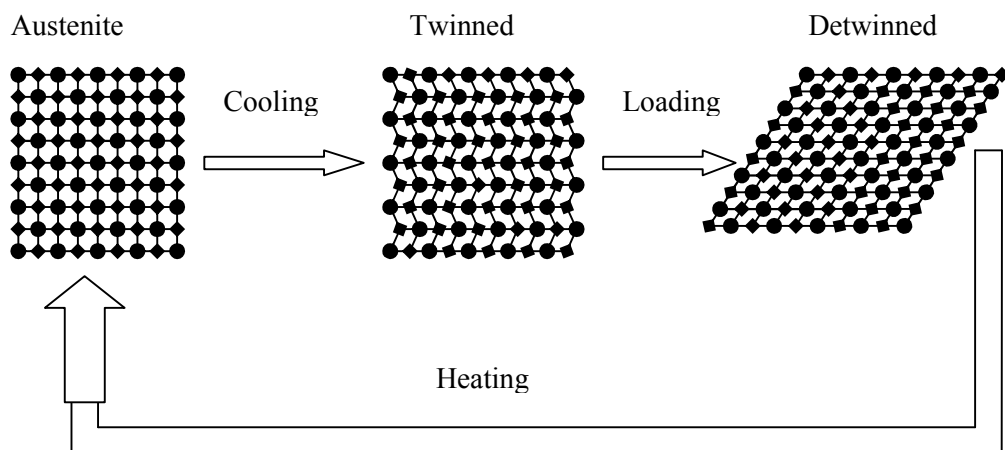


Figure 1.8: Austenite BCC, twinned and detwinned martensite structures.

In a case of martensite, the structure may either form a monoclinic crystal lattice or rhombic crystal lattice. Several authors (Pai, 2007; Wie and Sandström, 1998) concur that the formation of these crystal structures is governed by the stress applied on the system. The formation of monoclinic lattice takes place when there is no stress applied and at low temperature conditions. Further, the monoclinic lattice has two configurations namely twinned martensite and detwinned martensite. See figure 1.8 for twinned and detwinned martensite structures. Twinned martensite is called such a name due to the availability of an atom on the boundary seeing the mirror image on the other boundary side. Twin boundaries exist at low temperature and are easily moved by the application of stress resulting in detwinned martensite state. Again the twinned boundaries actually dislocate to accommodate the applied stress hence the formation of a rhombic crystal structure.

According to Wie and Sandström (1998), the martensite phase consists of highly twinned polydomains (martensite variants). At this phase, when the material is subjected to an applied stress, the material variants undergo a self-accommodating pattern of shear-induced shrinkage, growth and reorientation by detwinning, resulting in twin-induced inelastic strains. Figure 1.8 illustrates the transformation process that occurs from twinned martensite to detwinned martensite. Pai (2007) noted that austenite and twinned martensite possess the same geometrical shape in macroscopic scale. When a load is applied to twinned martensite, the material transforms to detwinned martensite with a new lattice structure called rhombic. The orientation of rhombic structure is governed by the direction of the applied load, which, results in deformation of the structure. Above, on application of heat (known as Joule's effect), the transformation only follows one route of austenite BCC structure, which is the existence of Ti atoms at the vertex and Ni atoms at the centre of the cube. This transformation actually leads to the recovery of the original structural shape.

1.4.10 Interfacial bond strength test

Prior to embedding the SMAs, it is imperative to have a clear understanding of the SMA interfacial bond strength on reinforced e-glass / epoxy composite. The bond strength could be achieved by conducting single pull out tests on different conditioned specimens. The single pull out test provides a comparison of strength among specimens. The experiment could show that an untreated specimen is likely to possess better interfacial bond strength than the corroded and sanded specimens.

Evans et al (1999) acknowledged that the fibre-matrix interface had a significant influence on the fracture behaviour of fibre-reinforced materials. In their work, different parameters such as the interfacial shear strength (τ_i), the energy release rate (G_c), the frictional shear stress (τ_f), the coefficient of abrasion (A) during frictional pull-out and the Coulomb friction coefficient (μ) were proposed to characterise the mechanical properties of the interface of the composite material. A similar methodology needs to be applied in the case of reinforced composite embedded with NiTi alloys. An investigation would be conducted using the Single Rod Pullout (SRPO) test to gather empirical data. The SRPO method would allow resolving all the parameters which characterise the mechanical properties of the interface. The mathematical models allowing for the development of the interface parameters SRPO test were mainly based on the cylindrical geometry of the specimens. The model is based on the work by Penn et al (1989).

Evans et al (1999) noticed that the results obtained from SRPO tests were to some degree not convincing for industrial applications. However Sakai et al (2000) proposed that in order to overcome the disparity between models and reality, in cases of fibres, the fibre bundle pullout test should be applied. Similarly, in the case of SMAs (NiTi) embedded in the composite a bundle Pullout Test could be applied.

In Coulomb's friction model, the shear stress (τ_f) is expressed as the product of the friction coefficient (μ) and the clamping stress (q_0). Gao et al (1999) overcame the predicament to separate μ and q_0 parameters using the single fibre pullout (SFPO) tests by taking into account the Poisson contraction of both fibre and the surrounding matrix system during the pull-out process. In this work, similar methodology could be applied by substituting NiTi alloy as the material instead of fibres. Most reinforced composites embedded with NiTi need transfer of strain from the wire to the matrix. So it is favourable to have a very strong bond between NiTi alloy wire and epoxy AR 600 matrix. It is crucial to have some measure of the interfacial bond strength between the NiTi wire and the host matrix for the assessment of mechanical response.

According to Jonnalagadda (1997), bond strength is commonly defined as the mechanical resistance to separation of the bonding agent from the substrate. In this case, bonding is attributed to the interface region between the host matrix and the embedded NiTi alloy. Due to the nature of the material bonding, debonding normally proceeds in a weak boundary layer or interface region. The level of bonding is controlled by applying an appropriate surface treatment to alter the interface region.

Several researchers have conducted a number of testing methods such as pullout, pushout, single fibre critical length test, fragmentation test, Broutman test and microbond test for determining the interfacial bond strength of composites. In this research, a single rod pullout test is chosen as the best initial test method to evaluate the interfacial bond strength of the fibre-NiTi-epoxy resin interface. A pullout test diagram is shown in figure 1.9.

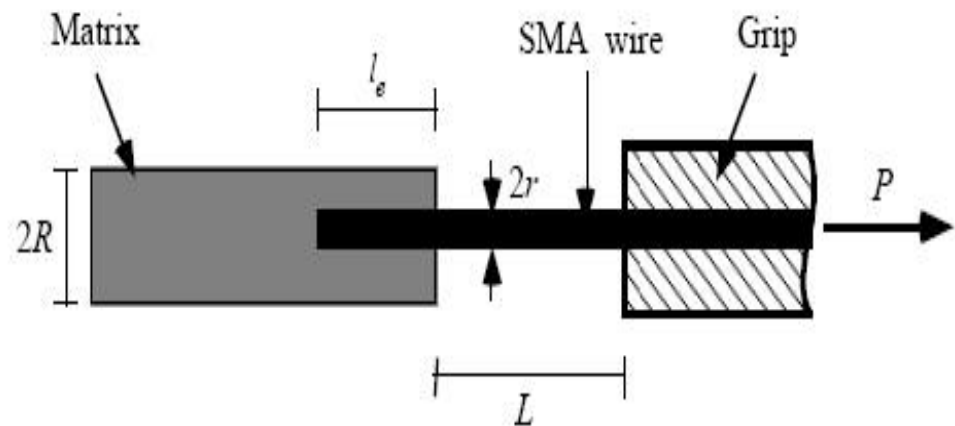


Figure 1.9: A pullout test schematic of tested specimens

A length (l_e) of the rod is embedded in the E-glass / epoxy matrix. The embedded length (l_e) is determined using the equation developed by Miller et al. (1986) and it is expressed as

$$L_e = (\sigma_f \times D) / 4T \quad (1.1)$$

The free length L of the NiTi rod is measured between the e-glass / epoxy matrix face and tensile machine grips. The free length parameter is a very significant one as it determines the extension and breakage of the NiTi rod wire.

There is ample literature on the standard pullout test of fibres. Wie and Sandström (1998) have shown that the load applied to the fibre end is recorded as a function of the displacement of this end with respect to a “stationary” point in the specimen, usually the grips. They also found that a force – displacement curve from the test consisted of three stages as follows:

- At the first stage, the fibre matrix interface should remain intact, the curve should be nearly linear for the system. ($0 \leq F \leq F_d$)
- At the second stage, when the external load F reaches some critical value, debond force (F_d), the fibre begins to debond off the host matrix through the interfacial crack propagation. ($F_d \leq F \leq F_{max}$), the registered force proceeds to increase with the fibre end displacement (or crack length), due to addition of frictional load in debonded regions being added to the adhesional load from the intact part of the interface.

- At the third stage, after a peak load, F_{max} is reached. The crack propagation becomes unstable and the whole embedded length debonds. The measured force drops from F_{max} to F_b . From this moment until complete pullout, the “tail” force is due to frictional interaction between the fibre and the matrix.

Zhandarov et al. (2004) proposed a model which relates the ultimate interfacial shear strength (T_d) to the debond force (F_d) as

$$T_d = (F_d \beta / \pi d_f) \coth(\beta l_e) + T_t \tanh(\beta l_e / 2) \quad (1.2)$$

where β is shear lag parameter, and T_t is a stress term due to thermal shrinkage. Further Zhandarov’s model gave a direct expression for the current load F applied to the fibre end, as a function of the crack length. In their second energy controlled debonding model, the model assumed that the debonding zone extended when the energy release rate, G , reached its critical value, critical energy release rate (G_{ci}). In the paper, a comparison of various approaches to the characterisation of the strength of the fibre / matrix interfaces based on micromechanical (single fibre) tests was performed. It was found that both energy based (critical energy release rate) and stress based (local interfacial shear strength) criteria can be successfully applied as interfacial parameters. Although both criteria could be applied, stress based criterion would be employed in this work.

Although there is abundant literature on SFPO test, the literature on the interfacial bonding strength of embedded SMAs is quite limited therefore this work will add to knowledge.

CHAPTER 2

RESIN INFUSION TECHNIQUE IN MANUFACTURING FLAT COMPOSITE MATERIAL

2.1 Introduction

This chapter describes the manufacturing procedure of resin infusion as an advanced composite manufacturing technique. Explanation on the benefits of selecting resin infusion as a manufacturing method is presented as well as step by step description of the experiments. Researchers such as Abraham et al. (1998) and Avila et al. (2003) conducted a comparative study on the material properties of e-glass/epoxy resin using different manufacturing processes. It was confirmed that the vacuum assisted process out performed the hand lay-up process in terms of strength and stiffness.

The curing process of the composite is presented by means of temperature vs. time graph. The curing process model is suitable to analyse the effect of temperature on the composite. The curing of the composite is found to be a four step process, also known as a dwell process. A temperature deviation of 1°C was observed from the start of first dwell to the finish of fourth dwell. The flow of the resin during processing was observed as a function of distance and time. Firstly, we looked at the process where the composite was embedded with a sacrificial mat. Secondly, we looked at the process where the sacrificial mat was replaced by toughened glass. Both processes were covered by a vacuum bag to create the dome. Through observation there is resemblance on the graph profiles, although the flow speeds seemed to be varying. The flow speed with the toughened glass was found to be deviating by 34.9 % compared to that with sacrificial mat.

The toughened glass was employed to ensure the production of a flat composite surface. The composite fibre volume content was determined to ensure a free resin rich composite. An average fibre volume of 62.42 % content was achieved with the weight of the glass fabric approximately 250 g and the weight of the whole composite approximately 324 g. In this case, ten fabric mats were utilised.

2.2 Manufacturing the composites

The composites were manufactured by first pre-packing the moulds with fibres, usually arranged in mat form. This was followed by infusing the resin under pressure into the closed mould. This procedure allows close control which results in high quality products. Hyer (1998) reported that, “Defects such as incorrect overall fibre volume fraction, misaligned or broken fibres, non-uniform distribution of fibres, with resultant matrix-rich regions, pores or voids in matrix-rich regions, gaps or overlaps in the arrangement of sheets of reinforcement in any given lamination, inter-laminar debonded regions (delaminations), incorrect state of resin cure, resin cracks or transverse ply cracks resulting from thermal stresses during cooling after manufacture are likely to arise from the processes of manufacture .”

Our composites were made up of three components; E-glass fibre, epoxy resin and NiTi alloys as an embedded material (expected to increase strength and stiffness of the structure).

2.3 Description of Resin Infusion Process (RIP)

The resin infusion process is the process whereby:

- 2.3.1** Fabrics are laid up as a dry stack of materials.
- 2.3.2** Material fabrics are then covered with different types of plies followed by a vacuum bag.
- 2.3.3** Vacuum bag is secured on a sticky tape to form a seal laid on the hardened glass.
- 2.3.4** The resin is allowed to flow into the fabric after the vacuum is created.
- 2.3.5** The resin is distributed over the whole stack of fabric, thus wetting the fabric stack.

The Resin Infusion Process (RIP) is done in two phases: fabrication and process modelling.

2.4 Fabrication Phase

In this phase, the e-glass fibre reinforcement and epoxy resin AR600 together with hardener AH 2338 are prepared to form a flat plate. The description of the required procedures for fabrication is dealt with on page 27. The fabrication of the flat plate was processed at room temperature under vacuum created using vacuum bag and pump. The vacuum allows the consolidation of fibre mat layers and reduces air voids between layers. Above that, the elimination of gases given off by the resin that pose a health risk, as it cures is achieved. In order to fabricate a flat plate, tools are required to form the geometrical shape of the plate during processing.

2.5 Tooling

The design and construction of the tool is a significant component during the fabrication phase. In view of the fact that the tool would be subjected to heat and pressure during the curing of the composite, a toughened glass (1052 x 911 mm) polished all round was sourced from Glassmen, Durbanville, South Africa. The glass was placed on a surface table (1502 x 915 x 920) mm on a rubber mat (1052 x 911 x 5 mm). The rubber mat was fitted to cushion the toughened glass, when resting on the surface table. The glass was chosen because it exhibits dimensional stability, good surface finish, is fairly durable and low cost.

The list of material and consumables applied for the fabrication of the flat plate composite is shown in table 2.1.

Table 2.1: Fabrication materials and consumables

Item no.	Description	Item no.	Description
1.	Glass 315g UD fabric	14.	Resin trap pot
2.	Peel ply fabric with tracer yarn	15.	Heat gun
3.	Tacky tape DTE/90	16.	Acetone
4.	Airbleed 100/1.9	17.	10mm diameter plastic tubing
5.	Absorption fabric	18.	10 mm T-piece connections
6.	Release film	19.	10 mm in-line pipe
7.	Resin Mixing Pot	20.	Rotary fabric shear
8.	Resin distribution fabric	21.	Hand roller brush
9.	Epoxy AR600	22.	Disposable masks
10.	Hardener AH2338	23.	Safety spectacles
11.	Vacuum bag	24.	Surgical gloves
12.	Vacuum pump	25.	Methylene chloride
13.	Wax polish –carnuba paste (Release agent)	26.	10 mm diameter spiral plastic tubing

2.6 Resin infusion process

The process offers many benefits in comparison to conventional hand lay-up techniques. As it is a closed mould process, the system allows for unlimited set-up time in that the resin system is not being introduced until the reinforcements and core materials are put in place. The vacuum bag facilitates good resin distribution and consolidation of the laminates. The hypothesis is that with infusion process the resulting mechanical properties of the complete product are likely to be higher than would be the case with hand lay-up techniques. The RIP process is also preferred because the existing moulds can continue to be utilised with little or no modification. One limiting factor of applying RIP is the use of sacrificial mat or net to facilitate resin distribution as well as layer of peel ply and release film. These consumables increase the cost of the moulds and lengthen lay-up time. In

addition, the consumables are difficult to dispose due to stringent hazardous waste legislation.

The RIP is achieved by following the steps below:

Step 1: Wax application

The surface of a 10 mm thick hardened glass used for (tooling/mould) is cleaned with acetone. A tacky tape is placed around the surface area of the glass. A wax polish is applied on the surface area to allow the easy removal of the finished product. See figure 2.1.

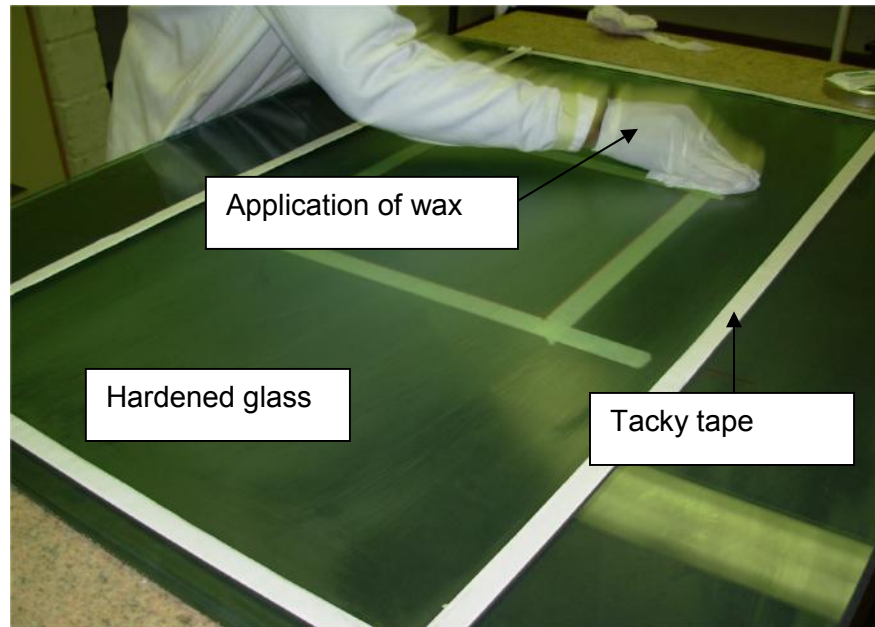


Figure 2.1: Preparation of the molding tool

Step 2: Heat application

A heat gun was used to speed up the drying process of the wax polish. The heat gun was kept at a position slightly higher from the glass surface to prevent hot spots. The distance of about 100 mm between heat gun and the wax polish surface was found adequate. See figure 2.2.

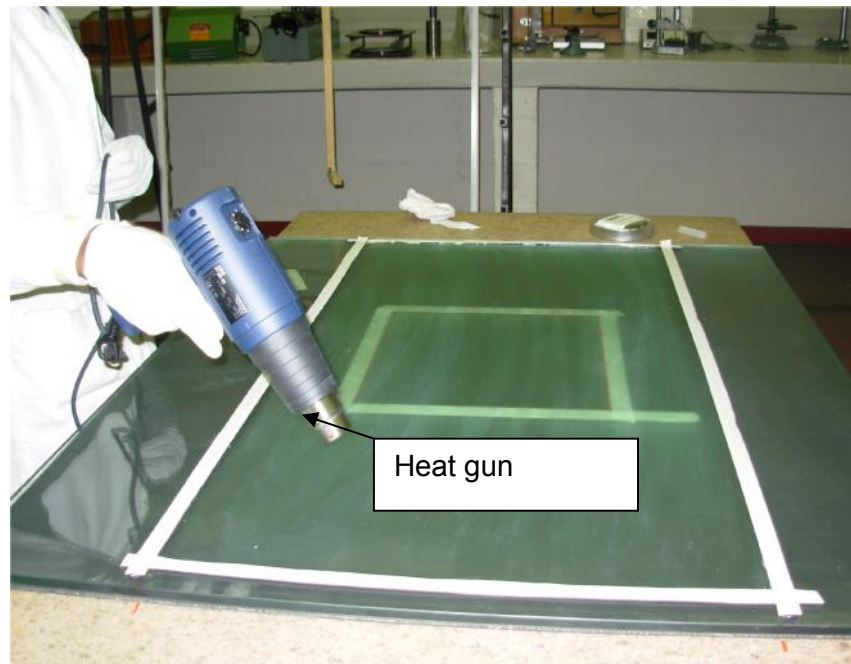


Figure 2.2: Application of the heat using heat gun

Step 3: Fabric layout

The carbon and e-glass fabrics were cut according to the design specifications using a roller shear cutter and laid up over the mould after the wax polish was dried up. The fabrics were placed one upon another according to the required end product size. The fabrics were grouped into sizes starting with two plies, four plies and six plies on both carbon and e-glass. See figure 2.3.

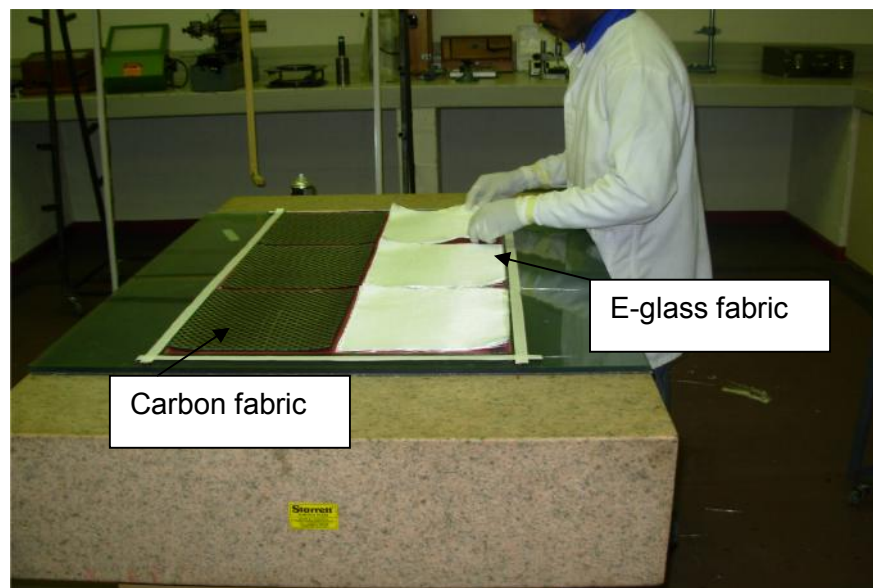


Figure 2.3: Placing 300 x 250 mm carbon fiber and e-glass plies onto the mould

Step 4: Lay-up release film

The release film is laid up over the plies to provide easy release from the epoxy resin. The film consists of perforated small holes to allow for bleeding and breathing. See figure 2.4.

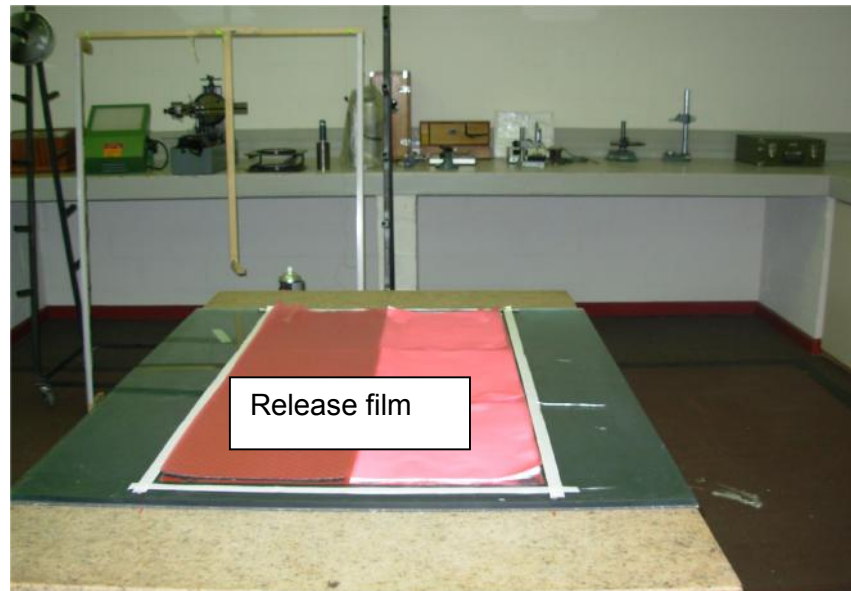


Figure 2.4: Release film layout

Step 5: Lay-up peel ply

The peel ply is applied to the texture surface in order to avoid sanding or braiding the surface. Excess resin can wick through and be peeled off after the composite has cured leaving a smooth textured surface. See figure 2.5.

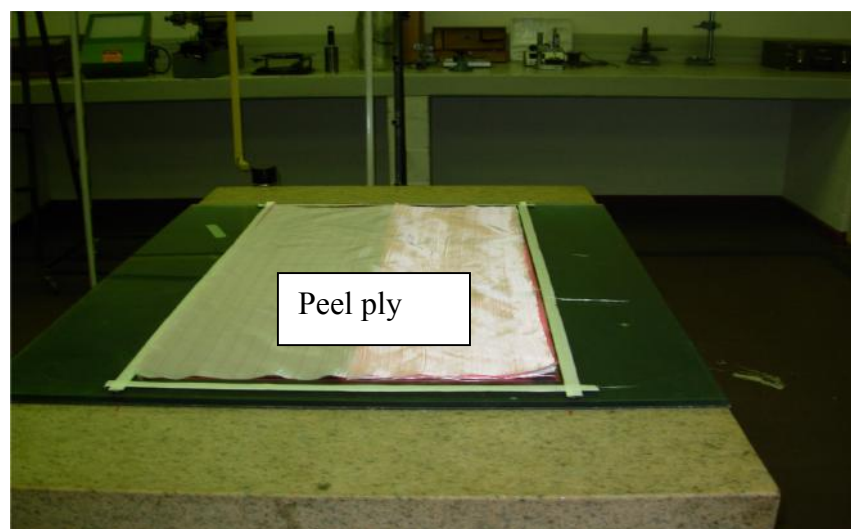


Figure 2.5: Laying peel ply

Step 6: Lay-up resin distribution fabric

The resin distribution fabric is employed to assist the flow of resin during the resin infusion process. The size of the fabric is tailored 50 mm more so that the spiral pipe could lie on the fabric. See figure 2.6 for lay-up illustration of resin distribution fabric.

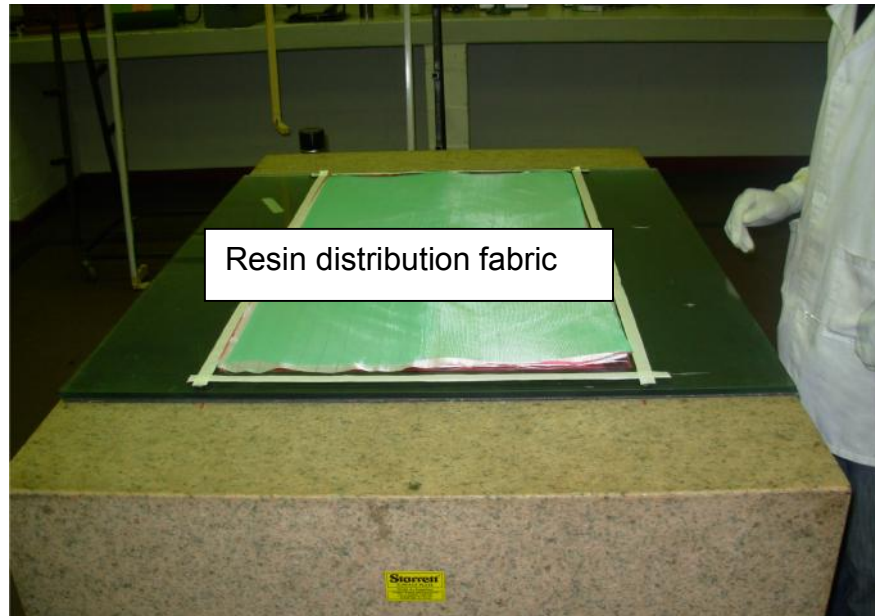


Figure 2.6: Laying resin distribution fabric

Step 7: Lay-up breather

The breather is laid-up above the distribution fabric as illustrated in figure 2.7. Hyer (1998:583) described the fabric as a porous, high temperature fabric employed to absorb excess resin during processing. The resin is absorbed to increase the fibre volume fraction and flush voids from the laminate. The breather allows “pulling” vacuum and removing volatiles without vacuum trap off that can wrap the composites. It is supposed to be placed over the entire surface of the lay-up. It further assists in removing creases.

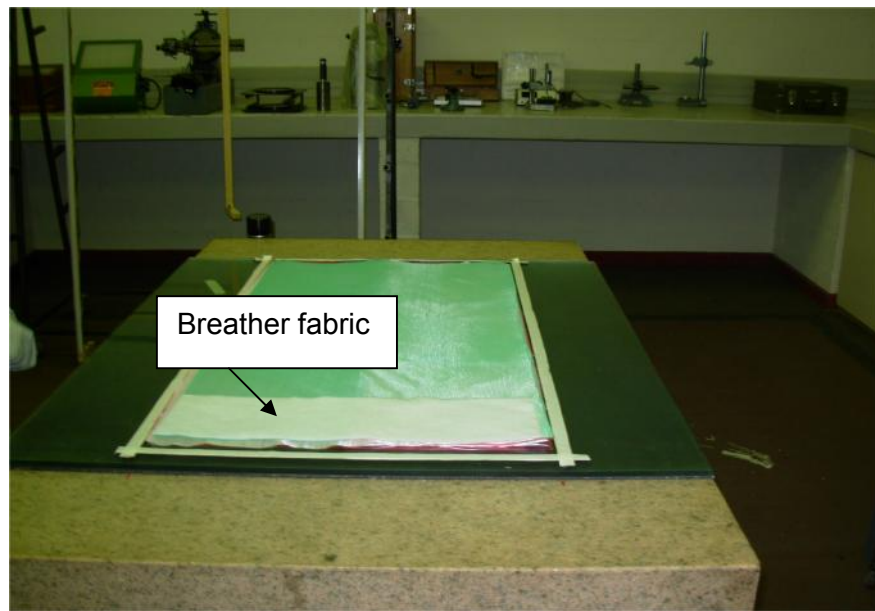


Figure 2.7: Laying breather or absorption fabric

Step 8: Lay-up spiral wrap

The spiral wrap allows the easy distribution of incoming and outgoing resin mix as illustrated in figure 2.8.

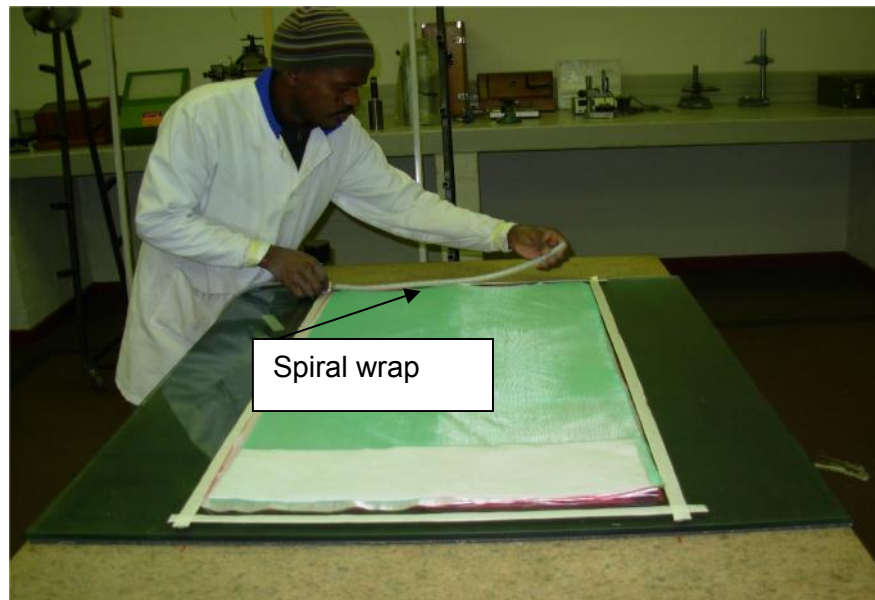


Figure 2.8: Insert spiral wrap at inlet and outlet side of the mould

Step 9: Lay-up vacuum bag

The vacuum bag is placed over the composite using the sticky tape as shown in figure 2.9 in order to facilitate good resin distribution and consolidation of the composite.

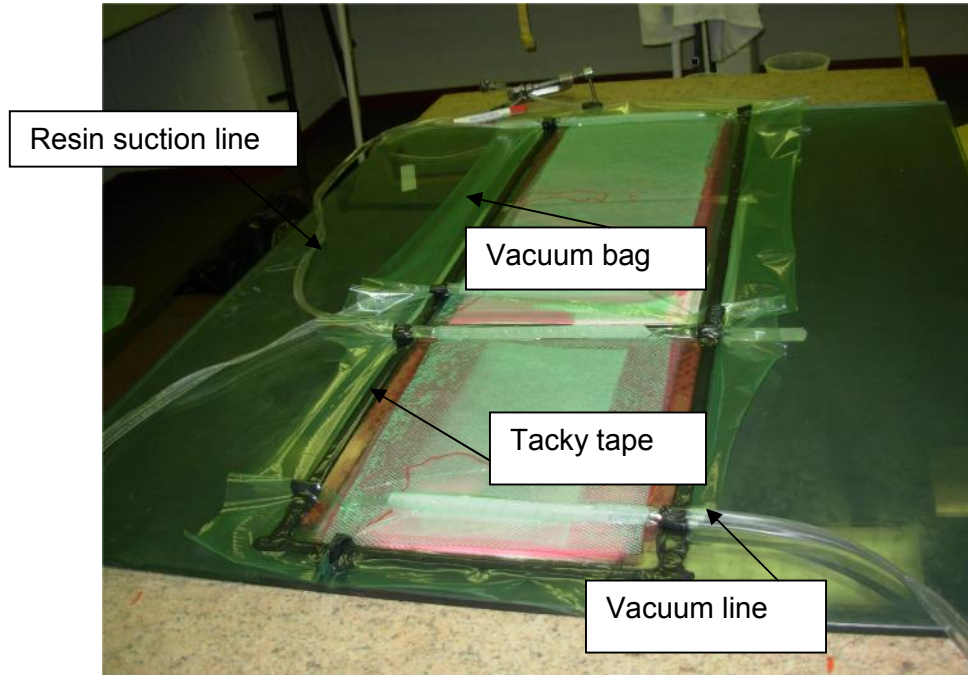


Figure 2.9: Apply vacuum bag using tacky tape

Step 10: Lay-up resin infusion equipment

The vacuum pump is employed to create vacuum in the mould. The resin trap box is installed to trap resin so that it does not damage the pump. The resin suction pot is fitted to mix resin and facilitates the drawing of resin to the system. All these accessories are shown in figure 2.10.

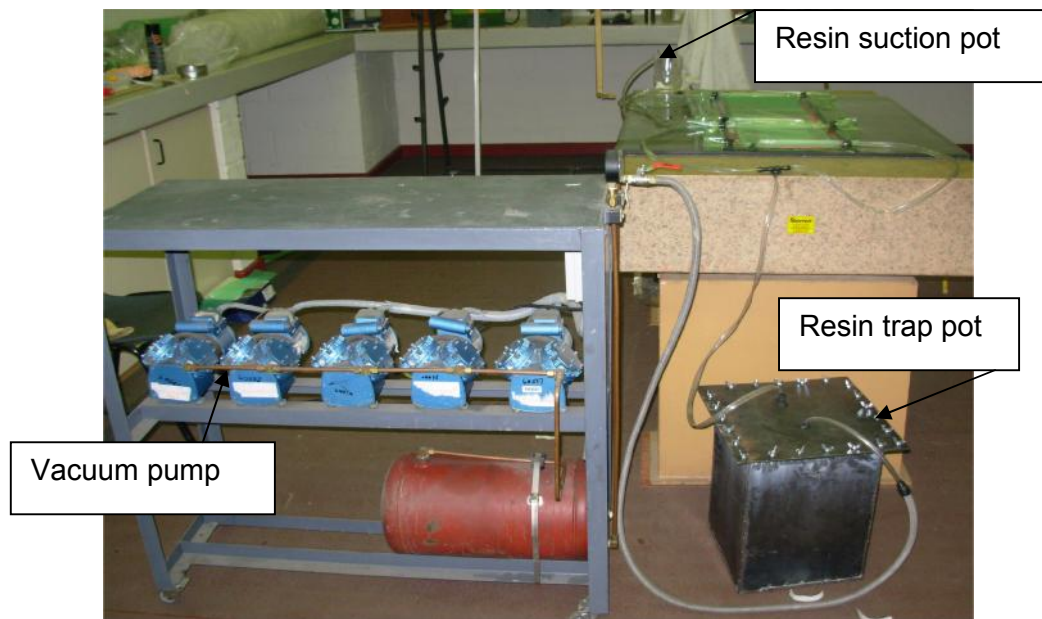


Figure 2.10: Resin infusion using vacuum pump

Step 11: Vacuum creation

The resin suction line is sealed at the end using tacky tape. The vacuum pump is switched on drawing air from inside the bag. The bag is pulled flat towards the glass mould. Once the air is pulled out and vacuum is created, the system is visually checked for leaks. During the leak test, the vacuum pump is switched off and the vacuum line is closed tightly using a small g-clamp. The leaks are detected once the pressure level within the bag lowers down and the bag is not tightly seating on the glass mould. The vacuum is allowed to hold for 30 minutes.

Step 12: Resin infusion

Once epoxy resin AR 600 is mixed with a hardener AH 2338, the tacky tape used to seal the end of resin suction line is removed. The resin is drawn into the system wetting up the fabrics. Once the fabrics are all wet, the resin line is closed using a g-clamp and the pump is left running to remove excess resin from the fabric.

2.7 The curing process phase

The objective of monitoring the curing process is to quantify any special effects on physical parameters such as the degree of cure, temperature, fibre volume fraction and residual stresses. Hyer (1998:596) highlighted that the epoxy resin material does not require high temperature during curing in comparison to polyimides. As a result of the low temperature process, the material is less prone to residual stresses. A data logger with a thermocouple was employed during the process to measure temperature vs. time. The data would provide an insight into the amount of temperature rise during the process of curing the composite.

An epoxy resin AR 600 and a hardener AH 2338 were mixed and infused into the fabric layers (laminates) to form a composite. The process was conducted at room temperature (22 °C). The pressure applied was approximately 1 bar below atmospheric, during the process. The room temperature is the temperature that cures the composite. The cure cycle for epoxy resin AR 600 is a four step cycle as shown in figure 2.11. In the process, initially the temperature of the epoxy resin AR 600 was constant at 24.6 °C. This is known as the first dwell. The temperature then increased after the first dwell to 24.9 °C. The temperature remained at 24.9 °C for an hour ten minutes (1 hour 10 minutes). This period is called the second dwell. Again the temperature rose to 25.3 °C and it remained constant for 30 minutes. This is called the third dwell. The temperature further increased to 25.6 °C after 30 minutes for more than two hours. This is the fourth dwell on the temperature vs. time graph.

During the first dwell, entrapped gases are allowed to escape from the system and epoxy resin flows smoothly through the laminate with no hindrance. During this interval the viscosity of the resin is still low hence allowing the easy flow of resin. Looking at the second dwell, this is the interval when the resin begins to settle, forming a gel for a period of about 1h10 min. As the temperature continues to increase to the 25.3 °C level, the resin begins to cure very rapidly. The last dwell interval indicates the end of curing of the resin and this is the critical stage. During this stage the strength and the stiffness of the composite are developed. The temperature

is kept constant until the pump is switched off. This is the period the composite is “touch” dry and it is kept under vacuum. Vacuum is employed to ensure epoxy resin AR 600 / e-glass fibre interaction as well as consolidation of the composite. The flat straight line indicates that curing is in a finished state. During processing of the composite, the temperature of the system deviated by approximately 1 °C. This simple means that the composite did not overheat and residual stresses were avoided. The final curing temperature record indicated an anomaly between 3:20 and 3:40 which was caused by the vacuum pump switch off.

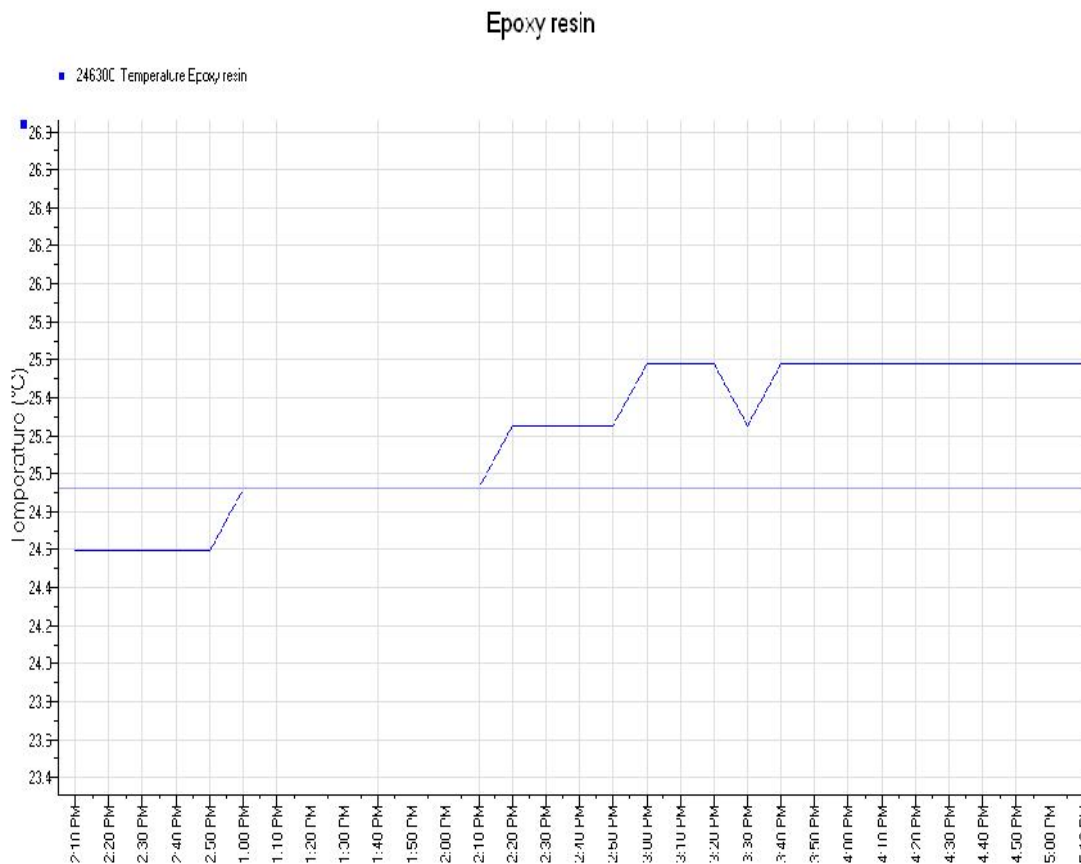


Figure 2.11: Four step cure cycle

2.8 Elimination of sacrificial mat

During the processing of the composite, it was found that the use of two glass moulds gave a better surface finish on both sides, thus eliminating the use of sacrificial mat or net. The introduction of the glass not only reduced the cost of the mould but also reduced the time taken to lay up the mats. The elimination of the sacrificial mats offered a very significant change in flow speed. In figure 2.12, the flow speed is shown as a function of the flow distance and time. The graph shows almost a linear relationship between distance and time. The mat took 5 minutes to roughly wet a surface of approximately 26 mm. See figures 2.13 for the set up of glass moulds.

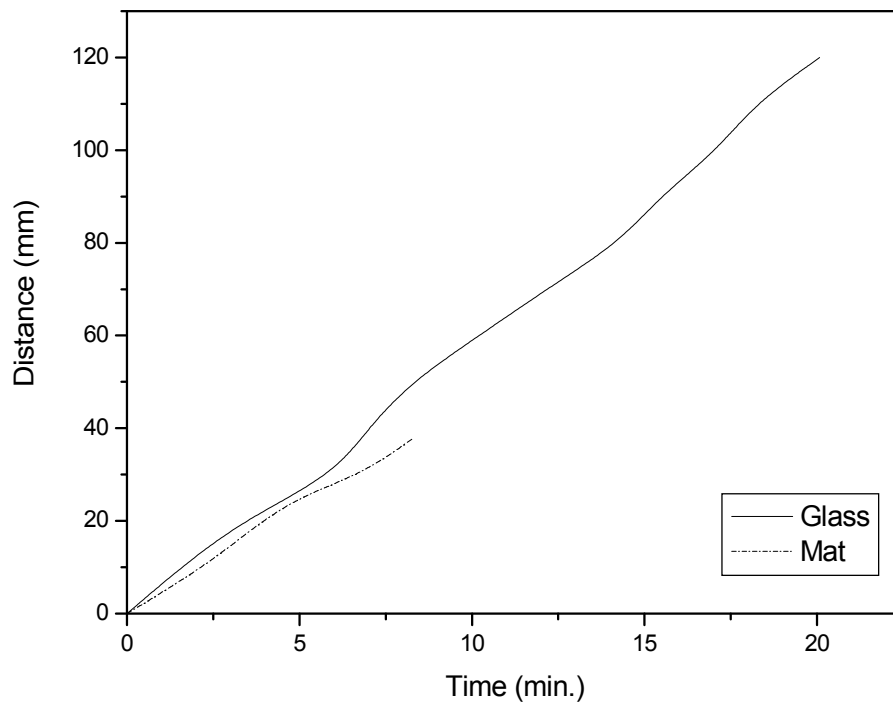


Figure 2.12: Flow speed of unidirectional (UD) material mat

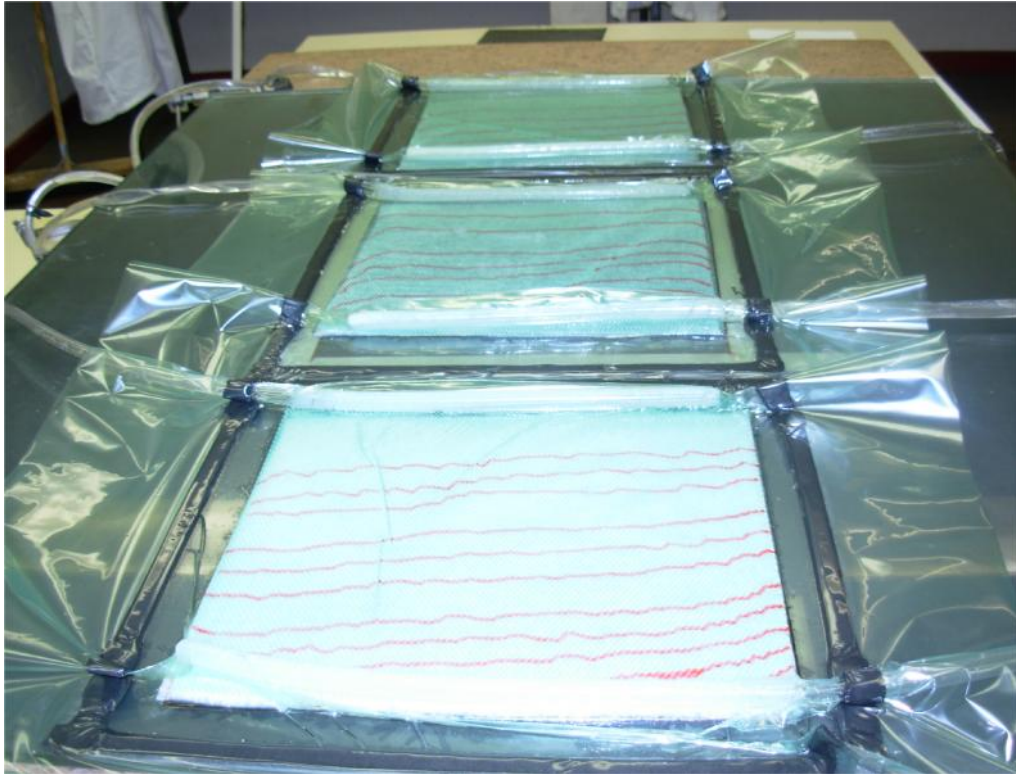


Figure 2.13: Set up with one and two glass moulds

2.9 Results

The composites formed from the resin infusion process were found to be approximately 330 mm long x 330 mm wide x 1.6 mm thick. Their thickness varied according to the number of fabric mats embedded and the surface thickness was found to be uniform across the composite. Following the work of Gomes et al. (2007), the embedded e-glass fibre volume content was determined using the following equation:

$$V_f = 1 - \frac{W - W_f}{\rho_m V} \quad 2.1$$

where W and V are, correspondingly, representing the weight and volume of the fabricated composite. W_f is the weight of e-glass fabric embedded in the composite and ρ_m is the density of the epoxy resin AR 600. In our case, the weight of the e-glass fabrics was found to be approximately 250 g and for the whole composite was found to be approximately 324 g, measured using a Toledo Digital scale. The average volume e-glass fibre content of

fabricated composites was found to be approximately 0.6242. In Appendix A, the calculations for the e-glass fibre content are shown.

2.10 Summary

An experimental investigation was performed to master the manufacturing procedure known as resin infusion in the production of flat composites. A complete resin infused flat plate was manufactured. A summary of the findings are presented below.

2.10.1 A manufacturing procedure has been successfully developed for the production of flat composites.

2.10.2 The tooling for the manufacturing of the composites was set up to facilitate fabrication of flat composite plates. It was found that a glass mould and a vacuum bag can be utilised.

2.10.3 Although a glass mould with sacrificial mats and a vacuum bag were found to be suitable for this application, two glass plates and a vacuum bag were sufficiently adequate in addition to reducing the cost of the mould and lay up time.

2.10.4 A change in flow speed was observed when the sacrificial mat was eliminated. It was found that the average deviation in flow speed is approximately 34.9 % and it is attributed to less resistance to flow.

2.10.5 During processing, the cure cycle for an Epoxy resin AR 600 was found to be a four step cycle presented in figure 2.11. The process displayed a temperature deviation of approximately 1 °C from start to finish of the whole composite manufacturing. It is assumed that thermally induced stresses will be low due to the low temperature deviation.

2.10.6 The composite shows no sign of voids, cracks, matrix rich regions and signs of debonding. The composite is very compact and shows good consolidation. This indicates that vacuum pressure eliminated voids.

2.10.7 Initially, two e-glass fabric mats of 0.15 mm thickness were tested and they were found to provide a laminate thickness of approximately 0.4 mm when embedded in an epoxy resin AR 600.

2.10.8 Subsequently, when ten fabric e-glass mats were laid up, a 1.6 mm thickness composite was achieved.

2.10.9 The flat composites produced when two glass plates were used, have the same surface finish on both sides. However, when one

glass plate and a vacuum bag were used, there were differences in surface finishes.

2.10.10 The average volume of e-glass fibre content of fabricated composite was found to be approximately 0.6242.

2.11 Conclusions

Resin infusion technique in manufacturing flat composite material has been developed. Two fabrication process tools of flat composite plates were examined and it was found that both composite manufacturing tools could be used. Possible range of surface finish was demonstrated. The two glass plates, and one glass plate and a vacuum bag had differences in surface finish. We therefore say that in order to optimise cost and time, two glass moulds and vacuum bag are sufficiently adequate to manufacture composites.

CHAPTER 3

DETERMINE THE PROPERTIES OF FIBRE COMPOSITES LAMINATES WITHOUT NiTi SMAs

3.1 Introduction

The purpose of this chapter is to describe the process of determining the mechanical properties of e-glass fibre composite laminates manufactured to embedding NiTi alloys. This chapter deals with the fabrication of composites consisting of AR 600 epoxy resin mixed with AH 2338 hardener and e-glass fibres. In the past few years, e-glass fibres have made an impact in the South African economy. Toyota South Africa has built centres to manufacture vehicle parts such as canopies out of e-glass fibre. Boat building companies have gained success in the application of e-glass fibres mixed with epoxy resin. In this work, E-glass fibres were used as the best material for composites embedded with NiTi alloys. A unidirectional (UD) e-glass fibre composite was fabricated by resin infusion process (RIP). The e-glass fibre and epoxy resin AR600 together with hardener AH 2338 were prepared to form a composite. The fabrication of the composite was done at room temperature under vacuum created using vacuum bag and pump.

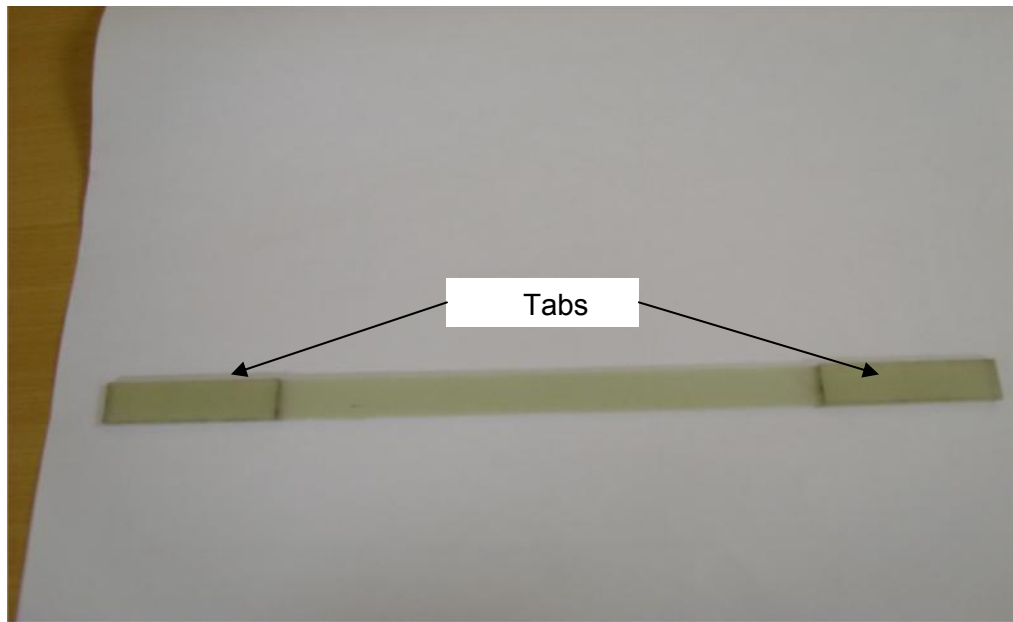
3.2 Problem statement

It was desired to determine the mechanical properties such as tensile strength and stiffness of the manufactured composites.

3.3 Sampling and testing of specimens

The specimens that were manufactured using resin infusion process were left to dry under vacuum conditions at room temperature (23°C) for 24 hours. Thereafter the vacuum was stopped and the specimens were allowed to hard cure for a period of seven days. Specimens were then taken from three different sets of composites made from ten-layer laminates with the e-glass fibres oriented at 0°, 90° and 45°. All the loads on the specimens were applied at 0° (unidirectional) during specimen testing.

The tensile specimen geometry was of rectangular shape with dimensions 250 x 15 x 1.6 mm as detailed in ASTM D 3039/D 3039M - 00¹ standards. E-glass fibre / epoxy AR 600 tabs were employed as material tabs. See figure 3.1 for the tabs position. The tabs were applied to grip specimen to avoid premature failure during the loading of the specimen. The tab material configuration was made to be [0 / 90]. These specimens were cut to size using a diamond cutting blade, as shown in figure 3.2. The specimens were distinguished from one another according to their sample



number.

Figure 3.1: E-glass fibre reinforced / epoxy AR 600 tabs



Figure 3.2: Diamond cutting blades

3.4 Experimental procedure

3.4.1 Tensile test of UD composites specimen

The UD composite tensile tests were carried out for all specimens. There were five specimens prepared for each sample as illustrated in figure 3.3. A specimen without grips was first tested, and the results showed that the specimen failed pre-maturely and outside the gauge length as seen in figure 3.4 (a). Subsequently, emery cloth was used unsuccessfully as the grips were slippery. Finally e-glass reinforced tabs were glued using epoxy AR 600 mixed with hardener AH 2338 on both ends of the specimens as shown in figure 3.4 (c), and were found to be suitable.

The tabs attached to the specimens were cured at room temperature for 24 hrs. The tabs were cut at a 90° angle as recommended by ASTM 3039/D 3039 - 00ε¹. The gauge length of the composite specimens was 150 mm. The strain gauges were attached at the centre of each specimen for measuring longitudinal and transverse strains so that the material's Young modulus could be determined. The resistance of the strain gauges was 120 ohms (Ω) with a gauge factor of 2.075±0.5%. The transverse strain gauges were separated from the longitudinal strain gauges to facilitate easy recording of readings. Figure 3.5 illustrates the strain gauge connections. A quarter bridge connection was chosen as the preferred simplest way of connecting the strain gauges. Tensile tests were conducted for the prepared composite specimens using a Hounsfield - type tensile testing machine as illustrated in figure 3.6. The cross-head speed of the machine was set at 2 mm / min, as recommended in ASTM D. Figure 3.7 illustrates specimen dimensions in mm.

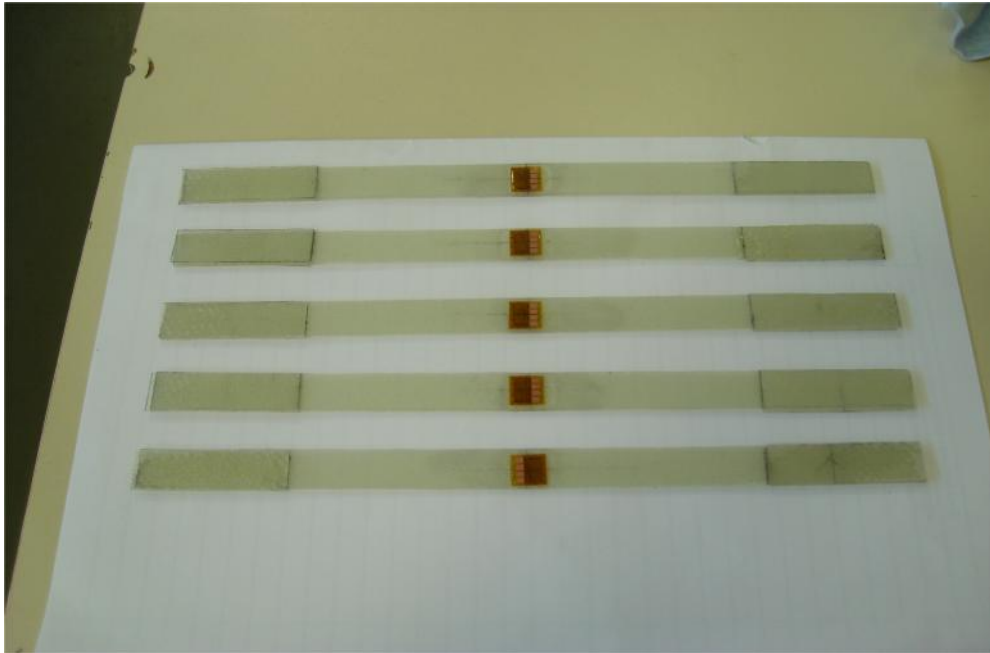


Figure 3.3: Specimens as finally prepared with “tabs”

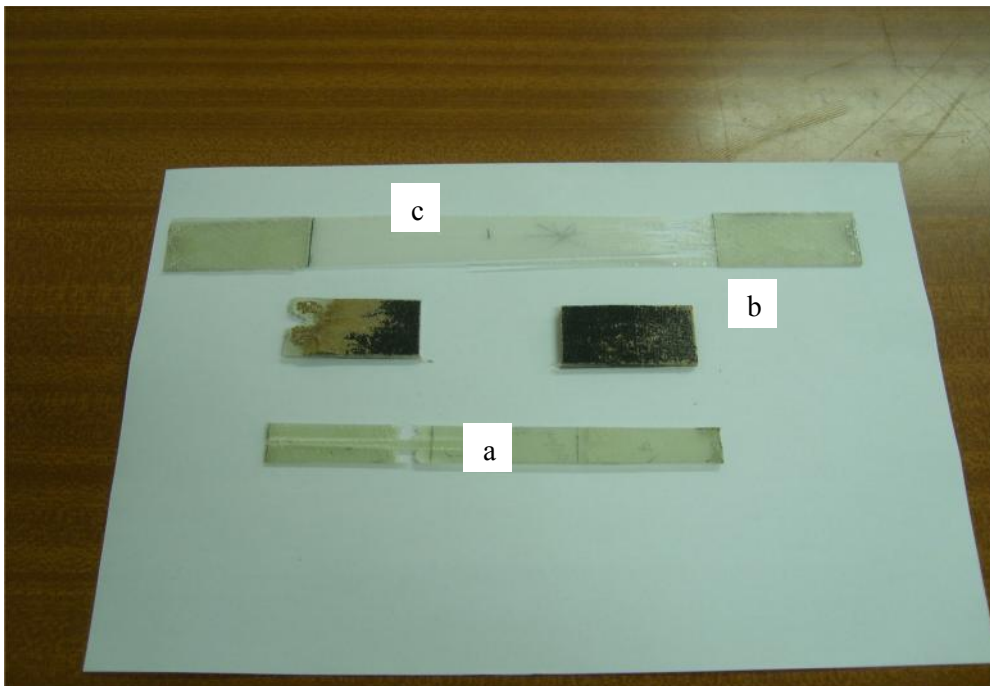


Figure 3.4: Specimens initially tested



Figure 3.5: A quarter bridge strain gauge connection



Figure 3.6: Test specimen secured in the tensile machine's jaws

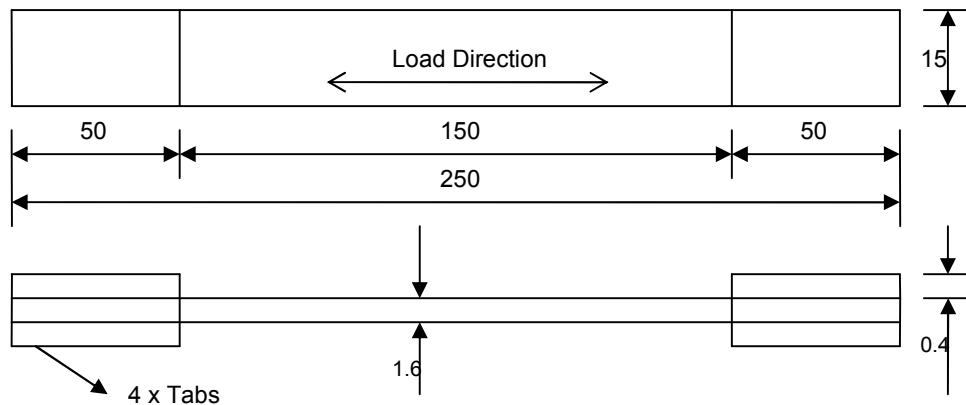


Figure 3.7: Dimensions and geometrical shape of Tensile test specimens.

3.4.2 Fibre orientation

In the experiment, the fibre plies were orientated in three different directions such as 0° , 45° and 90° . This was performed to determine which orientation would give the higher tensile strength and better stiffness properties. The better orientation would enable the embedding of NiTi alloy to the best advantage. All specimens were tested according to the orientations described above with the same loading condition (axial loading).

3.5 Experimental results

3.5.1 Tensile properties of an e-glass / epoxy material with fibre plies orientated at 0°

Table 3.1 shows the results of tensile tests of the e-glass / epoxy composites with fibre plies orientated at 0°, 45 and 90°. All the values shown in the table are average values obtained from the 3 specimens for each orientation.

Table 3.1: Statistics for Engineering Materials Constants

Longitudinal strain ε_1	Orientation	n	\bar{x}	S_{n-1}	CV (%) x 100	Chord Long.
	0°	3	0.0197	0.0108	0.3585	0.0359
	45°	3	0.0023			0.011
	90°	3	0.0002	0.0001	0.0054	0.0004
Transverse strain ε_2	Orientation	n	\bar{x}	S_{n-1}	CV (%) x 100	Chord Trans.
	0°	3	0.0058	0.0031	0.1042	0.0101
	45°	3	0.0041			0.0159
	90°	3	0.0043	0.0036	0.1797	0.0115
Poisson's ratio ν_{12}	Orientation	n	\bar{x}	S_{n-1}	CV (%) x 100	
	0°	3	0.282	0.0052	0.1733	
	45°	3	0.214			
	90°	3	0.0397	0.0230		
Deformation $\Delta l(mm)$	Orientation	n	\bar{x}	S_{n-1}	CV (%) x 100	Max deform
	0°	3	11.07			14.505
	45°	3	6.65			
	90°	3	3.02			6.03
Young's chord modulus E Tensile strength F^{tu}	Orientation	n	E (GPa)	F^{tu} (MPa)	G₁₂ (GPa)	Load_{max} N
	0°	3	17.4	625		15011.67
	45°	3		88.83	3.09	
	90°	3	6.36	72.9		1844

A typical force – deflection diagram of the composite specimens $[0^\circ]_{10}$, is illustrated in figure 3.8. Initially the curve had an exponential form in the range of 0 to 4.14 mm and thereafter for the range of 4.14 to 14.5 mm, the curve behaved linearly. This particular behaviour could be attributed to the fibres initially not properly aligned but as a result of the tensile test they were realigned. It can be assumed that the fibres which were not oriented at 0° had their orientation improved by the tensile loading. Further, a typical graph of stress – strain is illustrated in figure 3.9 and it showed a linear behaviour.

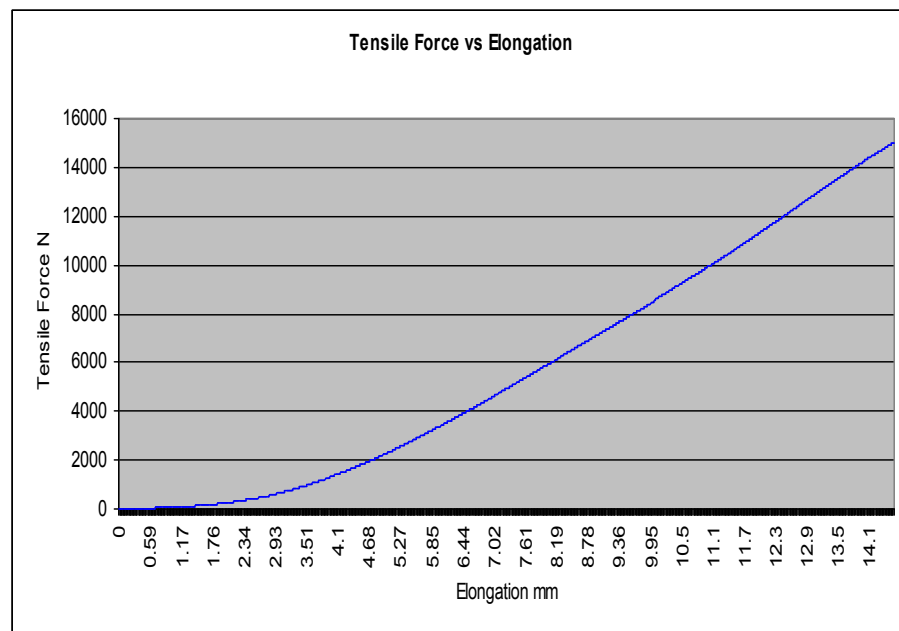


Figure 3.8: Force vs elongation for the 0° fibres oriented specimen

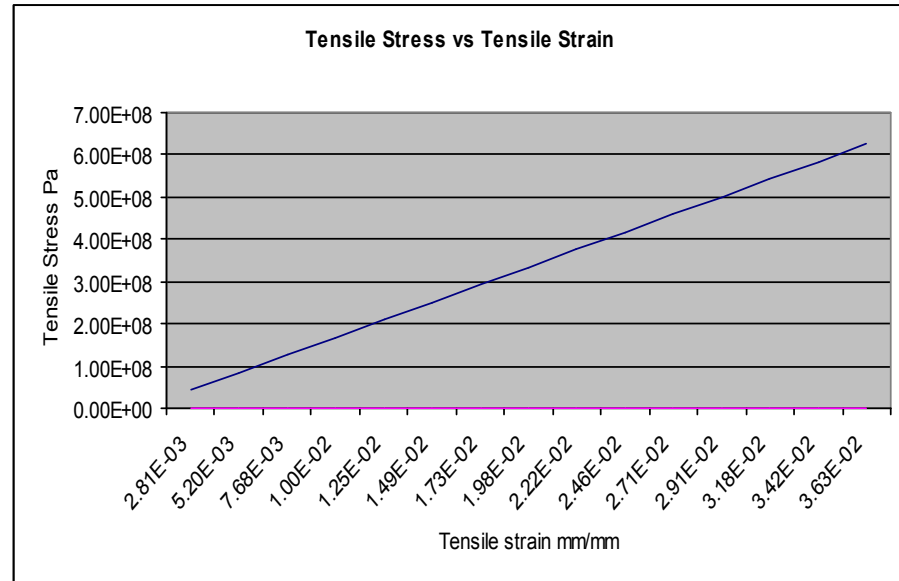


Figure 3.9: Stress-strain graph for the 0° fibre oriented specimen

3.5.2 Axial tensile tests of UD e-glass / epoxy with fibre plies oriented at 45° (Diagonal)

Tensile tests for the 45° oriented fibre specimens were performed under same conditions. The objective of the test was to characterise the shear behaviour of the e-glass / epoxy composite. The tests were conducted using the Hounsfield tensile testing machine with a load cell of 50 kN (model H50KS). The tests were controlled by means of a displacement with a speed of 2 mm/min. Both the load and displacement were recorded using a computer. The specimen behaviour was measured using strain gauges placed in the axial and perpendicular directions. Table 3.1 shows the average values of the results obtained.

In figure 3.10, we see a typical force vs. extension graph for the 45° oriented fibres. At the beginning, the curve had an exponential form in the range of 0 – 5.88 mm. This exponential form was then followed by a linear behaviour of the curve. At approximately 8.09 mm, the curve started to behave non linear forming another exponential form. This non linearity could be associated with the stretching and reorientation of the fibres.

The calculated tensile shear stress (τ_{12}) of the specimens was found to be approximately 83.33 MPa. The shear modulus (G_{12}) was found to be approximately 3.09 GPa. The value of the shear modulus deviated by 39.2% from the one calculated by Paepegem et al. (2005). Yet the specimen failed at a shear stress of 14.79% greater than the one calculated by Paepegem et al. (2005). This simple means that there is an improvement in the composite properties manufactured using RIP.

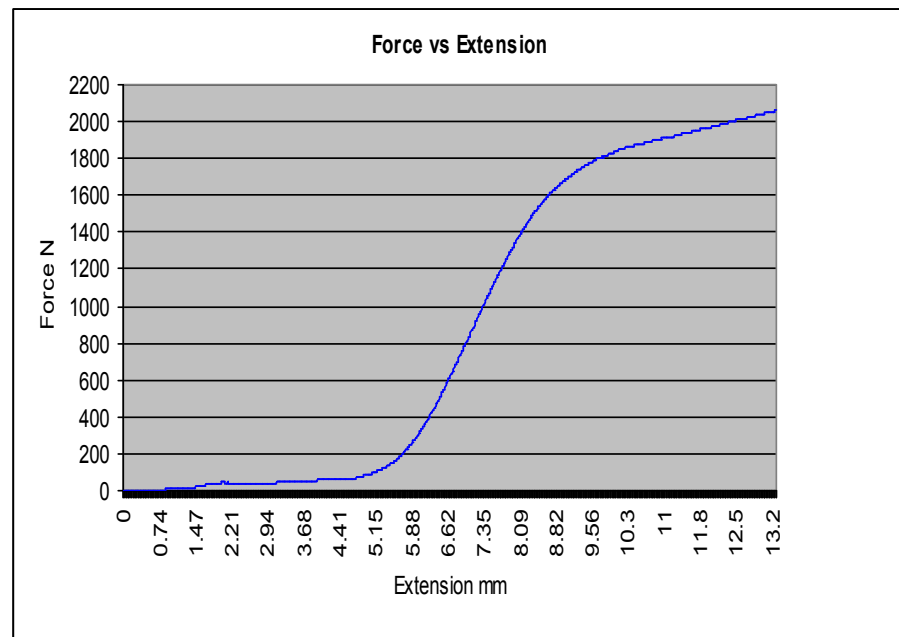


Figure 3.10: Force vs. Extension for the oriented fibres specimens $[45^\circ]_{10s}$

3.5.3 Axial tensile tests of UD e-glass / epoxy with fibre plies oriented at 90° (Perpendicular to the longitudinal axis).

Tensile tests for the 90° oriented fibre specimens were performed under same conditions as those of fibre plies oriented at 0° . Table 3.1 showed the average values of the results obtained. The tensile strength of the specimens was found to be approximately 72.9 MPa. The value was quite lower than that for the fibre plies oriented at 0° and 45° . The value of fracture strains was much lower compared to the fibres oriented at 0° which achieved a fracture strain of 1.97%.

It is observed that the curve behaviour was much similar to the 45° specimen curve except that the exponential form occurred at different extension rates. See figure 3.11.

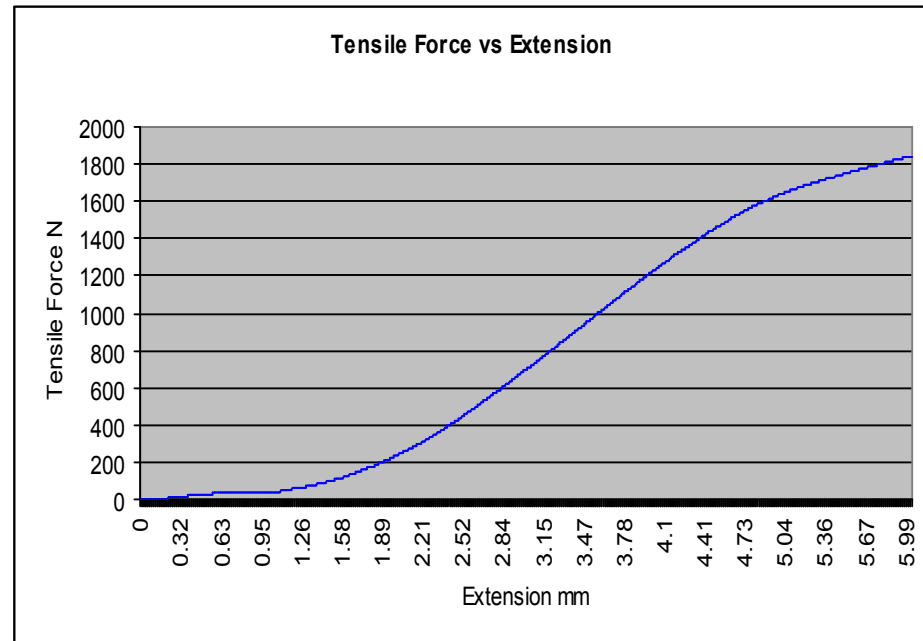


Figure 3.11: Force vs. Extension for the 90° fibre oriented specimens

3.5.4 Morphology of failure of UD e-glass / epoxy reinforced composite specimens oriented at 0°, 45° and 90°.

Morphology of failure of UD e-glass / epoxy (Eg/ep) reinforced composite specimens was conducted to show the difference in failure mode of the specimens oriented as mentioned in the above sub-headings. The two part failure mode codes (SGM and LGM) mentioned in ASTM standards D 3039 / D 3030M - 00¹ were closely followed. The failure mode codes stand for:

S → Long Splitting
 G → Gripp / gage
 M → Multiple areas

L → Lateral
 G → Gage
 M → Middle

Looking in figure 3.12, the specimen had a long, splitting failure between the tabs. The failure occurred in multiple areas along the gauge length in the middle part. The failure analysis was for the specimens with the plies oriented at 0° . Observation of the failure surface of tensile specimen was performed using digital microscopy. Figure 3.13 showed a specimen fractured along the gauge length with fibres showing traces of resin on the surface. This showed good interfacial bond between the material constituents.

The mode of fracture of the tested $[45^\circ]$ e-glass / epoxy specimens is shown in figure 3.14. The failure occurred in the gauge length away from the tabs. It was a shear dominated failure due to the shearing off of the specimens along the 45° fibre direction. In the case of the fibre oriented $[90^\circ]$ e-glass / epoxy specimens, the failure was found to be occurring lateral on the gauge length around the middle of the specimen (LGM). See figure 3.15 for the $[90^\circ]$ tensile test specimen failure. The specimen results indicated that most of the failures occurred at the gauge except the 0° is different.



Figure 3.12: $[0^\circ]$ tensile test specimen failure.

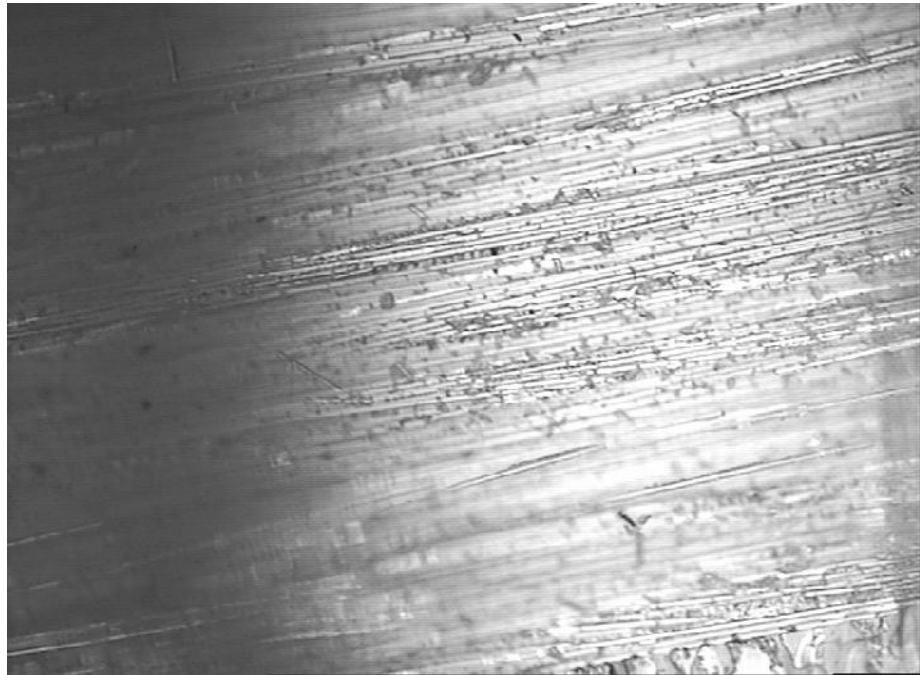


Figure 3.13: Failure surface under tensile load for the UD Eg/ep [0°]

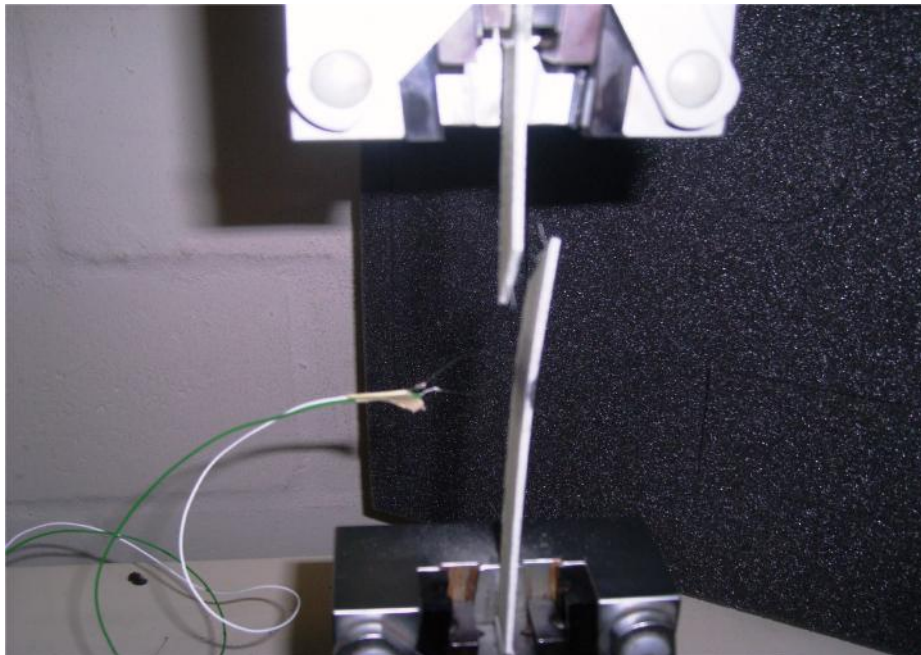


Figure 3.14: [45°] tensile test specimen failure



Figure 3.15: [90°] tensile test specimen failure

3.5.5 Engineering material coefficient of variation analysis

The idea of conducting a material coefficient of variation analysis was to show the variation of each mechanical property as a function of the ply orientation and record the findings. Similar study was done by Gomes et al. (2007) who tested the coefficient of variation of fibre's strength that were alkali treated and those that were untreated. It was found that the variation in fibre strength decreased largely through alkali treatment.

In our case, calculation of the coefficient of variation (CV) was done on longitudinal and transverse strains. According to table 3.1, the coefficient of variation in longitudinal strain at 0° ply was approximately 35.85% while in transverse strain at 90° ply was approximately 17.97%.

3.6 Discussion of the results

The results of the tensile tests showed that the strength for fibres oriented at $[0^\circ]$ was approximately eight times larger than that for the fibres oriented $[90^\circ]$. The average value of deformation was found to be approximately 11.07 mm for fibres oriented at $[0^\circ]$ in comparison to those fibres oriented at $[90^\circ]$ found to be 3.02 mm. The large value of deformation proved that the range of various shapes could be formed when the material was axially oriented.

Looking at figures 3.10 and figure 3.11, the increase in ply angle increased the non-linearity of the graph, and, the tensile strength was reduced as shown in table 3.1. The shear modulus of the composites was determined when the composite plies were oriented at 45° direction. The value of the shear modulus was found to be 3.09 GPa. This value was approximately 22% lower than the one found by Gommers et al., 1998 and Van Paepegem et al., 2005. The value of the shear strength (83.83MPa) shown in table 3.1 was found to be within their experimental range from 65 to 140 MPa.

3.7 Conclusions and Recommendations

3.7.1 With these results, we therefore conclude that laying of the plies at 0° direction would be a suitable methodology for embedding NiTi.

3.7.2 Numerical analysis results are validated using experimental method and small deviations were noted. Yet in order to make possible the practical analysis of these composites, environmental factors such as moisture, UV, etc should be taken into consideration.

3.8 Comments

The surface of this composite material manufactured using the respective RIP system is shown in figure 3.13. The figure simply clarified that fibre arrangement and stacking on the surface of RIP composite system was very good. The good fibre arrangement and stacking was probably attributed to drawing of vacuum from the system. The drawing of vacuum accelerated the elimination of voids and air bubbles between fibre plies. It was also envisaged that stacking of the fibre plies under vacuum conditions promoted the alignment of fibres during processing. Figure 3.13 further illustrated the digital microscopic photograph of cross-sectional area of RIP composite. It was therefore easy to deduce that the reason for the magnitude of that strength level achieved was mainly related to their good fibre longitudinal alignment and stacking arrangement.

Above this, the Young's modulus of the RIP composite material had achieved a value of approximately 17.4 GPa, which was a value similar to Curaua fibre green composites, which had a Young's modulus of 13.4 GPa. The value was further compared to laminate properties arising from wet lay-up with autoclave consolidation and RTM. Abraham et al. (1998) reported that these processes achieved approximately 13.91 GPa (RTM) and 16.36 GPa (autoclave). The fracture strain value of RIP composite had a value of 0.0197 which was comparable to those GRPF such as Epoxide + 70% glass fibres tested by Mathews et al. (1999:40). The fracture strain of GRPFs was 0.0178 which was also less than the RIP composite fracture strain. The value of fracture strain was measured quite accurately using strain gauges placed at the centre of each specimen. Based on the fracture strain achieved by RIP composite laid at 0° with average volume of 62.42%, we could say the fracture strain of this unembedded composite was approximately 1.97 %. Yet, the maximum strain value achieved at 0° was 3.59%.

CHAPTER 4

PREDICTING MATERIAL PROPERTIES USING MICROMECHANICS EQUATIONS AND AN ANSYS SOFTWARE MODEL

4.1 Introduction

The chapter focuses on determining material properties of unidirectional composites using theoretical micromechanics, plane stress equations and finite element analysis. The UD composite is firstly treated as two constituent materials with the axis of reinforced e-glass in the same plane as the axis of loading. The composite is assembled by putting together UD plies of identical material properties with adjacent layers placed above each other and oriented symmetrically with respect to the reference axis. The constitutive governing equations are: the generalised Hooke's law, the Maxwell-Betti reciprocal theorem and the relation between in-plane stresses and strains. The material coefficients are expressed as functions of the material constituents and ply parameters.

Computed composite moduli were evaluated using the data of the constituents and the analytical relations presented by (Beihl, 2000; Hyer, 1998). It was observed that the most significant contribution to the axial stiffness of the composite was made by the e-glass fibre. The calculated theoretical tensile modulus was found to deviate by approximately 30.56 % from the experimentally determined results. The shear modulus was found to deviate by approximately 42.07 % from the experimental results. In addition, the theoretical Poison's ratio was found to be greater than the experimental value with a margin of 4.08 %.

4.2 Problem statement

The purpose of this chapter is intended to predict material properties obtained in the previous chapter using micromechanics equations and an Ansys software model.

4.3 Unidirectional composite laminate

The unidirectional reinforced composite laminate is made up of UD fibre mat embedded in an epoxy resin. A laminate is fabricated from orthotropic layers of UD fibre mat using RIP. The governing equation of the composite laminate is represented by the following stress-strain relation in the fibre local coordinate system:

$$\begin{Bmatrix} \sigma_1 \\ \sigma_2 \\ 0 \\ 0 \\ 0 \\ \tau_{12} \end{Bmatrix} = \begin{bmatrix} Q_{11} & Q_{12} & Q_{13} & 0 & 0 & 0 \\ Q_{12} & Q_{22} & Q_{23} & 0 & 0 & 0 \\ Q_{13} & Q_{23} & Q_{33} & 0 & 0 & 0 \\ 0 & 0 & 0 & Q_{44} & 0 & 0 \\ 0 & 0 & 0 & 0 & Q_{55} & 0 \\ 0 & 0 & 0 & 0 & 0 & Q_{66} \end{bmatrix} \begin{Bmatrix} \varepsilon_1 \\ \varepsilon_2 \\ \varepsilon_3 \\ \gamma_{23} \\ \gamma_{13} \\ \gamma_{12} \end{Bmatrix} \quad (4.1)$$

Note: σ_3 is ignored for each layer and the subscripts 1 and 2 are, both correspondingly, the fibre and the normal to fibre in-plane directions. The subscript 3 is the direction normal to the plate.

The reduced stiffness components, Q_{ij} , are represented in terms of the appropriate engineering constants as:

$$Q_{11} = \frac{E_1}{1 - \nu_{12}\nu_{21}} \quad (4.2)$$

$$Q_{12} = \frac{\nu_{12}E_2}{1 - \nu_{12}\nu_{21}} = \frac{\nu_{21}E_1}{1 - \nu_{12}\nu_{21}} \quad (4.3)$$

$$Q_{22} = \frac{E_2}{1 - \nu_{12}\nu_{21}} \quad (4.4)$$

$$Q_{66} = G_{12} \quad (4.5)$$

Once the expressions for these mentioned engineering constants are evaluated in terms of material and geometric parameters, the composite orthotropic stiffness for any angle can be analysed directly.

4.3.1 Prediction of axial stiffness of UD composite

The prediction of axial stiffness of UD composite (E_1) is based on rule of mixtures models and the equation is represented as

$$E_1 = E_1^f V^f + E^m (1 - V^f) \quad (4.6)$$

where

E_1 is the axial stiffness of UD composite

E_1^f is the fibre Young's modulus

E^m is the epoxy resin Young's modulus

V^f is the fibre volume fraction

The theory assumes the use of the unit cell which is subjected to a stress σ_1 such that the cell stretches in 1 direction, and due to Poisson effects, contracts in the 2 direction. Due to bonding of the fibre and the matrix, the assumption is that these constituents will stretch and contract the same amount in 1 and 2 directions.

4.3.2 Prediction of transverse stiffness of UD composite

The transverse stiffness, E_2 , of a UD composite is also based on the rule of mixtures models and the equation is represented as

$$\frac{1}{E_2} = \frac{V^f}{E_2^f} + \frac{(1 - V^f)}{E^m} \quad (4.7)$$

In this equation, the transverse modulus is a function of the transverse moduli of the fibre and matrix, and the fibre volume fraction. The parameter is derived by considering a unit cell that is subjected to a transverse stress, σ_2 .

4.3.3 Prediction of major Poisson's ratio of UD composite

The major Poisson's ratio, ν_{12} , is computed by considering the overall contraction of the unit cell in the 2 direction. In addition, the rule of mixtures expression for the major poison' ratio is as follows:

$$\nu_{12} = \nu_{12}^f V^f + \nu^m (1 - V^f) \quad (4.8)$$

where

ν_{12} is a major poison's ratio of UD composite

ν_{12}^f is a fibre poison's ratio

ν^m is an epoxy resin poison's ratio

This expression is very similar to the rule of mixtures expression for the modulus E_1 because of the variable linearity's.

4.3.4 Prediction of shear modulus of UD composite

The shear modulus, G_{12} , of a UD composite is derived by looking again to rule-of-mixtures model for E_2 . In this case the fibre and epoxy resin are considered to be subjected to a shear stress, τ_{12} . If truth be told this theory says that the shear stress on the fibre mat has to be equal to the shear stress on the epoxy resin matrix on conditions that the equilibrium conditions hold. The rule-of-mixtures expression for G_{12} is represented as

$$\frac{1}{G_{12}} = \frac{V^f}{G_{12}^f} + \frac{1 - V^f}{G^m} \quad (4.9)$$

Where

G_{12}^f is the shear modulus of the e-glass fibre mat

G^m is the shear modulus of the epoxy resin matrix

4.4 Computing the contribution of material parameters of the constituents to the composite moduli

The contribution of each material or geometric parameter was found out using the above mentioned analytical relations. In case of the composite laminate model, the combination of constituent materials required to produce the best composite was determined using the same analytical relations. In table 4.1 is the data of material constituents that is used to work out the composite material moduli as well as computed moduli ((Beihl, 2000) http://www.rbsbattens.com/tech/physical_prop.cfm).

Table 4.1: Material constituent's data and computed moduli

E_1^f (GPa)	E^m (GPa)	E_2^f (GPa)	V^f	ν_{12}^f	ν_m	G_{12}^f (GPa)	G^m (GPa)
38.6	2.6	10.34	0.2642	0.29	0.3	3.447	1
Computed composite moduli							
E_1 (GPa)		E_2 (GPa)		ν_{12}		G_{12} (GPa)	
25.06		4.88		0.294		1.79	

Observing the computed composite moduli, it was obvious the e-glass fibre made the most significant contribution to the axial stiffness of UD composite E_1 . Similarly, epoxy resin matrix made a contribution to the transverse, E_2 , and diagonal, G_{12} , stiffnesses. These values look reasonable. It was much easier to express the composite moduli as analytical functions of the material parameters, hence the results.

4.5 Comparison of the theoretical predictions to experimental composite moduli measurements

The comparisons between the experimental and theoretical results of the mechanical properties for composite laminates are presented in table 4.2.

Table 4.2: Comparison of the mechanical properties for composite laminates

Material Properties (GPa)	Experimental values	Theoretical values	Deviation (%)
Tensile modulus E_1	17.4	25.06	30.56
Transverse modulus E_2	6.36	4.88	23.27
Shear modulus G_{12}	3.09	1.79	42.07
Poison's ratio ν_{12}	0.282	0.294	4.08

Using the data on table 4.2, calculated theoretical E_1 was found to deviate by 30.56% from the experimental tensile modulus results. The results were understandable since the theoretical material constituent's data applied was obtained from the general mechanical and physical properties of the materials. Similarly with the variation shear modulus, G_{12} theoretical was found to be deviating by 42.07% from the experimental value. The evaluation of Poison's ratio and tensile modulus obtained higher values than those obtained experimentally.

4.6 Finite element simulations

A beam element of 250 mm x 15 mm x 1.6 mm in dimensions is shown in figure 4.1. The beam is loaded axially with a uniform pressure of -625 N/mm^2 . The negative sign showed that the pressure was applied away from the area of the beam. Above, the beam is again made of an e-glass / epoxy composite material with the fibres oriented in the same direction as the applied load.

In this topic, the tensile tests on $[0^\circ]_{10}$ composite laminates are simulated with finite element analysis software (Ansys) where the engineering constants determined experimentally are implemented in the user material subroutine. Since the 0° orientation had significant results for this work, validation of the results is restricted to this direction only.

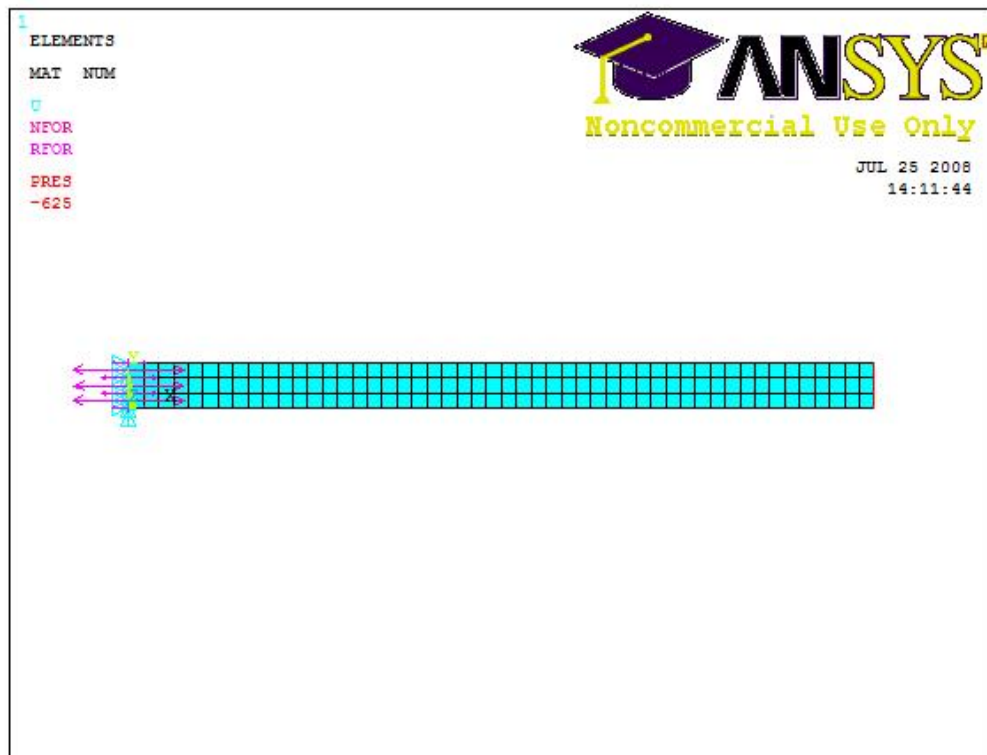


Figure 4.1: Finite element mesh and boundary load application for the $[0^\circ]$ specimen.

4.7 Tensile tests $[0^\circ]_{10}$ specimen results

The finite element mesh and boundary load application for the $[0^\circ]_{10}$ specimen are illustrated in figure 4.1. For the beam of the specified material properties, a plane82 element, which was an 8-node 82 structural type element was chosen. Each lamina was modelled with one element through the thickness. The displacement, u_x , was set at zero along 1 direction which lied in the x-axis while for displacement, u_y , was set at one along 2 direction which lied in the y-axis. Since the effects of slip in the specimen grips were eliminated, the displacement results in the experiments were compared to the simulated results. The simulation was done up to the level of 3.592 % total extensional strain, ε_1 , was reached. The value of total extensional strain corresponded to the ultimate measured value in the experimental results.

The simulated contours for the displacement, u_x , are shown in figure 4.2. The maximum displacement achieved was found to be approximately 8.98 mm. These results were fairly close to the experimental results. The difference was 18.5% lower than the experimental results. Simulated displacement contours are shown at figure 4.2. The lines of constant displacement are parallel with the end grip. As can be seen from figure 4.3, the simulated contours of longitudinal strain ϵ_1 showed a constant value of 0.033727 for the strain in the whole specimen, apart from the area close to the grip. The maximum strain occurs in the vicinity of the constrained part. The fibre ply orientation in the composite laminate is 0° .

The tensile stress σ_1 also showed a constant stress of $601.326 \text{ MN} / \text{mm}^2$ although in the grip vicinity, the stress concentrations did occur. Figure 4.4 presented the simulated contours of tensile stress. However, the transverse stress reached a value of $-16.907 \text{ MN} / \text{mm}^2$ while also still showed maximum transverse stress in the grip vicinity. See figure 4.5 for simulated contours of transverse stress for the $[0^\circ]$ specimen. Again, in this part, the orientation of the fibre ply was kept at 0° .

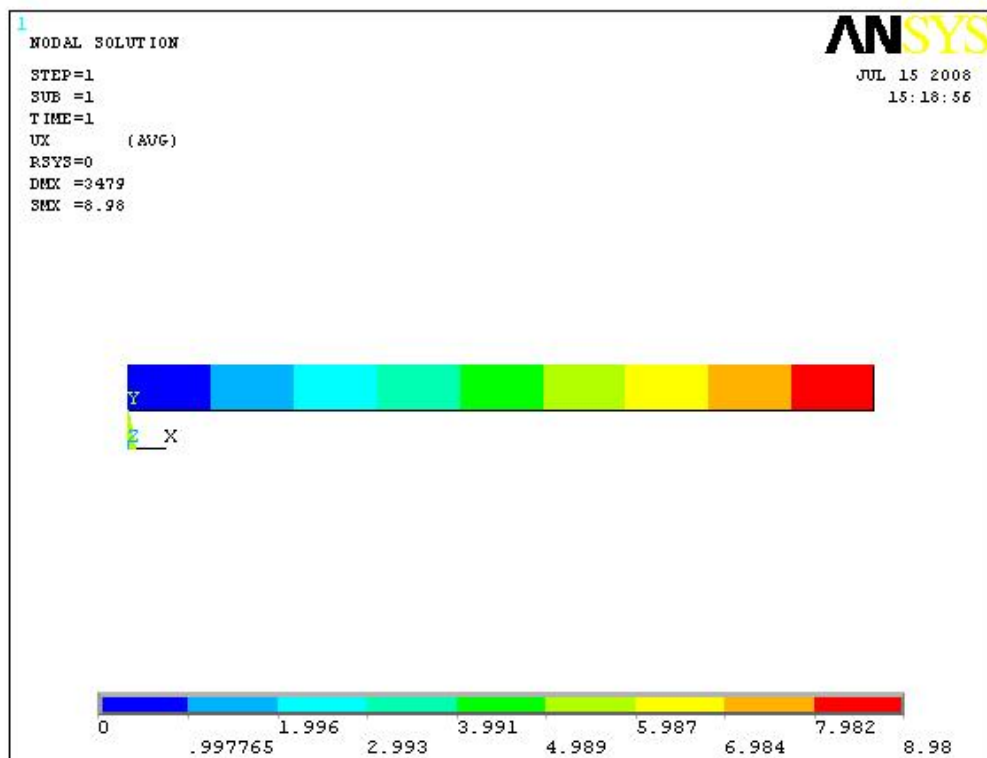


Figure 4.2: Simulated contours of nodal displacement u_x for the $[0^\circ]$ specimen.

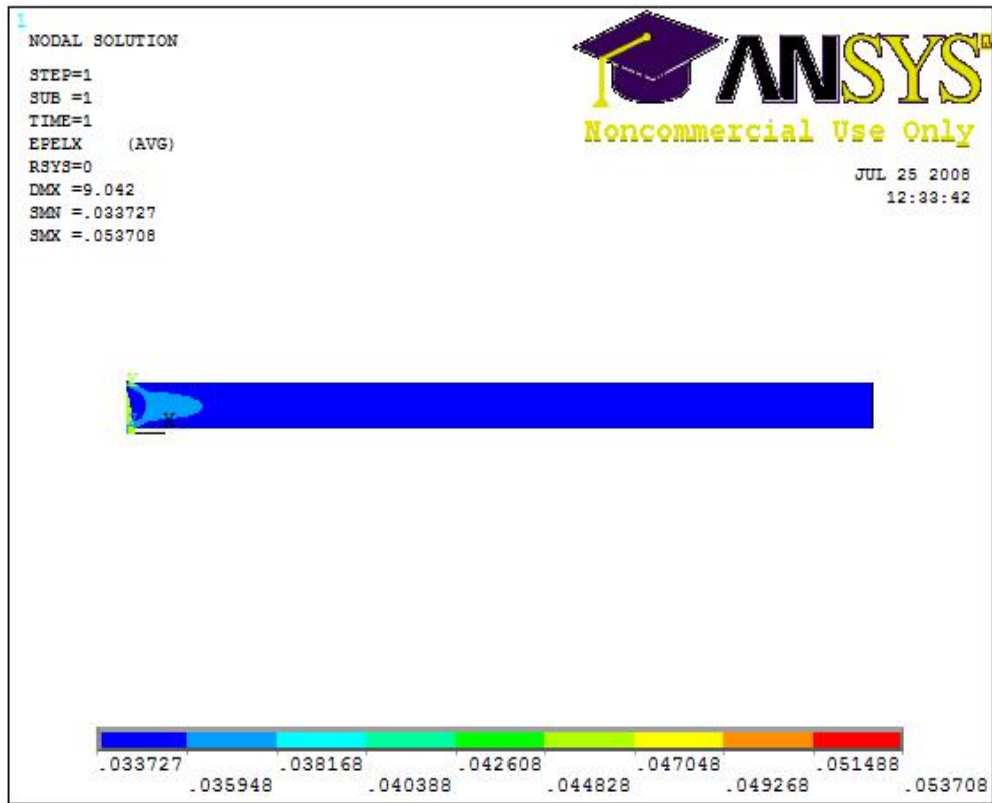


Figure 4.3: Simulated contours of nodal strains for the [0°] specimen.

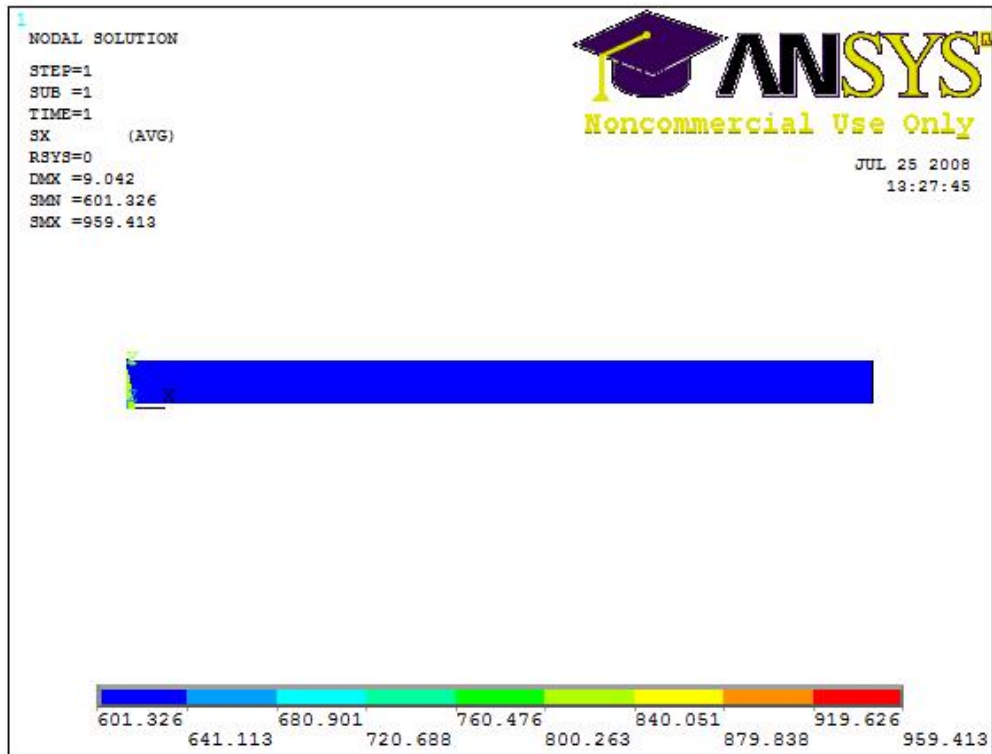


Figure 4.4: Simulated contours of tensile stress σ_1 for the [0°] specimen.

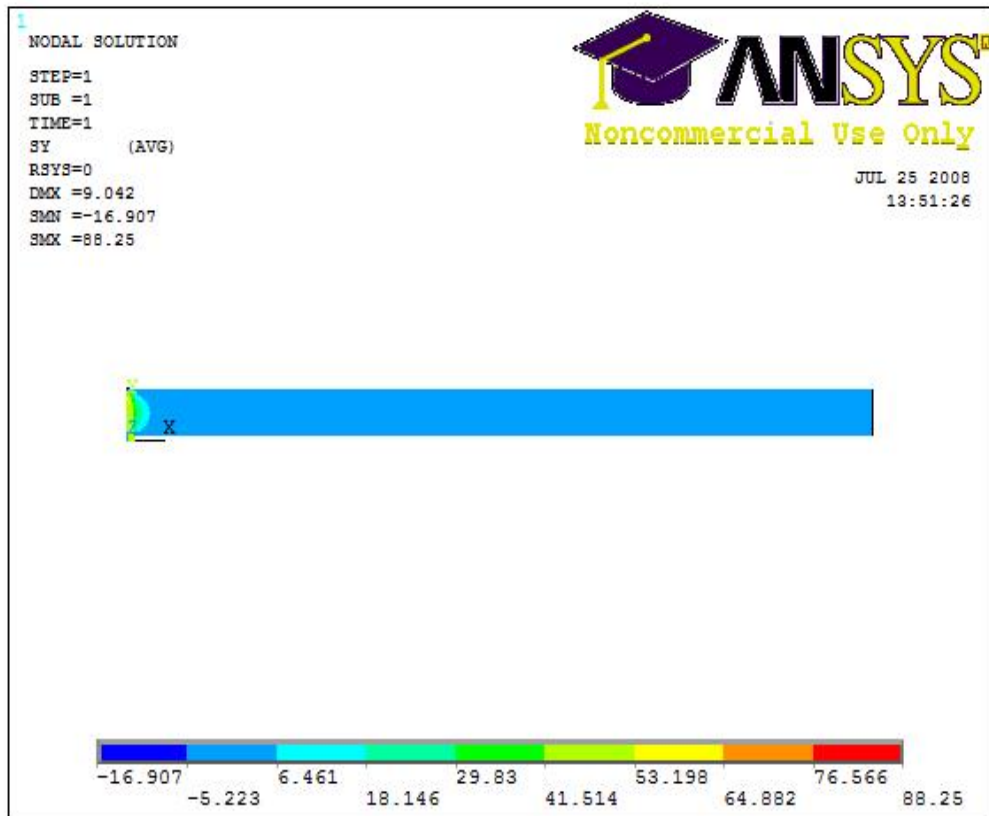


Figure 4.5: Simulated contours of transverse stress for the [0°] specimen.

4.8 Conclusions

- 4.8.1** Computed composite moduli has been evaluated using material constituent's data obtained and analytical relations mentioned above. Through tabulated data in table 4.1, E-glass fibre made the most significant contribution to the axial stiffness of UD composite.
- 4.8.2** Calculated theoretical tensile modulus was found to deviate by approximately 30.56 % from the experimental tensile modulus results. The deviation is attributed to the theoretical material constituent's data obtained from general mechanical and physical properties of the material.
- 4.8.3** The shear modulus was found to deviate by approximately 42.07 % from the experimental results.
- 4.8.4** The theoretical Poisson's ratio is also found to be greater than the value calculated experimentally.
- 4.8.5** The finite element simulations of the tensile tests on E-glass / Epoxy resin laminates [0°] showed a fairly close agreement with the measured experimental displacement and strain results. The difference of experimental displacement to simulated one was found to be approximately 18.5 % lower.
- 4.8.6** The simulated contours of longitudinal strains indicated a constant value of 0.033727 for the strain in the whole specimen, apart from the area close to the grips. The maximum strain was observed in the vicinity of the constrained part.

CHAPTER 5

CHARACTERISING MATERIAL INTERFACE STRENGTH USING THE PULLOUT TEST

5.1 Introduction

The Pull-out test is employed as the best approach in characterising the interface strength of fibre/epoxy material embedded with NiTi SMAs. Interface plays the key part in determining to great extent the properties of a reinforced composite embedded with NiTi SMAs. A reinforced composite consists of epoxy/resin material embedded with NiTi SMAs as an insert. The fibres ensure the strength of the material while the epoxy assists in keeping the shape of the part. NiTi SMAs are embedded in order to increase the material's strength and as a result their application requires transfer of strain from the wire to the reinforced fibre/epoxy material. Thus, the interface is a key element of the reinforced composite embedded with NiTi SMAs.

Zhandarov et al. (2004) describes four structural levels such as (molecular, micro, meso and macro) of analysing reinforced composite materials. In this chapter, micro analysis of the interface is employed as a technique to characterise fibre/epoxy material embedded with NiTi SMAs. The technique considers the selection of parameters such as debond strength, debond force, displacement, as well as the pull-out test, as a micro mechanical test for the interface characterisation.

The objective of this chapter is to present a procedure of characterising the interfacial strength and evaluating interfacial properties in fibre/epoxy material embedded with NiTi SMAs.

5.2 Selected Materials

A commercially available unidirectional (UD) reinforced material (E-glass), 220 grams (g) fabric, was bought from Aerontec cc, Kenilworth, Cape Town. The fabrics are wetted with epoxy resin AR 600, covered in unidirectional stacking order, cured under vacuum pressure at room temperature of ± 24 °C. This process is applied because of its exceptional advantages such as reduction of resin rich laminates, elimination of voids, etc. The fabrication is completed by hard curing the material at room temperature (± 24 °C) for a period of 5 to 7 days. These are the recommendations from the supplier, Aerontec. The hard curing of the laminate specimens at room temperature would influence the microstructure, elastic moduli and the shear strength. Some properties of unembedded composites were presented in table 3.1 of chapter 3. NiTi shape memory alloy wire of 1 mm diameter (Φ) is employed as the element to be pulled-out from the reinforced e-glass / epoxy resin laminate. The SMA material was bought from Johnson Matthey (supplier) in USA. Table 5.1 below presents the material data for the NiTi SMA.

Table 5.1: NiTi SMA material data

Diameter(mm)	Chemical Composition					Temper	Surface	Active A_f (°c)
	Ni	Ti	C	O	All others			
1	55.32	44.67	≤ 0.05	≤ 0.05	0.20	Straight annealed	Oxide	60.7
All others are: Al, Co, Cr, Cu, Fe, Mn, Mo, Nb, Si, W								

5.3 Specimen preparation

Specimens for the pull-out tests were initially cut to a length of 125 mm. The length was chosen so that the first 50 mm length is embedded in the e-glass / epoxy resin laminate while at the same time the next 50 mm length is chosen as a free length. The free length is compensated to allow measuring the extension of the specimen during loading. In addition, a 25 mm length is chosen to place the grips during testing. See figure 5.1 for a pullout test schematic of test specimens. Nine specimens were dipped into ethanol 98% solution to remove surface impurities and oils. These specimens grouped into three and each group was composed of three samples. The samples were grouped as follows:

5.3.1 Untreated NiTi specimens.

5.3.2 Corroded NiTi specimens, and

5.3.3 Hand sanded NiTi specimens.

Hand sanded samples were prepared by sanding the wires for about 15 passes with a 600 grit sandpaper. During the process of hand-sanding, the grooves were made axially to the surface of the NiTi rod wire. Corroded specimens were dipped into nitric acid 2% solution for 5 minutes.

The samples were placed in the heating furnace for the duration of 10 hours after preparation. The temperature of the furnace was set to 230 °C. Thereafter they were taken out and cooled at room temperature. Masking tape was applied over 75 mm length to facilitate the alignment of the wires to the laminate, prevent wetting of the entire wire as well as facilitate the cutting of the specimen into size. See figure 5.2 for the application of masking tape.

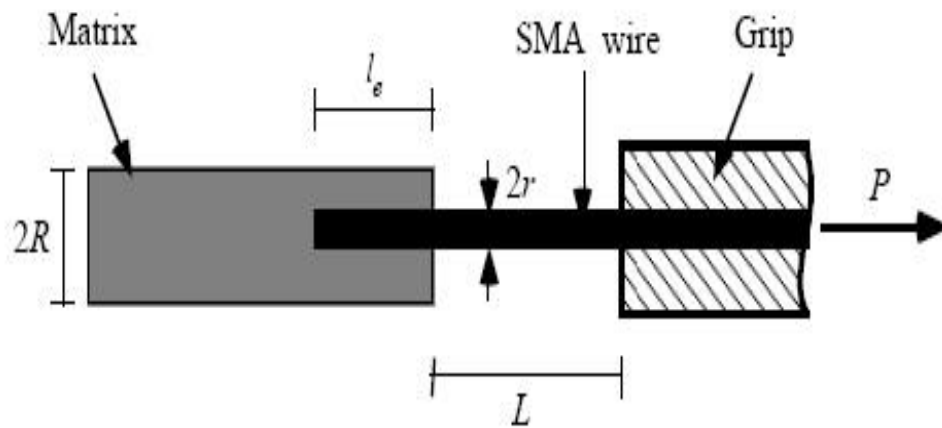


Figure 5.1: A pullout test schematic of test specimens



Figure 5.2: Masking tape application

The samples were fabricated using the resin infusion process. The wires were placed in the centre of the composite plies to achieve symmetry of the composite laminate. After putting the wires in between the plies, the vacuum bag was placed over the mould tool to create vacuum. See figure 5.3 for vacuum application. Once vacuum was achieved, infusion was initiated while the pump kept running for approximately 1 - 2 hours. The samples were cured for 24 hours subsequently for 5 days. Three flat specimens were cut out of 1.6 mm thick plates embedded with one rod of NiTi alloys. These flat specimens are cut out to the specimen geometry using a diamond cutting blade.

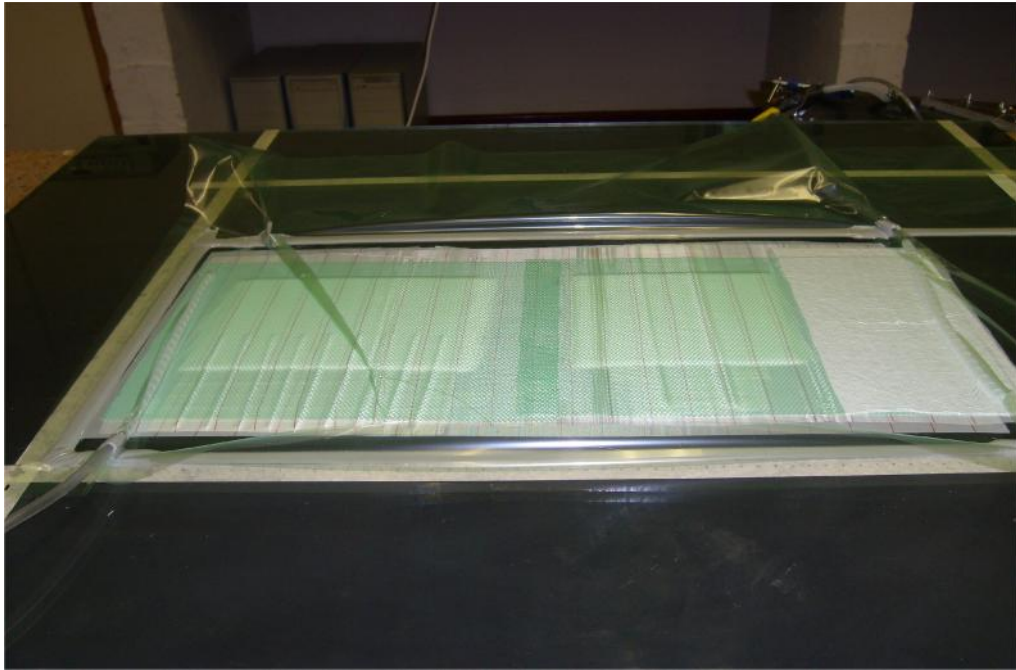


Figure 5.3: Vacuum application

NiTi rod wires have the composition of 55.32 % nickel and 44.67 % titanium. An austenite start temperature A_s for 1 mm diameter wire was 51.1 °C and an austenite finish temperature A_f was 60.7 °C. Above that the value for martensite finish temperature M_f is found to be 36.2 °C. A comparison is done on untreated surface specimens to treated surface specimens.

5.4 Effect of surface treatments

The effect of surface treatments would be modelled using Miller's model et al. (1986). This would be achieved by a single rod pullout test using an Instron tensile testing machine with a crosshead speed of 1 mm/min. A typical force-displacement curve was plotted as shown in figure 5.4. Miller et al. (1986) assumed that the shear strength of the bond can be determined assuming negligible frictional effects using the expression,

$$\tau = \frac{F_p}{\pi D l_e}, \quad (5.1)$$

where τ = apparent interfacial shear strength, F_p = the pullout force, D = the NiTi alloy diameter and l_e = NiTi alloy embedded length. The assumption of negligible friction allows the determination of the bond strength reliability and the calculation of the efficiency of the NiTi / host matrix bond. In a subsequent work by Zhandarov and Mäder (2004), the pullout force F_p or debond force F_d were related to the ultimate interfacial shear strength τ_d by

$$\tau_d = \frac{F_d \beta}{\pi d_f} \coth(\beta l_e) + \tau_T \tanh \frac{\beta l_e}{2} \quad (5.2)$$

where β is a shear lag parameter found using the Nayfeh (1977) model, and τ_T is the stress term due to thermal shrinkage. Also in this case interfacial friction was ignored.

Penn and Lee (1989) modelled the debond force using energy-controlled debonding, which in terms of the interfacial work of fracture G_i was expressed as

$$F_d = 2\pi r^2 \sqrt{\frac{E_f G_i}{r \tanh(ns)}} \quad (5.3)$$

Where E_f = fibre elastic modulus, r = pullout fibre radius, R_1 = radial extent of the shear stress in the matrix, n = fraction of the fibre interface length debonded and s = dimensionless parameter for embedded length.

$$n^2 = \frac{E_m}{E_f (1 + \nu_m) \ln\left(\frac{R_1}{r}\right)} \quad (5.4)$$

$$\text{and } s = \frac{l_e}{r} \quad (5.5)$$

Then interfacial shear strength can be expressed as

$$\tau_d = n \sqrt{\frac{E_f G_i}{r}} \quad (5.6)$$

The material properties were taken from the tensile test conducted as fibre elastic modulus (E_f), matrix elastic modulus (E_m), fibre Poisson's ratio (ν_f) and matrix Poisson's ratio (ν_m). For simplicity of material interfacial strength calculation, the debond stress would be calculated from equation (5.1) using the average pullout force for each of the surface treatments.

5.5 Experimental procedure for the pullout tests

The objective of this work is to measure the interfacial bond strength of SMAs in reinforced composite material. All specimens were subjected to the same procedure. The pullout tests were performed with an Instron machine using a cross-head speed of 1 mm/min.

5.6 Experimental results

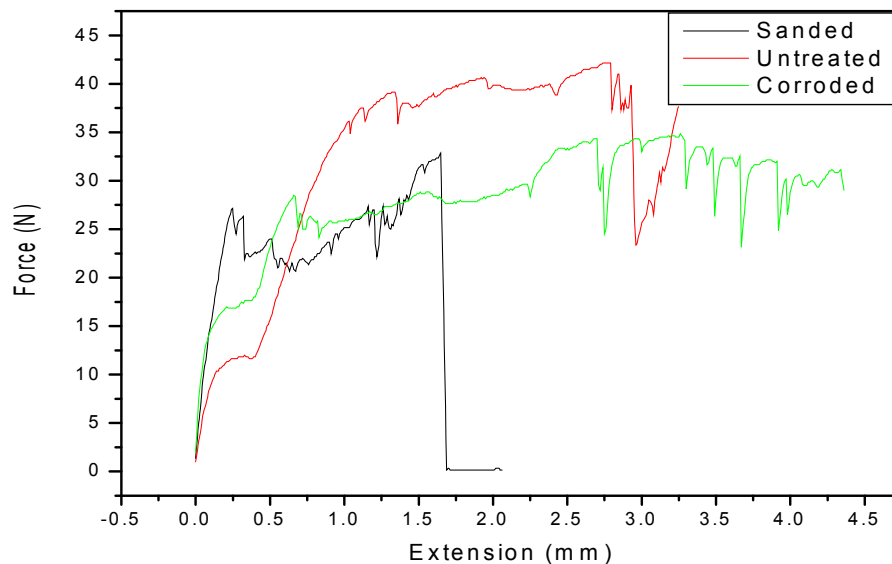


Figure 5.4: Typical force - extension curves for tested specimens

5.6.1 Hand sanded specimens

Using the Instron tensile testing machine, typical load vs. extension graphs were obtained as the one shown in figure 5.4. The nearly linear elastic region for these specimens starts at approximately (0.028 mm, 6N) and terminates at approximately (0.232 mm, 26.5 N) point. Point (0.232 mm, 26.5 N) shows the start of continuation of debonding until point (1.64 mm, 32.65N) is reached. At (1.64 mm, 32.65N), interfacial debonding occurs through to one end of the specimen. During the interfacial debonding process from 26.5 N to 32.65 N, interfacial friction plays a role on the waste of energy. It is noted that in this graph, point (1.64 mm, 32.65N) represents the maximum extension and load the NiTi carried during debonding process. Again, the point signifies complete debond. After the interfacial debond is completed, a drop in load is observed. A drop in load is shown as a vertical line from 32.65 N to 0.15 N. At this point (2.06 mm, 0.15 N), a steady frictional sliding is actually noticed.

5.6.2 Corroded specimen

For these specimens, the first kink occurred at (0.185 mm, 16.6 N) as presented in figure 5.4. It is noted that the kink was caused by sliding of the specimen grips. From point (0.185 mm, 16.6 N) to (0.385 mm, 17.8 N), there is uniform frictional force. This could be due to Poisson's contraction of the SMA. The point that illustrates the beginning of interfacial debonding of the embedded material is (0.65 mm, 28.15 N). From (0.65 mm, 28.15 N) to (2.695 mm, 34.35 N), the curve indicates the continuation of interfacial debonding until the specimen gives up some of the energy used. After (2.695 mm, 34.85 N), a steady drop in load is observed. This situation is attributed to the entire length of debonded NiTi contributing to the interfacial friction.

5.6.3 Untreated specimen

These specimens exhibited the first kink at point (0.2 mm, 11.15 N) illustrating the sliding of the specimen grips. A typical load vs. extension graph is also presented in figure 5.4. From point (0.2 mm, 11.15 N) to point (0.404 mm, 12 N), the curve remains constant in terms of applied load. Point (0.93mm, 33.83N) signifies the start of interfacial debonding of the specimen. Again, from (0.93 mm, 38.83 N) to point (2.78 mm, 42.15 N), the interfacial debonding occurred along the NiTi length until the NiTi is separated through one end of the specimen. Thereafter the specimen shows a complete interfacial debonding. Although there is complete interfacial debonding along the NiTi SMA, it was observed that the behaviour of the curve did show load increments. This again is attributed to the entire length of interfacial NiTi alloy contributing to the interfacial friction. Further it can be associated with the alignment of the embedded element, hence, a load increase after a sudden drop.

5.7 Discussion of the results

A pull-out test technique aimed at determining maximum debonding force and apparent interfacial shear strength (IFSS) parameters was applied. The results of the pullout tests showed that the debond stress was greater on the untreated SMA samples than the corroded and the hand sanded SMA samples. This is illustrated in figure 5.5 and figure 5.6. We can therefore say that the untreated samples have good adhesion with the e-glass/epoxy resin laminate.

Apparent IFSS (τ_{app}) is a parameter employed to characterise the quality of interfacial bonding. The parameter is calculated using the maximum debonding force equation in equation 5.1. Figure 5.7 presents a typical plot of apparent interfacial shear strength versus the embedded length. The experimental data shows that an apparent IFSS will only increase if the magnitude of the embedded length is reduced and vice versa. At approximately zero magnitude of embedded length, it is shown that the

magnitude of apparent IFSS was approximately 0.268MPa. This is also justified by theoretical equation developed by Miller et al. (1986).

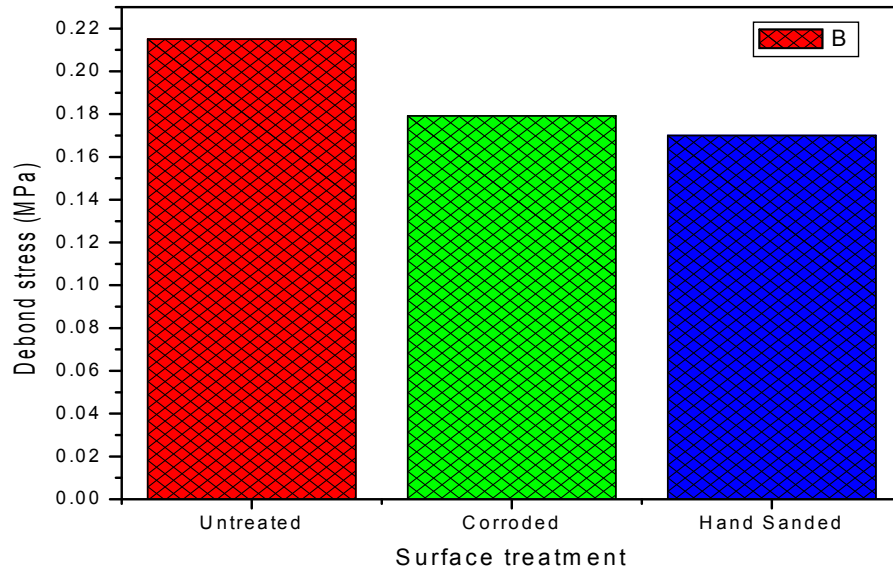


Figure 5.5: Difference in initial debond stress of various surface treatment cases

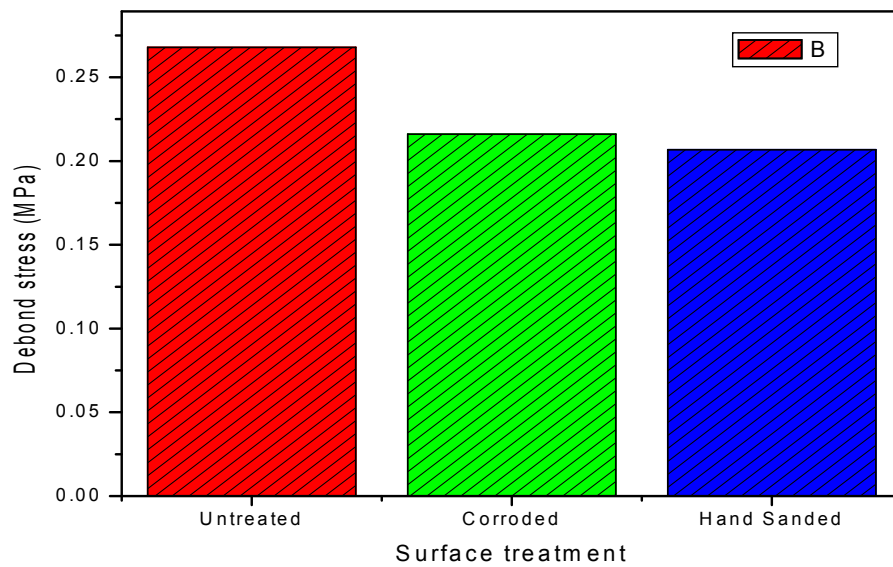


Figure 5.6: Difference in final debond stress of various surface treatment cases

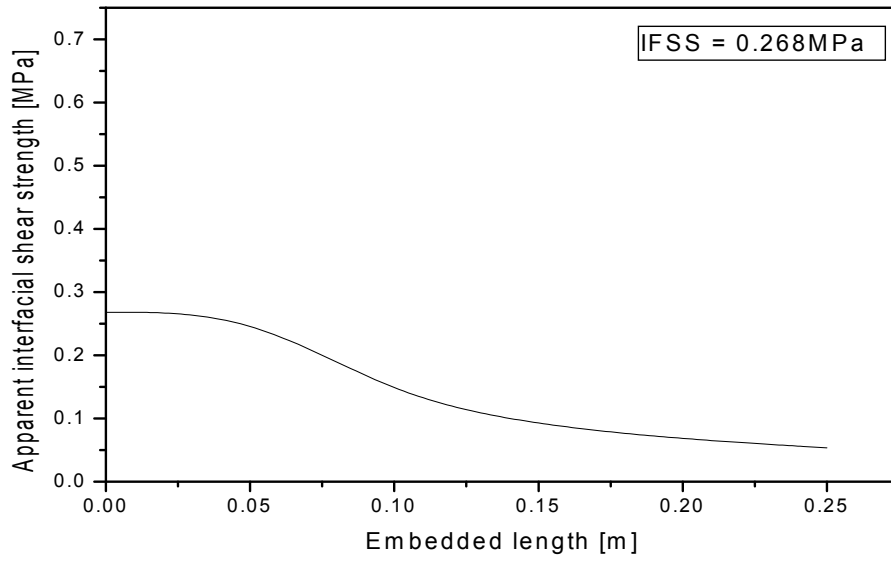


Figure 5.7: Apparent IFSS plotted as a function of embedded length

5.8 Conclusions

The interfacial bond strength on different surface treatments was investigated using the standard pullout test. The desirable properties for this application were to achieve maximum adhesion and hence maximum load. A maximum adhesion would provide a better structural integrity of the final composite laminate embedded with NiTi SMAs.

- 5.8.1** Hand sanding of the wires as a surface treatment resulted in an initial decrease of debond stress while corroded and untreated wires showed an initial increase in debond stress.
- 5.8.2** Although the first kinks in the load extension curve occurred earlier for corroded and untreated wires, the debond force was found to be greater than the sanded specimens. The first kinks were attributed to grip slippage.
- 5.8.3** Untreated wires exhibited the highest interfacial debond stress of approximately 0.268 MPa. The recorded maximum debond force was found to be approximately 42.15N at an extension of 2.78mm.
- 5.8.4** Hand sanded wires had lower interfacial debond stress of approximately 0.207 MPa. The recorded maximum debond force was found to be approximately 32.65N at an extension of 1.65mm.
- 5.8.5** The corroded wires exhibited an interfacial debond stress of approximately 0.216 MPa with a maximum debond force of approximately 34.85N at an extension of 2.695mm.

5.9 Recommendations

The use of double sided mould would avoid profiling of the specimen and would eliminate high stress concentrations. There is a possibility that the laminate is resin rich at the bottom than at the top. Thus, two sided moulds might improve the surface structure as well as reduce stress concentrations around the wires. It is important to investigate the local stresses induced in the reinforced laminate by means of actuating the SMA wire. Since the sliding effect is noticed in both untreated and corroded specimens, it is therefore recommended that proper wire specimen grips be utilised.

CHAPTER 6

THE MECHANICAL BEHAVIOUR OF SMA WIRES

6.1 Introduction

This chapter describes the experiments on the mechanical behaviour of SMA wires. The purpose of the experiment is to confirm the following key features of the NiTi SMA mechanical behaviour:

- 6.1.1** The loading behaviour of the NiTi SMA based upon alloy percentages available on the material at ambient and
- 6.1.2** at elevated temperatures.

The results would lead to determine an actuating force.

6.2 SMA selection

SMA's are metallic alloys that exhibit the shape memory effect upon deformation. The shape memory effect begins either by application of load where large strains are generated or upon the application of heat where the original geometrical shape of the structure is fully recovered.

The generation of recovery stresses by prestrained SMA elements upon heating is the direct result of their unusual thermo-mechanical behaviour. Therefore the selection of proper material constituents is crucial for obtaining the best functional behaviour. In this work, Nitinol (NiTi) was selected as it exhibits the shape memory effect, with notable stability during long term loading. In addition, this material has shown dependence on the activation temperature, initial deformation as well as the presence of the martensite percentages in the material.

6.3 Experimental procedure

The experiment consisted of using 1 mm diameter, NiTi wire. Four NiTi wires were cut into 250 mm length. The specimens were surface cleaned using ethanol. Three of these specimens were put into a temperature controlled furnace for conditioning. The temperature in the furnace was set to 230°C. The specimens were kept inside the furnace for a period of 10 hours to refine their grain structure. The specimens were taken out to cool down at room temperature. The fourth specimen was rigged into a tensile testing machine as presented in figure 6.1.

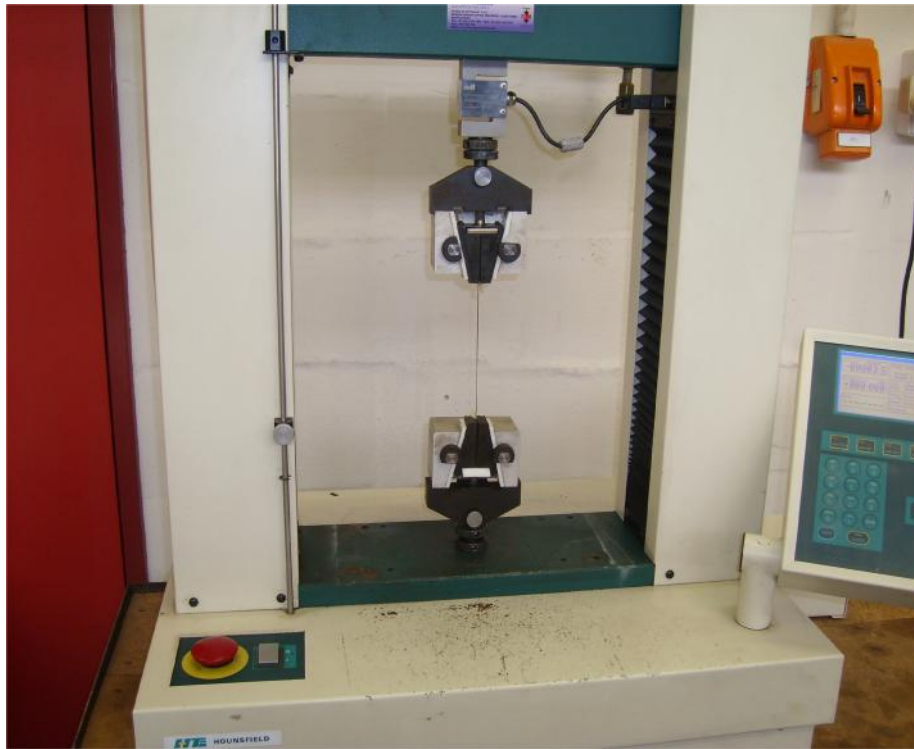


Figure 6.1: NiTi SMA attached to the crosshead of the tensile testing machine.

The tensile testing machine was equipped with a load cell of 5 kN. One end (about 25 mm) of the NiTi wire specimen was fastened with the clamp and attached to the fixed end of the tensile testing machine. The other end was attached to the machine's movable crosshead. Firstly, the wire specimens were loaded with approximately ± 120 N to achieve both twinned and detwinned martensite shapes. The displacement rate of the machine was set at 1 mm/min. Figure 6.2 shows the path taken by NiTi specimens on a martensite load – extension graph.

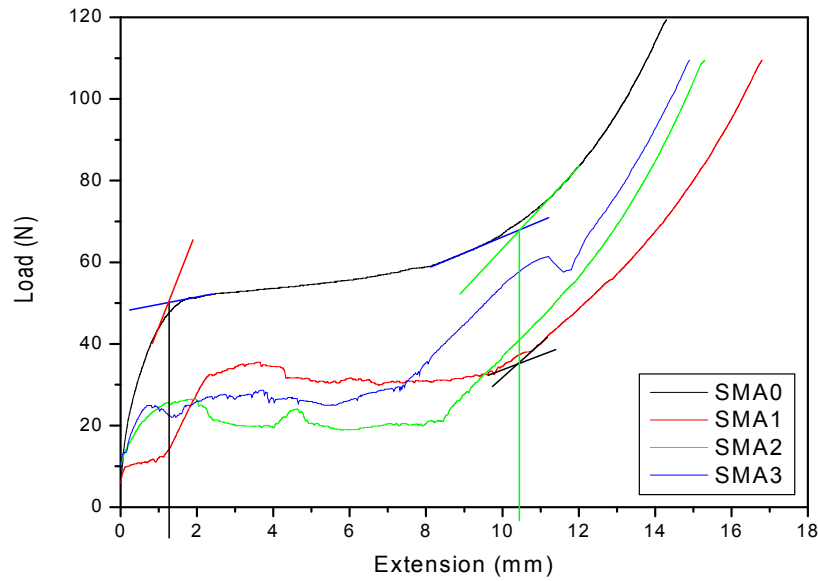


Figure 6.2: Martensite load – extension curve showing loading profile for the four specimens.

6.4 Characteristics of the NiTi SMA specimens at ambient temperature

Figure 6.2 presents the martensite load – extension graph of all specimens. Specimen SMA0 was formed with three different phases. The first phase occurred when the material extended from 0 to 1,25 mm. At that particular point, it was observed that the load was approximately 50 N. The material is said to be in the twinned martensite phase. This is a region where the first yield load point takes place. After this yield load point, the material begins to detwin and as a result there was a combination of twinned and detwinned martensite phases in the specimen. The second yield load point takes place at approximately 10,4 mm of extension with the load approximately 68 N. At this yield load point, the material is fully detwinned. At this phase, as reported by Pai (2007), atomic bonds that form a rhombic structure are stretched. Wie (1998) explained that when subjecting a material in the martensite state to an applied load, the variants underwent a self-accommodating pattern of shear-induced shrinkage, growth and reorientation by detwinning, resulting in twinned–induced inelastic strains.

Based on the current behaviour of the graph, it is noticed that when the material is fully twinned martensite, it experiences elastic unloading conditions. Yet, when the material is fully detwinned martensite, it does not experience the same elastic unloading conditions as mentioned before. The material's Young modulus is quite different from the one in the first phase. Again, where the material is a combination of twinned and detwinned martensite, the material experiences a Young's modulus which is proportional to the fraction of twinned and detwinned martensite available at the unloading point. It is observed that the material experiences a residual strain upon unloading. With the application of heat, the residual strain would be recovered. In addition, the transformation line of the curve is not a horizontal line and this perhaps may be attributed to un-conditioned specimen.

Looking at the martensite load - extension graph of SMA1, it is noticed that the material starts to experience the load initiation at 1.25 mm extension. This can be attributed to the fact that the material is not pre-strained as was the case for SMA2 and SMA3. From 1.25 mm to 2.3 mm, the material shows a twinned martensite phase as the load-extension relationship is linear and elastic. From 2.3 mm to 10.4 mm, the material shows the combination of twinned and detwinned martensite phases. Observations indicate that the martensite load-extension for the SMA1 specimen obtained a yield load of approximately 35 N in comparison to 68 N of the SMA0 specimens. This can be attributed to conditioning of the SMA1 specimen.

Considering both un-conditioned and conditioned SMAs (SMA0 and SMA1), the shape of loading curve tends to take the same profile but differs in terms of material properties. The arrangement of the twinned and detwinned layers influences the properties of the material. This is indicated by a difference in the loading results data shown in table 6.1. The results are quite significant because they show that an increase in applied load results in an increase in yield stress. Yet, the material's Young's modulus decreases while the material's strain increases correspondingly. Although there is similarity in these two mentioned specimens, the magnitude of their properties is quite different. This could be attributed to the way of

conditioning the material. The difference is demonstrated by the inclination of the SMA0 curve and the flat SMA1 curve in figure 6.2.

Table 6.1: Properties of SMA 0 and SMA 1 at ambient temperature (Gauge length = 150 mm)

Specimen Description	Load (P) N	Tensile Yield Stress (σ) MPa	Young's modulus (E) GPa	Tensile Yield Strain (ϵ) mm/mm	Phase type (Martensite)
SMA0	50	63,66	12,73	0,005	Twinned
	68	86,59	2,08	0,0416	Detwinned
	59	75,12	2,29	0,0328	Combined
SMA1	32	40,74	4,35	0,00936	Twinned
	35	44,56	1,07	0,0416	Detwinned
	33,5	42,65	1,09	0,03912	Combined

6.5 Characterisation of the NiTi SMA specimens at elevated temperature (115°C)

The NiTi SMA element was activated through an elevated temperature of approximately 115°C. The effect was simulated in figure 6.3 by electrically activating the NiTi SMA through resistive heating. Turner (2000) described the advantages of the methodology as: simple operation, relatively uniform heating, good control as well as easy operation. Experiments are conducted on fully annealed specimens to determine the baseline mechanical properties of the material. In addition, these experiments are performed to quantify the material properties as function of temperature. The tests are performed on a 1 mm diameter NiTi rod element, 250 mm long.

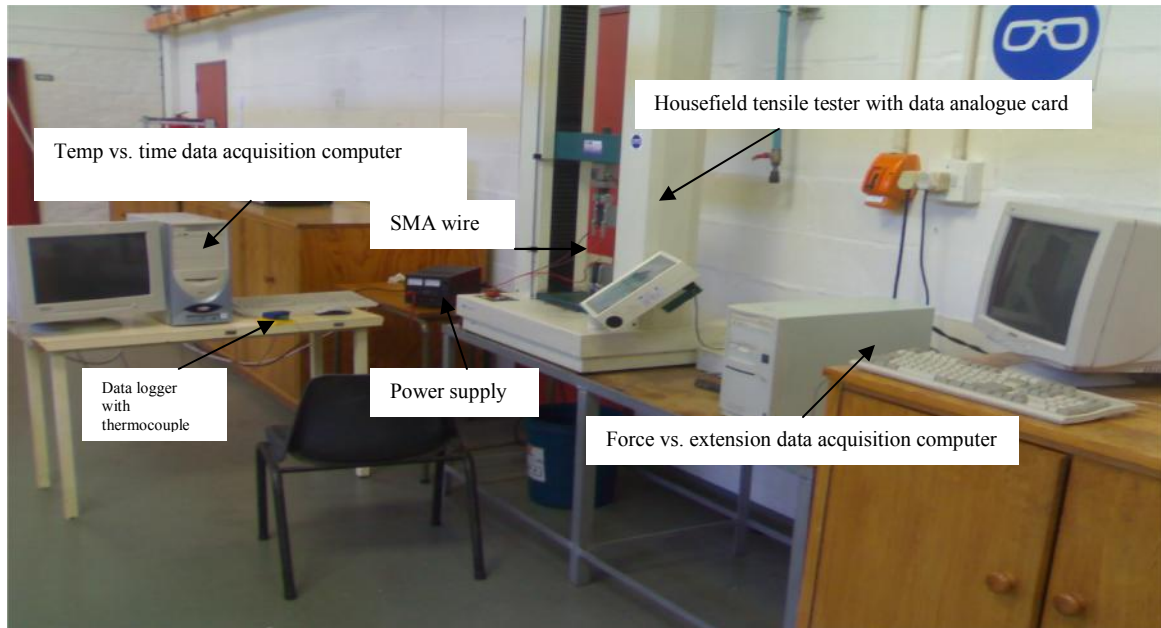


Figure 6.3: Equipment employed when electrically activating the NiTi SMA through resistive heating

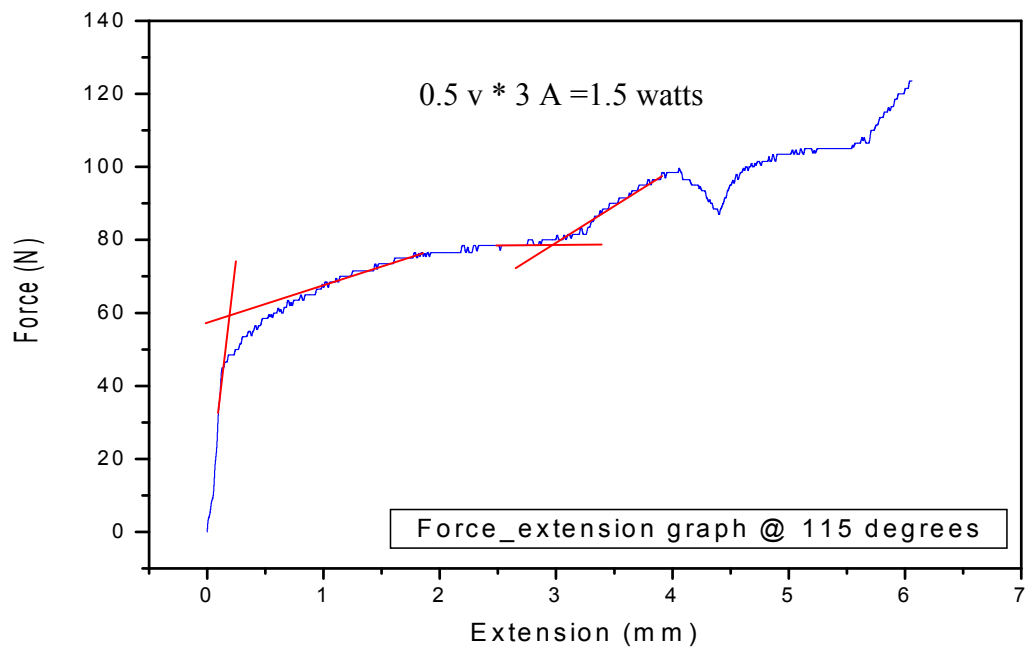


Figure 6.4: Martensite force – extension graph demonstrating loading behaviour

Figure 6.4 is a force – extension graph of the fully annealed specimen similar to SMA1 at ambient temperature. Fully twinned martensite is observed to occur at 59.1 N and at 0.2 mm extension. The material at this point obeys Hooke's law and this is the region where the first yield point occurs at elevated temperatures. After the yield load point, the material begins to detwin hence a combination of twinned and detwinned martensite are observed. The second yield load point is found to occur at approximately 78.64 N and at 2.97 mm. At the second yield load point, the material behaves linearly elastic. This is again attributed to stretching of atomic bonds that form a rhombic structure. The material at this stage does not obey Hooke's law unless resistive heating is applied to the specimen.

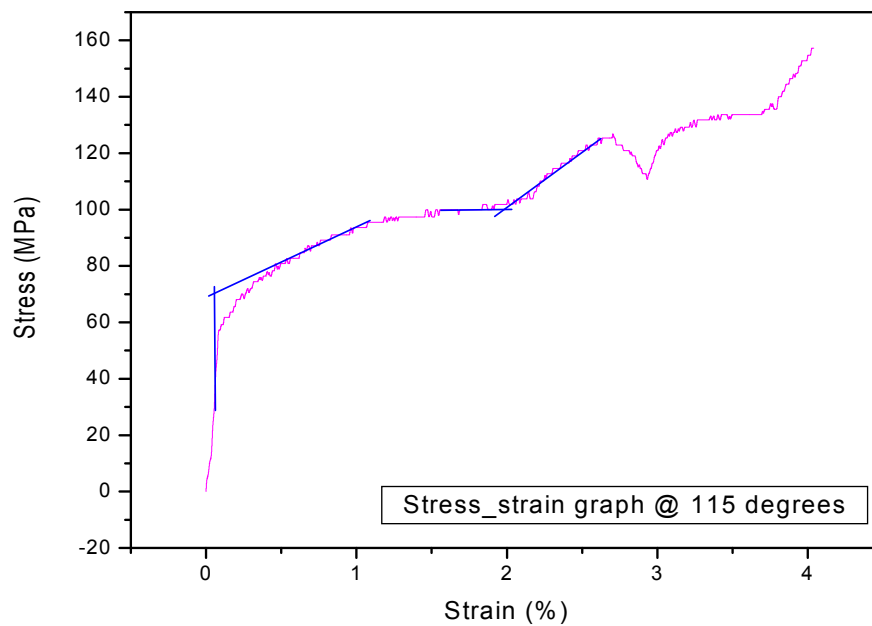


Figure 6.5: Stress-strain relation

Figure 6.5 shows the stress – strain relations and indicates that the stress – strain relationship is linear and elastic up to 0.0586 %. A combination of twinned and detwinned martensite in the specimen is observed at 0.65% strain. The material is found to be fully detwinned at approximately 1.97% strain which is the second yield load point of the specimen. When the strain is beyond 2.66% or the stress is beyond 125.48 MPa, it shows an irrecoverable deformation. The deformation is attributed to breakage of atomic bonds. In a force – extension relationship, irrecoverable deformation

occurs beyond 98.51 N. The material's Young's modulus is quite high at twinned martensite phase than at combined twinned and detwinned martensite phases, indicating that it is quite stiff when it is in the twinned state. All the data for the properties of SMA at elevated temperature are presented in table 6.2.

The temperature change along the NiTi SMA wire was measured during heating process with a thermocouple of type K, carefully attached at the gauge length centre of the SMA specimen. (See figure 6.3 for SMA wire attached with the type K thermocouple). The thermocouple was connected to the data logger which was linked to the computer (figure 6.3). Figure 6.6 shows the temperature profiles of the SMA wire during heating. The SMA wire was heated by means of resistive heating and the temperature peak was found to be increasing uniformly to approximately 115°C in 75 seconds (s). At 175s, heating of the SMA wire was stopped and it was allowed to cool down at ambient temperature. The wire is found to cool down uniformly. The temperature profiles give an indication of how the wire is heated and cooled during the loading process. In addition, figures 6.7, 6.8 and 6.9 present temperature – force, temperature – stress and temperature – strain graphs. It is observed that when the temperature increases the force, stress as well as strain also increases. This was also confirmed by Parlinska et al (2000).

Table 6.2: Properties of SMA 1 at elevated temperature (Gauge length = 150 mm)

Specimen Description	Load (P) N	Tensile Yield Stress (σ) MPa	Young's modulus (E) GPa	Tensile Yield Strain (ϵ)%	Phase type (Martensite)
SMA 1	59.1	70.33	120.02	0.0586	Twinned
	78.6	99.96	5.07	1.9700	Detwinned
	68.8	85.14	13.09	0.65	Combined

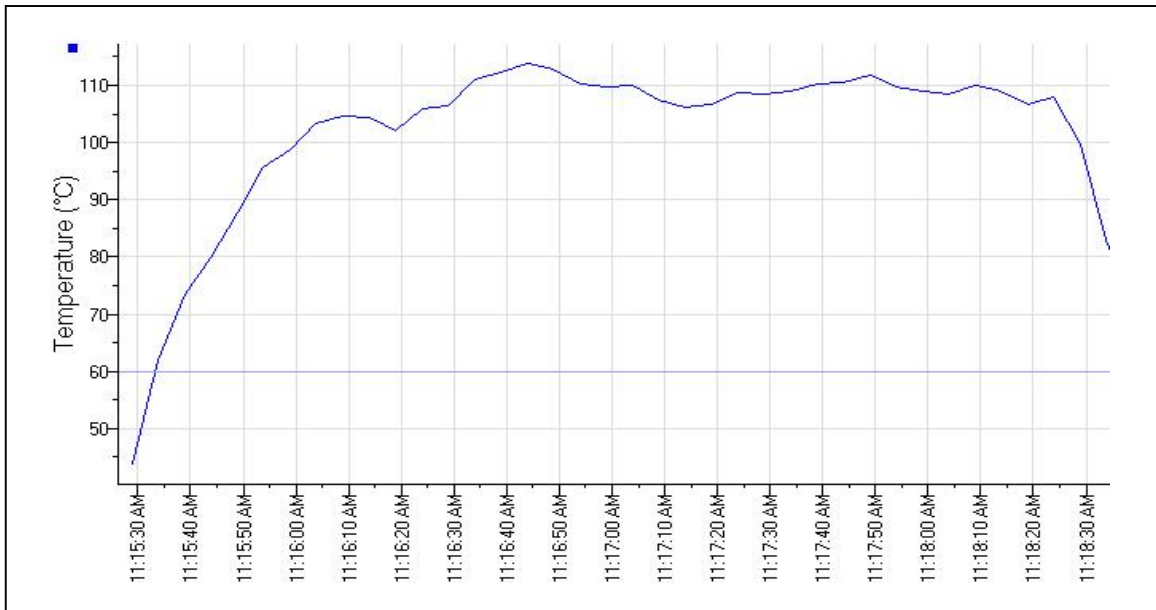


Figure 6.6: Temperature profiles of NiTi SMA wire during heating

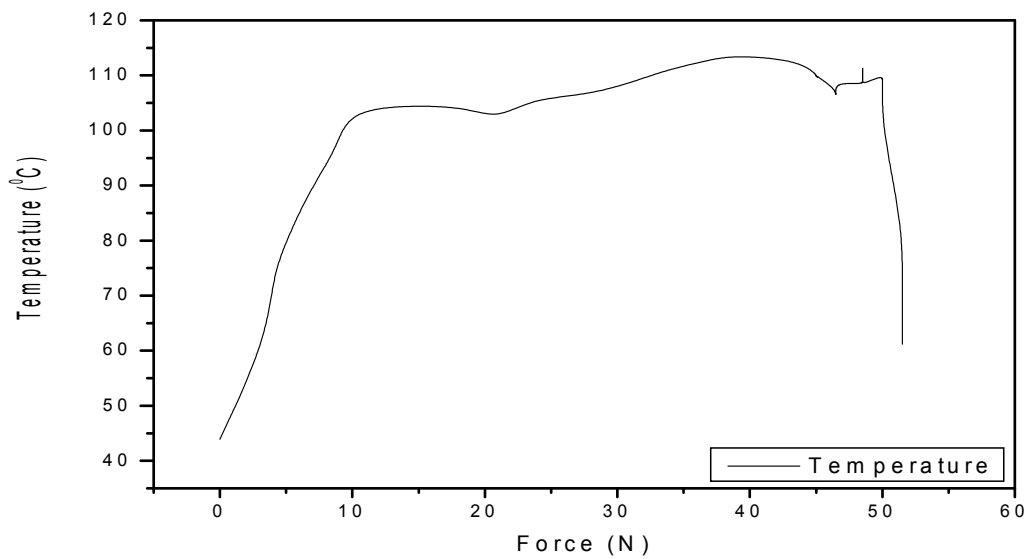


Figure 6.7: Force – Temperature graph

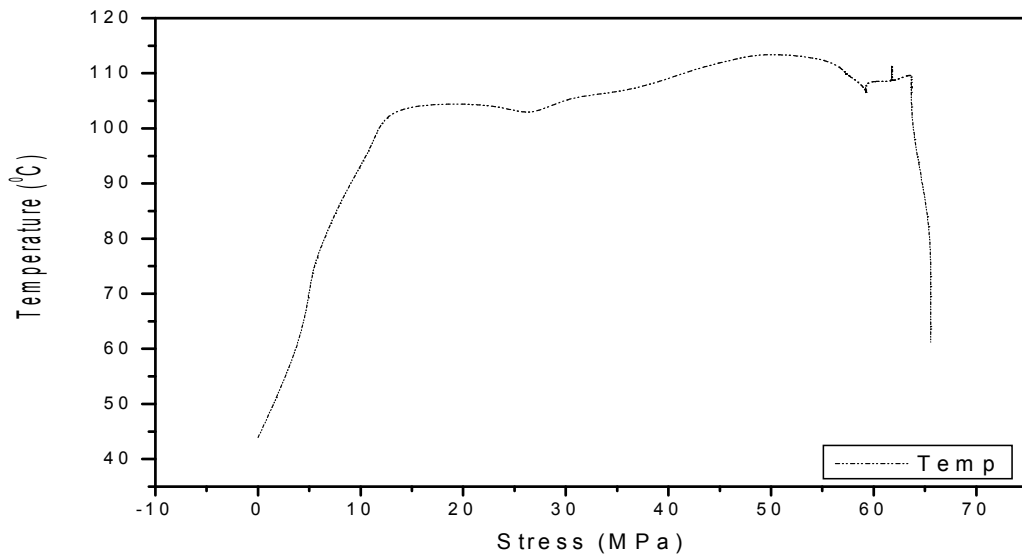


Figure 6.8: Stress – Temperature graph

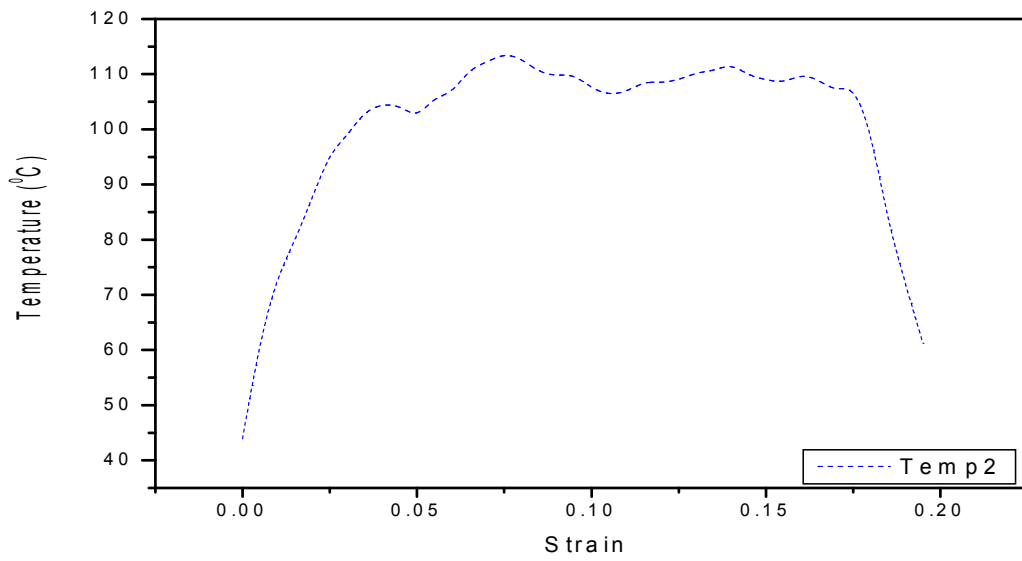


Figure 6.9: Temperature – strain graph

6.6 Conclusions

- 6.6.1 The mechanical behaviour of the NiTi SMA at fully twinned martensite phase was found to behave elastically.
- 6.6.2 When the material is at fully detwinned martensite phase, the material shows Young's modulus of different magnitude in comparison with the fully twinned martensite phase. This is illustrated in table 6.1.
- 6.6.3 Different Young's moduli are observed when the material is a combined twinned and detwinned martensite. The combined twinned and detwinned martensite together with detwinned martensite produced a residual strain in the material upon unloading. This residual strain could only be recovered by applying a Joule's effect.
- 6.6.4 It was observed that when the material was subjected to elevated temperature while loaded, the transformation load was quite high in comparison to those specimens loaded at ambient temperature. The residual strains were quite low at elevated temperature than those at ambient temperature.
- 6.6.5 Both at ambient and elevated temperatures, the SMA wire exhibited high tensile yield stress, tensile yield strain and a lower stiffness at detwinned martensite.
- 6.6.6 At twinned martensite, the NiTi SMA demonstrated lower tensile yield strains and higher stiffness.

6.7 Recommendations

The study is limited to the behaviour of the material at detwinned martensite, thus, properties of the material beyond detwinned would need further investigation.

CHAPTER 7

INVESTIGATING AND DETERMINING THE MATERIAL PROPERTIES OF REINFORCED COMPOSITES EMBEDDED WITH NITI SMAs

7.1 Introduction

This chapter describes the procedure of determining the tensile strength and stiffness of reinforced composites embedded with NiTi alloy wires. The results are compared with those of reinforced composites without embedded NiTi SMAs. The strains were observed when the SMA elements (SMA1, SMA2 and SMA3) were activated.

7.2 Experimental procedure

The NiTi wires (250 x 15 x 1 mm) were first placed in a furnace for a period of 10 hours at 230°C. Thereafter, the specimens were cooled at room temperature. The wires were subsequently pre-strained to approximately 3% prior to embeddement. A tensile testing machine was employed to pre-strain the wires. All the wires were pre-strained at the same rate of 2 mm/min. The assumption is that pre-straining is kept in the wire as long as the epoxy resin cures at room temperature of approximately 24°C, i.e., the wires do not recover their initial shape.

Un-strained and pre-strained NiTi wires were placed at different positions to prepare for laying on the e-glass mat. Three set of wires were prepared for embedding i.e. 1 wire per 15 mm width (placed at the centre), 2 wires per 15 mm width (placed 6.5 mm from edge) and 3 wires per 15 mm width (one wire placed at specimen centre and two wires placed 2.5 mm from centre at each side) of the composite. Laying the wires in this fashion ensured that there was equidistance between wires from the centre of the composite. Figure 7.1 presents a picture of Un-strained and pre-strained NiTi wires embedded in the epoxy matrix with e-glass fibres. The NiTi wires were placed along the epoxy / e-glass fibres at 0° axes which yielded higher strength and stiffness (Chapter 3). The epoxy resin was cured at room temperature under vacuum conditions over 24 hours. The specimen was

allowed to post-cure over a period of five days. The weight of the formed composite was 108g and the weight for NiTi wires was approximately 12 g. The average volume of NiTi alloy content in fabricated composite laminate was approximately 51.24%. The flat bar type tensile specimens were cut out from the composite sheet using a diamond cutter.

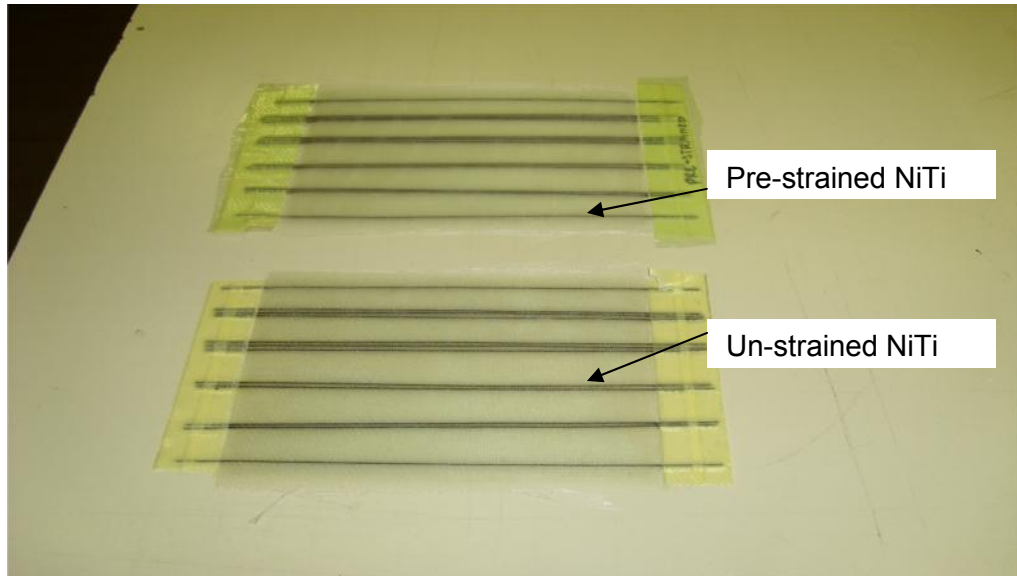


Figure 7.1: Embedded un-strained and pre-strained NiTi alloys

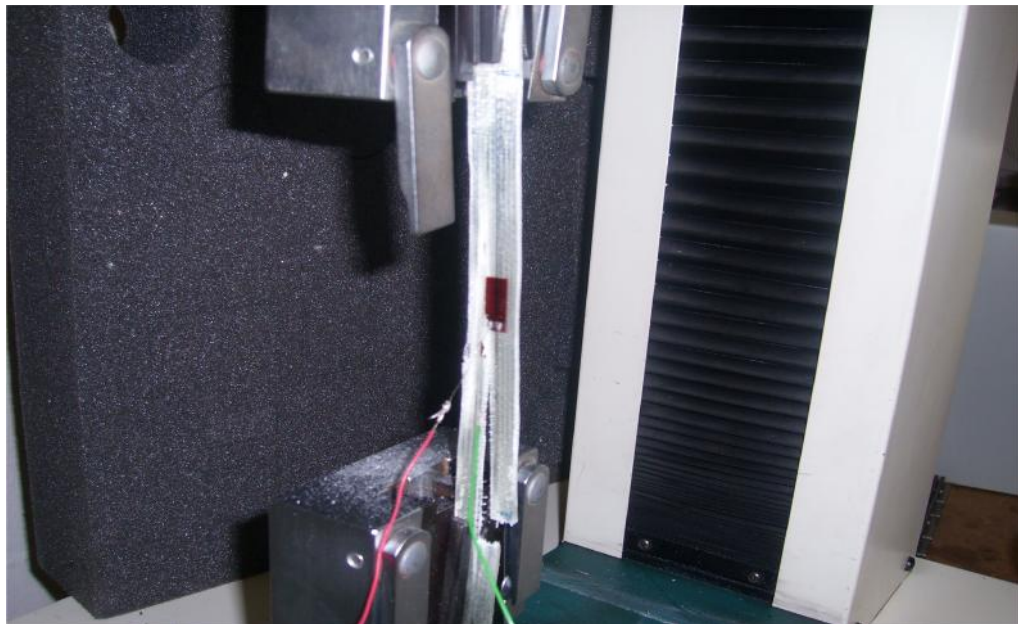


Figure 7.2: Experimental set up

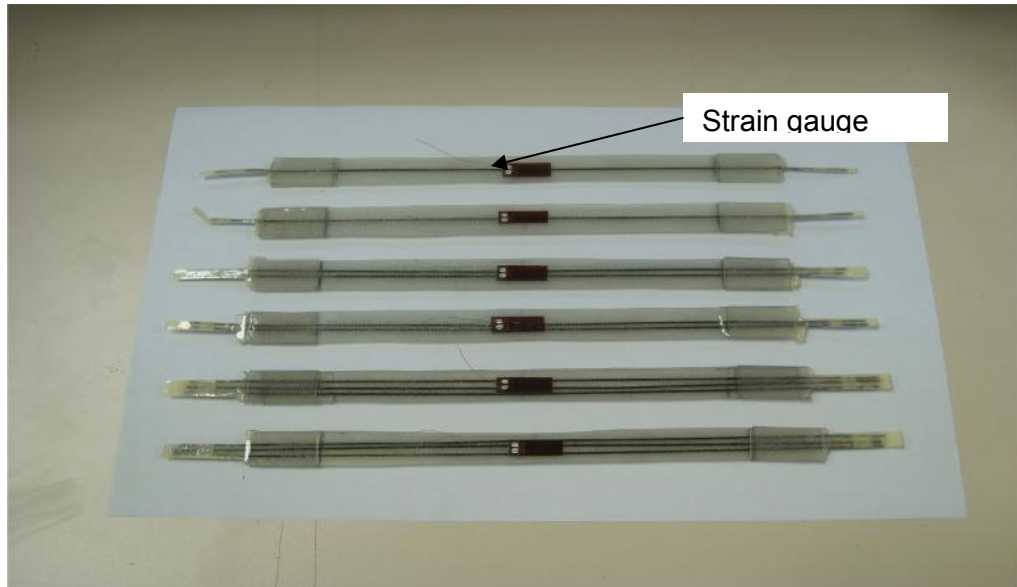


Figure 7.3: Strain gauge sensors attached to the specimens

In order to determine the tensile strength and stiffness of the combined material constituents, a tensile testing machine is employed. The experimental set-up comprised of the tensile testing machine, tensile specimen grips and a computer to allow recording the data. See figure 7.2 for the experimental set-up. The specimens were fitted with tabs of 50 mm in length and 15 mm in width on each side. The tabs protected the specimens from being damaged by the grips of the tensile testing machine. The composite specimens were placed on the grips and measurements of the applied force and specimen's extension at room temperature, were obtained. The strain gauge sensors depicted in figure 7.3 were placed longitudinally to the specimens in order to facilitate the recording of strain along the axis. The material's Young's modulus was determined as a function of the material's strains and stresses. The specimens to be tested were a 10 cross-ply epoxy resin / e-glass fibre laminate embedded with one wire, a 10 cross-ply epoxy resin / e-glass fibre laminate embedded with 2 wires and a 10 cross-ply epoxy resin / e-glass fibre laminate embedded with 3 wires at the centre or mid-plane of the composite. The following tensile testing of the 3 different specimen embedded with un-strained NiTi alloys is conducted:

7.2.1 Testing of 1 embedded NiTi wire in the unidirectional (UD) reinforced e-glass / epoxy composite

The tensile tests of the 1, 2 and 3 embedded NiTi wires in the UD reinforced e-glass / epoxy composite were carried out similarly. Three specimens were available for each sample. Tabs were fitted to the specimens to avoid specimen damage during grip application. The gauge length of the specimens was 150 mm and strain gauges were attached at the specimen's centre to measure the longitudinal strain. The strain measurement allowed for the determination of the material's Young's modulus, which provides an indication of the composite's stiffness. The strain gauges supplied by Instruments for Engineering Measurement (IEM), being the 10/120 type with gauge factor of $2.05 \pm 1\%$. A quarter bridge connection was selected for the strain gauge connections. Tensile testing of the specimens was conducted with a Hounsfield type tensile machine as illustrated in figure 7.4. The crosshead speed of the machine was set at 2 mm/min.

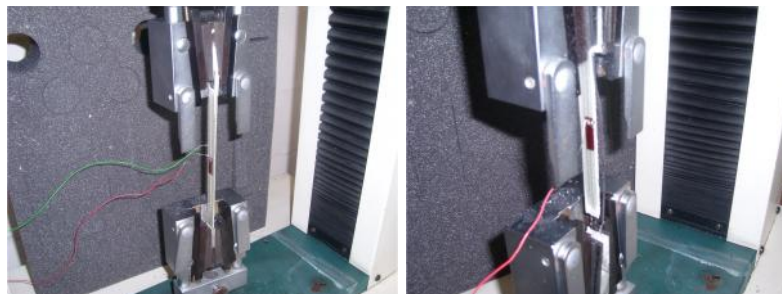


Figure 7.4: Experimental specimens tested using Hounsfield tensile testing machine

The tensile load for example of the 1 embedded wire was found to be approximately 10.74kN at an extension of 11.64 mm (See figure 7.5). In addition, a failure analysis of the specimen was conducted to show the failure mode of the specimen embedded with 1 NiTi alloy wire. The part failure mode code (SGM) mentioned in ASTM standards D3039 / D 3039M – 00^{E1} was closely followed. Looking at figure 7.6, the specimen had a long splitting failure between the tabs. The failure occurred closely to the embedded element along

the gauge length in the middle part. The specimen showed visible damage along the embedded wire indicating the interface as a weak point in the composite.

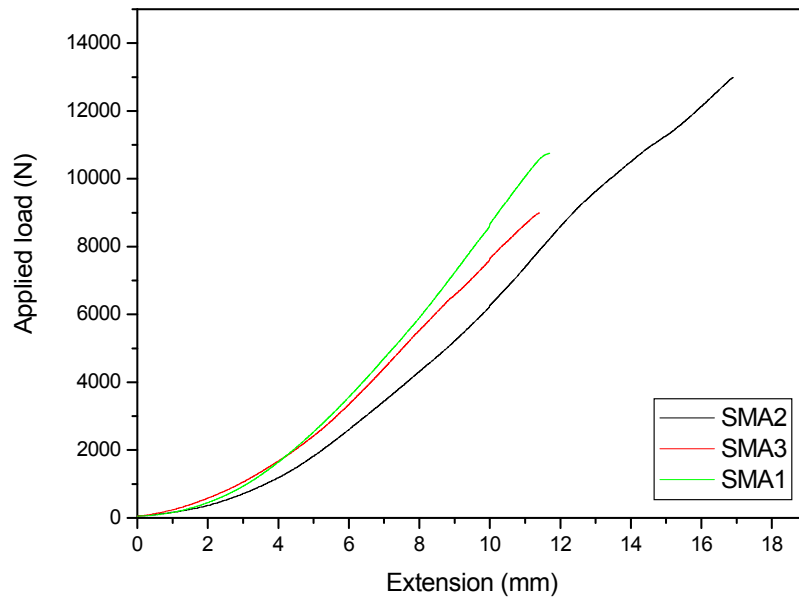


Figure 7.5: A typical load vs. extension curves for (embedded NiTi SMA wires) composite specimens



Figure 7.6: Tensile failure mode of the specimen with 1 embedded NiTi alloy wire

7.2.2 Testing of 2 embedded NiTi wires in the e-glass / epoxy composite

In this case, the tensile loading of the specimen was found to be approximately 12.97kN at an extension of 16.88mm. The part failure mode codes: lateral, at grip/tab, top (LAT) & edge delamination, gage, middle (DGM) were followed in analysing the specimen. The specimen showed the signs of edge delamination from the grip at multiple areas of the gauge length. Further there were signs of lateral failure at the top left of the grip. This failure mechanism is shown in figure 7.7.



Figure 7.7: Tensile failure mode of 2 embedded NiTi wires in the composite specimen

7.2.3 Testing of 3 embedded NiTi wires in the e-glass / epoxy composite.

In this case the tensile loading of the material was found to be approximately 8.99kN at an extension of 11.39mm. Amazingly, the tensile load and extension were lower than those of 1 and 2 embedded NiTi SMA wires, specimens.

The part failure mode code: longitudinal splitting, gage, middle (SGM) was followed for the failure analysis. The specimen failure was long splitting from the top to the bottom of the grip along middle of the outside NiTi alloy wire. This is illustrated in figure 7.8.

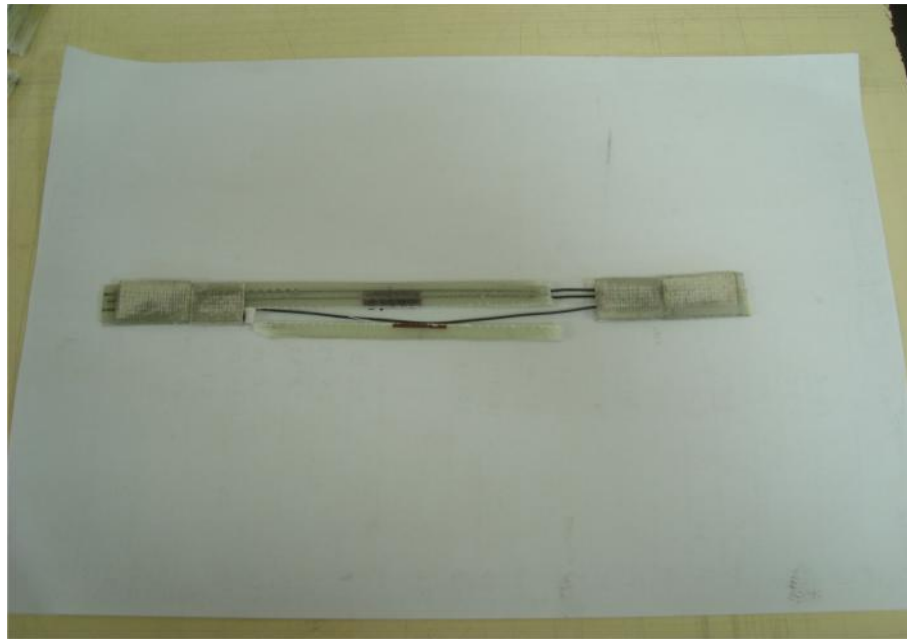


Figure 7.8: Tensile failure mode of 3 embedded NiTi wires in the composite specimen

7.2.4 Discussion on stress vs. strain graphs

Specimen load vs. extension graphs are shown in figure 7.5. These curves are obtained for embedded SMAs at a load range of 0 – 14000N. The relevant tensile stress – strain graphs are also presented in figure 7.9. Looking at the curves, it is obvious that the general shape of the curves is similar. The minor fluctuations observed in both curves of SMA2 and SMA3 could be associated with slight changes in properties of NiTi SMAs, laying up position and the interaction of NiTi SMAs to fibre / epoxy material composite. Figures 7.9 illustrate the stress – strain curves at a loading range of 0 – 14000N for specimens with different number of embedded NiTi SMAs. Looking at the shape of the curves, the number of embedded elements greatly impacted the value of the ultimate tensile strength as well as the stiffness of the material. It is observed that increasing the number of embedded NiTi SMAs into two had increased the ultimate tensile strength of the material. This could be attributed to the laying down position of NiTi SMAs. The three embedded elements were found to be in contrast with one or two embedded elements.

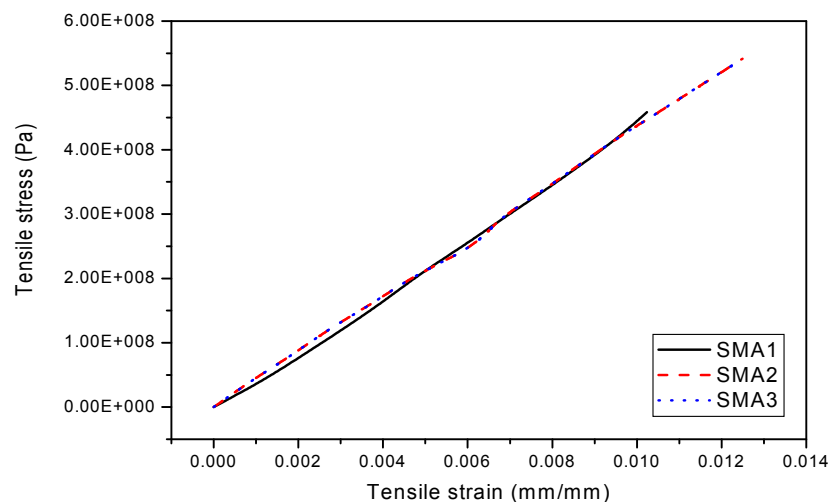


Figure 7.9: A typical tensile stress – strain curves for (1, 2 and 3 embedded NiTi SMA wires) for composite specimens.

7.2.5 Results on ultimate tensile material strength and longitudinal stiffness

The ultimate tensile strength (σ_u) and longitudinal stiffness (E_{11}) parameters determined based on these graphs in figure 7.9 are presented in table 7.1. From the table, it is found that the embeddement of 1 NiTi SMA resulted in an increase of 18.07% for ultimate strength and an increase of 1.97% for longitudinal stiffness in comparison to specimen embedded with 3 NiTi SMAs. In a case of 2 NiTi SMAs embedded, it was found that an increase of 30.33% in ultimate strength over 3 SMAs and 14.97% over 1 SMA was achieved. Yet, the longitudinal stiffness for 2 NiTi SMAs was found to be 1.21% less than 3 NiTi SMAs and 3.16% less than 1 NiTi SMA embedded in the virgin specimens. This simple means that an increase in ultimate strength of embedded composite will result in decrease in stiffness of the composite. Therefore, we could say, the ultimate tensile strength is affected by the number, position of embedded specimens and the size of the composite. It is noted that the ultimate strength of epoxy / e-glass fibre composite is greater than all tested embedded specimens. The magnitude of the un-embedded composite specimen deviated by 14.07% to 2NiTi SMAs, 26.93% to 1NiTi SMA and 40.13% to 3 NiTi SMAs. Although the ultimate strength is better for epoxy / e-glass fibre composite than embedded composite specimens, the longitudinal stiffness is in contrast with un-embedded specimens. The longitudinal stiffness is found to be better for embedded composite specimens than un-embedded ones. The magnitude of the un-embedded specimens is found to deviate by 60.74 to 1SMA and 3SMA, and, deviated by 59.45% to 2SMA specimens.

Table 7.1: Ultimate tensile strength and longitudinal stiffness of reinforced composite embedded with NiTi SMAs.

Embedded SMAs	σ_u (MPa)	E_{11} (GPa)
SMA 1	456.66	44.57
SMA 2	537.05	43.16
SMA 3	374.16	43.69

Figure 7.10 presents the variation of ultimate tensile strength with longitudinal stiffness for specimens with different number of NiTi SMA wires. The spline lines were employed to best fit the sampling points (UTS – Ultimate tensile strength). It was clear from the figure that the strength is a function of the number of embedded wires and longitudinal stiffness. Nevertheless, it was found that increasing the number of wires perhaps either decreased or increased the ultimate strength and longitudinal stiffness of the composite depending on the position of the wires. Based on the experimental results gained from the tests and using polynomial regression analysis, an empirical relationship was developed for the ultimate tensile strength in terms of longitudinal stiffness for specimens embedded with different number of wires as follows:

$$Y=A+B_1*X+B_2*X^2 \quad (7.1)$$

where Y stands for UTS.

X stands for E_{11} .

$$\text{And } R^2=1(\text{unity}) \quad (7.2)$$

Appendix B presents results of polynomial regression analysis. It is proven that the value of R-square showed exact fitness of function $Y = A + B_1*X + B_2*X^2$ on the experimental data. It could be seen that for SMA2 and SMA3 samples, the values of longitudinal stiffness are close to each other indicating a polynomial fit of the curves. The above equations are applied only to estimate the ultimate strength for the values in between of SMA1, SMA2 and SMA3.

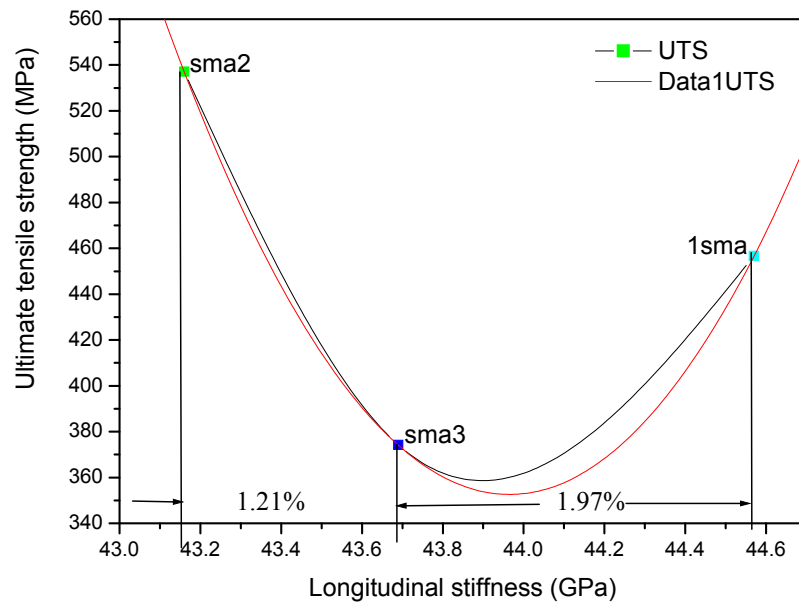


Figure 7.10: Effects of embedding different number of NiTi SMA wires on the ultimate tensile strength and longitudinal stiffness of epoxy / e-glass fibre / NiTi composite.

7.3 Heating of embedded pre-strained NiTi wires

The following experimental setup and procedure were adopted when heating was applied to the pre-strained NiTi wire elements.

7.3.1 Experimental setup for heating an embedded pre-strained NiTi wires

Figure 7.11 illustrates the experimental setup. The experiment apparatus consisted of a 3 – 15 volts (V) dc / 18A (HEP-920) power supply, configured as a voltage controlled current supply. It has a built-in ammeter and voltmeter which is adjustable manually in order to set the required voltage and prevent overheating of the NiTi wire element. The embedded pre-strained NiTi specimen was modelled as a cantilever beam. The specimen surface was parallel to the surface of the table.



Figure 7.11: An experimental setup for heating an embedded pre strained NiTi alloy wires

A strain gauge sensor was attached to the bottom surface at the centre of the specimen for strain measurements. The output of the strain gauge sensor was recorded by a strain indicator, Vishay Measurements Group, Raleigh, North Carolina. A K-type thermocouple was attached on the top side of the specimen surface by means of super-glue. The K-type thermocouple was connected to the computer through a Tiny Data Logger (TDL). An interface cable was employed to connect the TDL to the computer. The purpose of the K-type thermocouple was to measure the temperature of the specimen when heating was applied. The data output from the experiment, were: the voltage / amperage from the power supply, the strain of the cantilever, and the record of the temperature-time of the SMAs.

7.3.2 Experimental Procedure

For all the specimens tested, after being clamped to the table and attached with lead wires, the power supply was switched on and the voltage switch was adjusted to the set point giving a current of 5A. After reaching the set point, the wire was heated under no load conditions to recall the original geometry of the material. At this stage, the specimen shrank and the temperature varied in terms of magnitude. The strains were measured by the strain gauge sensor and displayed on the strain gauge indicator. A stop watch was employed to check the value of the strains over certain time intervals. The strain values obtained were made to be the function of the temperature and time. Once the strain value reached the maximum point, the power supply was switched off. As a result the specimen was left to cool by convection to surrounding air for approximately +20 seconds.

7.3.3 Results of embedded pre-strained NiTi wires

The following tests of 3 different specimens embedded with pre-strained NiTi alloys were conducted:

7.3.3.1 Testing of 1, 2 and 3 pre-strained embedded NiTi wire

The experimental setup employed during the SMA activation is pictured in figure 7.12. This setup allowed the recording of the strain of the composite during SMA activation and, simultaneously, the measurement of the specimen's temperature. The wire/s in the composite was connected in-series and by adjusting the wire current, the strain was generated in a controlled manner. The temperature measurement was taken at the mid point on the surface of the specimen.



Figure 12: Testing of 1 pre-strained embedded NiTi wire

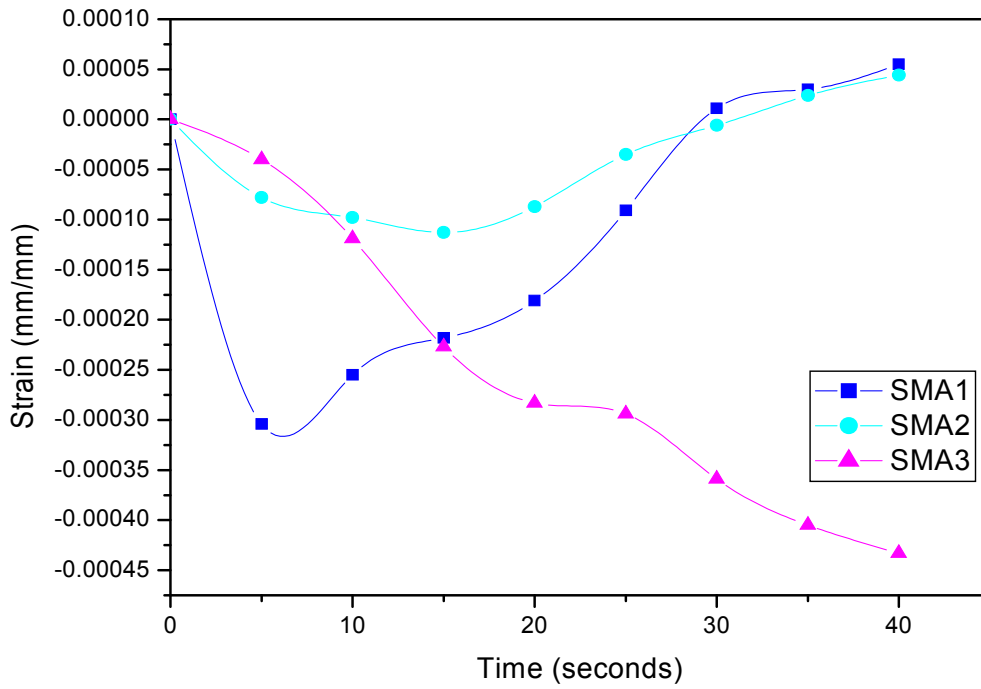


Figure 13: Strain vs. time graph for all SMA 1, 2 & 3

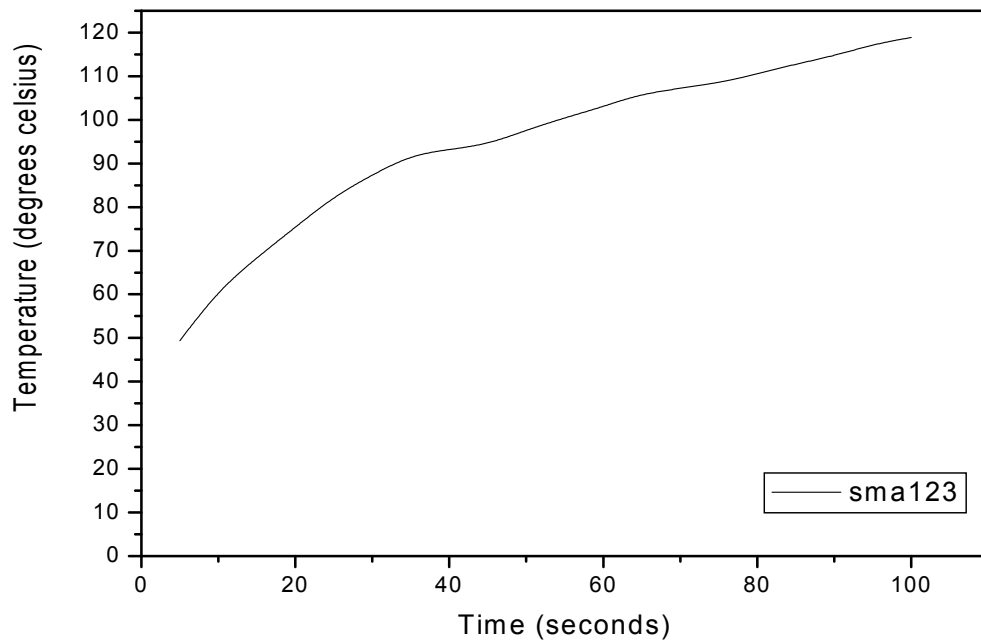


Figure 14: Temperature vs. time graph for SMA 1, 2 & 3

Looking at figure 13 and figure 14, it was observed that the pre-strained SMA wires over a period of time for an applied temperature created a different level of compressive strain. At approximately 49.4 °C, the generated compressive strain on SMA1 was approximately -304×10^{-6} mm/mm in 5 seconds (s). However, it was noted that as the time together with temperature had increased, the compressive strains started to decrease. The decrease was attributed to the slowly dissipation of heat generated by SMA wires into the composite specimen. Thus, the development of compressive strain field into the composite material was influenced by temperature changes. Further, it was observed that the heat generated by the specimens had caused softening of composite specimen. Although when the composite specimen was cooled down to room temperature, the specimen started to solidify returning to its martensitic state. This could be attributed to the wires overcoming the temperature hysteresis which occurred during activation of SMA element. At approximately 87 °C, the compressive strains started to decay away to tensile strains and again an indication of the change of state of the wire to austenite. In 40s, a positive strain of 55×10^{-6} was achieved on the tested specimen. In 1 embedded NiTi wire test, there was not much visible deformation or warping of the specimen.

The maximum compressive strain generated by the 2 embedded pre-strained wires was approximately -1.13×10^{-6} mm/mm in 15 seconds at a temperature of 68.4 °C. At intervals of 5s, the compressive strain started to decrease while the specimen temperature continued to increase. This was associated with the slow heat dissipation into the composite specimen. After 30s, the compressive strains changed forming a tensile strain. This could be related to the wires overcoming the temperature hysteresis which occurred during activation of SMA element and the change of state of the wire. It was noticed that the specimen became softer during the application of heat at the wires. It was further observed that, during cooling of the specimen, the heated specimen formed back to its original dimensions. Figure 15 illustrated the 2 pre-strained embedded NiTi wires and the results of the tests were also presented in figure 13 and figure 14.

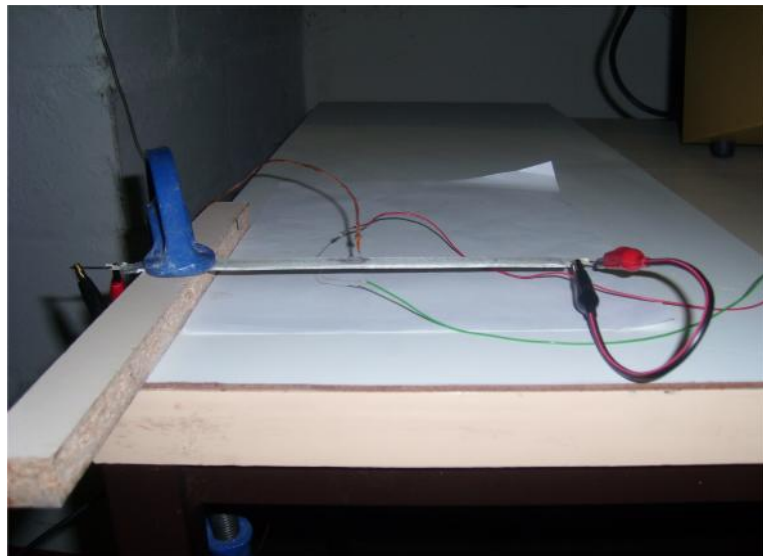


Figure 15: Testing of 2 pre-strained embedded NiTi wires

A total different level of compressive strain was shown by the growth of compressive fields inside the 3 embedded NiTi wires of the composite resulting in escalating the strain magnitude to the value of approximately $-4.33e-4$ mm/mm. It was observed that the heat generated by the activated pre-strained wires was slowly degenerated through the composite specimen resulting in the strain value of approximately $-4.33e-4$ mm/mm as shown in figure 13.

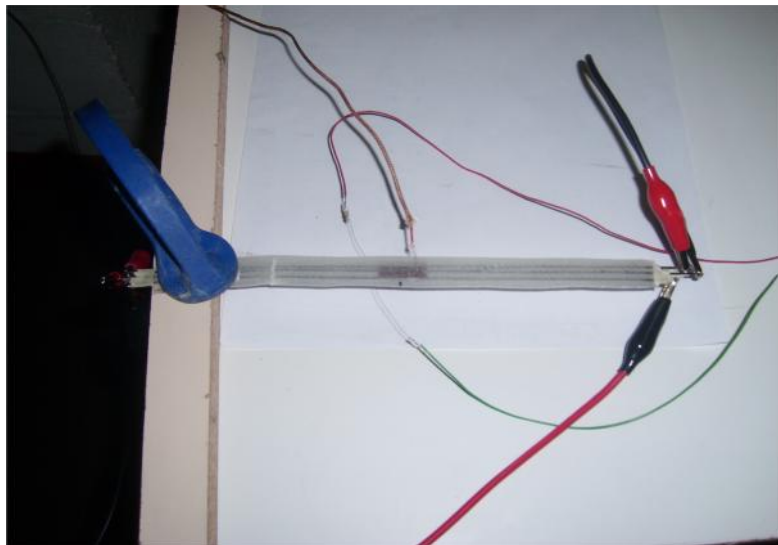


Figure 16: Testing of 3 pre-strained embedded NiTi wires

It was also observed that the generated strains had resulted in the geometrical failure (in compression) of the 3 embedded NiTi composite specimen. This is illustrated in figure 16. The induced compression of the composite specimen resulted into the warpage failure at activation temperatures of approximately 93 °C. It was noticed that when the activation temperature had exceeded 93 °C, as shown in figure 14, then a permanent buckling deformation was achieved when cooling down the specimen to room temperature. The results obtained as illustrated in figure 16 showed a single buckling wave in the traverse direction of the composite specimen. By increasing the volume fraction of embedded wires, the 10 ply composite specimen demonstrated a good picture of geometrical buckling failure mechanism. This is a clear indication that an increased stiffness environment of the composite specimen material had resulted in the generation of high recovery strains by pre-strained SMA wires. This type of failure mechanism presented a clear beam buckling under compressive load. This effect was not noticed in the case of SMA1 and SMA2 embedded wires because the generated strains during the experiment were of lower magnitude than the critical load required for geometrical beam buckling.

7.4 Conclusions

To prevent inaccuracies caused by variation in controlling, measuring and acquiring of data of different testing equipments, a 50 kN Instron, Hounsfield tensile testing machine was applied to carry out all the experiments in the present study. The tests were done for loads ranging from 0 to 14000 N with samples embedded with different number of NiTi SMAs at zero degree fibre and SMA orientation. Based on this experimental study, the conclusions are summarised as follows:

7.4.1 The mechanical properties of reinforced E-glass/ epoxy material embedded with different number of NiTi SMA were evaluated at load ranging from zero to 14000 N.

7.4.2 The experimental findings showed that the longitudinal stress achieved by 1 SMA embedded is approximately 456.66 MPa with a Young's modulus of 44.57 GPa. For 2 SMA embedded, the tensile stress was found to be approximately 537.05 MPa with Young's modulus of 43.16 GPa. Lastly, for 3SMAs embedded, the tensile stress was found to be approximately 374.16 MPa with a Young's modulus of 43.69 GPa.

7.4.3 It was observed that the tensile stresses of all tested embedded specimens were lower in terms of magnitude than that of un-embedded specimen at zero degree orientation. The magnitude of the un-embedded specimen deviated by 14.07% to 2NiTi SMAs, 26.93% to 1NiTi SMA and 40.13% to 3 NiTi SMAs.

7.4.4 Yet, the longitudinal stiffness of embedded specimens was found to be in contrast to the one of un-embedded specimens. The magnitude of the specimens is found to deviate by 60.74 to 1SMA and 3SMA, and, deviated by 59.45% to 2SMA specimens.

7.4.5 A variation of ultimate tensile stress with longitudinal stiffness for specimens with different number of NiTi SMAs was presented. It was found that increasing the number of wires perhaps either decrease or increase the ultimate strength and longitudinal stiffness of the composite depending on the position of the wires.

7.4.6 An equation presented in 7.1 is beneficial to evaluate the tensile stress values for longitudinal stiffness not incorporated in the experiment.

- 7.4.7** The strains that were generated in the fibre/epoxy specimens as a result of NiTi SMA wire activation were measured in composites embedded with different number of wires. The results showed that the presence of the wires generated compressive strains when the element was activated.
- 7.4.8** It was significant to note that when 3 SMA wires were employed, the generated strains in the specimen increased resulting in buckling failure mechanism. This could clearly signify the increased stiffness condition of the composite resulting in generating high compressive strains.
- 7.4.9** Although in contrast to 1 and 3 SMA wires, the activation of 2 SMA wires had resulted in reduction of the magnitude of the strains. This might be attributed to the position of the wires to the specimen or the heating method employed.

7.5 Recommendations

It is significant to check the influence of temperature when measuring the generated strains. During the manufacturing process of the composites, thermal strains are generated due to variation in thermal expansion coefficients of the e-glass fibre/epoxy resin/NiTi SMA. It is a well known fact that e-glass fibres are subjected to compression whereas epoxy is in tension. It is therefore significant to note that the pre-strained wires could have an influence on material strain distribution. It is therefore recommended that the strain distribution in the composite must be determined during and after the actuation of the element.

REFERENCES

Abraham, D., Matthews, S. & McIlhagger, R. 1998. A Comparison of Physical Properties of Glass Fibre Epoxy Composites Produced by Wet Lay-Up with Autoclave Consolidation and Resin Transfer Moulding. Engineering Composites Research Centre (ECRE), Department of Electrical and Mechanical Engineering, University of Ulster at Jordanstown, Shore Road, Newtownabbey BT37 0QB, Northern Ireland, UK.

Aerontec cc. Product Data Sheet – Resin System for Composites. blyth@cinet.co.za. March 2004.

ASTM D 3039/D 3039M - 00 1. Standard Test Method for Tensile Properties of Polymer Matrix Composite Materials¹. December 2002.

ASTM D 3171 – 99 Standard Test Methods for Constituent Content of Composite Materials¹.

ASTM D3518/D3518M-94. Standard Test Method for “In-plane shear response of polymer matrix composite materials. 2001.

Avila, F.A. and David T.S. Morais, 2004. A Multiscale Investigation on Variance Analysis for Hand Lay-up Composite Manufacturing. Mechanics of Composites Laboratory, Department of Mechanical Engineering, Universidade Federal de Minas Gerais, 6627 Antonio Carlos Avenue, Belo Horizonte, MG 31270-901 Brazil. 13 May 2004.*

Beihl, F. 2000. Glass Epoxy Thermal Shear Stress. www.hytecinc.com. Access 28 July 2008.

Buket, O, Aslan, Z. and Karakuzu, R. 2001. A Study of the Effects of Various Parameters on the Failure Strength of Pin-loaded Woven –glass-fiber Reinforced Epoxy Laminate. Department of Mechanical Engineering, Dokuz Eylül University, Bornova, İzmir, Turkey. 13 March 2001.*

Caron, J.F. and Carreira, R.P., 2002. *Interface behaviour in laminates with simplified model. Laboratoire d'Analyse des Matériaux et Identification, Ecole Nationale des Ponts et Chaussées, 6 et 8 avenue Blaise Pascal, Cité Descartes, Champs-sur-Marne, 77455 Marne-La-Vallée Cedex 2, France. 30 August 2002.*

Deng, S., Ye*, L. and Yiu-Wing, M. 1998. *Influence of Fibre Cross-Sectional Aspect Ratio on Mechanical Properties of Glass Fibre Epoxy Composites I. Tensile and Flexure Behaviour. Centre of Advanced Materials Technology, Department of Mechanical and Mechatronic Engineering, University of Sydney, NSW 2006 Australia. 1 October 1998.*

Evans, A.G., Hutchinson, J.W. and Wei, Y. 1999. *Interface Adhesion: Effects of Plasticity and Segregation. Acta Materialia, Volume 47, Issues 15-16, November 1999, Pages 4093-4113.*

Fereshteh-Saniee, F., Majzoobi, G.H. & Bahrami, M. 2005. *An Experimental study on the Behaviour of Glass-Epoxy Composite at Low Strain Rates. Mechanical Engineering Department, School of Engineering, Bu-Ali Sina University, Hamedan, Iran*

Gao, Y.C. and Zhou, L.M. 1999. *Energy Release Rate for Interface Debonding with Prestress and Friction. Theoretical and Applied Fracture Mechanics, Volume 32, Issue 3, November-December 1999, Pages 203-207.*

Gomesa,* A., Matsuo, T., Godab, K. and Ohgib, J. 2007. *Development and Effect of Alkali Treatment on Tensile Properties of Curaua Fibre Green Composites. a Graduate School of Science and Engineering, Yamaguchi University, Tokiwadai, Ube 755-8611, Japan. b Department of Mechanical Engineering, Yamaguchi University, Tokiwadai, Ube 755-8611, Japan. 22 April 2007.*

Gommers, B., Verpoest, I. & Houtte, P. 1998. *Analysis of knitted fabric reinforced composites: Part II. Stiffness and strength. Katholieke Universiteit Leuven, Department of Metallurgy and Engineering, de Croylaan 2, B-3001 Leuven, Belgium. 8 May 1998.*

Guide To Composites: Reinforcement

<http://www.netcomposites.com/education.asp?sequence=27>. Accessed: 24/ 07/ 2008.

Hyer, M.W. 1998. *Stress Analysis of Fibre Reinforced Composite Materials. International Edition, 1998. Library of Cataloging-in-Publication Data. ISBN 0-07-115983-5.*

Janke^{1,2}, L., Czaderski¹, C., Motavalli¹, M., and Ruth², J. 2004. *Application of Shape Memory Alloys in Civil Engineering Structures – Overview, Limits and New Ideas. (1) Empa, Swiss Federal Laboratories for Materials Testing and Research, Structural Engineering Research Laboratory, Überlandstrasse 129, CH-8600 Dübendorf, Switzerland. (2) Bauhaus-University Weimar, Faculty of Civil Engineering, Germany. 18 January 2005.*

Jonnalagadda, D.K., 1997. *Local Displacements and Load Transfer of Shape Memory Alloys in Polymeric Matrices. Graduate College of the University of Illinois at Urbana-Champaign.*

Mathews, F.L., Rawlings, R.D. 1999. *Composite materials: engineering and Science. WoodHead Publishing Limited; 1999, p.40.*

Miller, B., Muri, P. and Rebenfeld, L. 1986. *A Microbond Method for Determination of the Shear Strength of a Fibre / Resin Interface. Textile Research Institute, and Department of Chemical Engineering, Princeton University, Princeton, New Jersey 08542, USA. 6 May 1986.*

Pai, A. 2007. *A Phenomenological Model of Shape Memory Alloys Including Time-varying Stress. University of Waterloo, Waterloo, Ontario, Canada.*

Parlinska*, M., Clech*, H., Balta**, J.A., Michaud**, V., Bidaux+, J.-E., Manson**, J.-A.E., Gotthardt*, R. *Institut de Genie Atomique Departement de Physique, **Laboratoire de Technologie des Composites et Polymeres, Departement des Materiaux, EPFL, CH-1015 Lausanne, Switzerland, 2000. *Adaptive composite materials processing. Published by European Physical Society, Series Editor : R.M. Pick, Managing Editor : C. Bastian, Vol. Editor, A.M. Cunha, vol.241, p.33-34;*

Sept 24-28, 2000.

Penn, L.S. and Lee, S.M. 1989. *Interpretation of Experimental Results in the Single Pull-out Filament Test*. *J. Composites Science and Technology*, 11 (1), 23-30 (1989).

Philander, O. 2004. *The Development of A Computational Design Tool For Use in the Design of SMA Actuator Systems*. Doctor of Technology in Mechanical Engineering (DTECHME) in the Faculty of Engineering at the Peninsula Technikon. Submitted November 2004.

Physical Properties of Unidirectional "E" Glass.
http://www.rbsbattens.com/tech/physical_prop.cfm

Reuterlöv, S. 2002. *Cost Effective Infusion of Sandwich Composites for Marine Applications*. DIAB Technologies, Box 201, S-312, 22 Laholm, Sweden. Website: www.diab-group.com.

Sakai, M., Matsuyama, R. and Miyajima, T. 2000. *The Pull-Out and Failure of a Fiber Bundle in a Carbon Fiber Reinforced Carbon Matrix Composite*. *Carbon*, Volume 38, Issue 15, 2000, Pages 2123-2131.

Van Paepegem, W., De Baere, I. & Degrieck, J. 2005. *Modelling the Nonlinear Shear Stress-strain Response of Glass Fibre-reinforced Composites. Part I: Experimental Results*. Ghent University, Department of Mechanical Construction and Production, Sint-Pietersnieuwstraat 41, 9000 Gent, Belgium.

Wei, Z.G. and Sandström, R. 1998. *Review Shape – Memory Materials and Hybrid Composites for Smart Systems. Part 1 Shape –Memory Materials*. Department of Material Science and Engineering, Royal Institute of Technology, S – 100 44, Stockholm, Sweden.

Zhandarov, S. and M'ader, E. 2004. *Characterisation of fibre / matrix interface strength: Applicability of different tests, approaches and parameters*. Institute of Polymer Research Dresden, Hohe Strasse 6, D-01069 Dresden, Germany. 5 July 2004.

APPENDICES

APPENDIX A: CALCULATIONS OF E-GLASS FIBRE CONTENT

$$V_f = 1 - \frac{W - W_f}{\rho_m \times V} = 1 - \frac{324 - 250}{1130 \times 0.17424} = 0.6242$$

APPENDIX B: RESULTS OF POLYNOMIAL REGRESSION ANALYSIS

[2010/02/27 17:15 "/Graph1" (2455254)]

Integration of Data1_UTS from zero:

i = 1 --> 3

x = 43.16 --> 44.57

Area Peak at WidthHeight

607.03145 43.161.41 537.05

[2010/02/27 17:17 "/Graph1" (2455254)]

Linear Regression for Data1_UTS:

Y = A + B * X

Parameter ValueError

A 2285.16784 4664.23074

B -41.75646 106.4637

R SD N P

-0.36513 107.23102 3 0.76205

[2010/02/27 17:22 "/Graph1" (2455254)]

Polynomial Regression for Data1_UTS:

Y = A + B1*X + B2*X^2

Parameter ValueError

A 550198.153120

B1-25012.75361 0

B2284.46073 0

R-Square (COD) SD N P

1 0 3 <0.0001

[2010/02/27 17:24 "/Graph1" (2455254)]

Fit Data1_UTS to $y_0 + A_1e^{-x/t_1} + A_2e^{-x/t_2} + A_3e^{-x/t_3}$:

Chi²/DoF --

R² -1.22603E24

Parameter ValueError

y0 350.78152 --
A1-4.39354E14 1.31613E-124
t1 1 7.47944E-141
A2-2.19677E14 3.09364E-141
t2 10 3.05202E-155
A3-1.09838E14 --
t3 100 --

[2010/02/27 17:28 "/Graph1" (2455254)]

Lorentz (2) fit to Data1_UTS:

Chi²/DoF --

R² 0.12023

Peak Area Center WidthHeight

1 381.81 42.817 0.011236 21633
2 227.29 41.442 1.8219 79.421

Yoffset = 446.33969

[2010/02/27 17:30 "/Graph1" (2455254)]

Gauss fit to Data1_UTS:

Chi²/DoF --

R² -3.9968E-15

Area Center WidthOffset Height

1.9796E7 4347.7 0.013607 455.96 1.1609E9

[2010/02/27 17:30 "/Graph1" (2455254)]

Fit Data1_UTS to $y_0 + A_1e^{-x/t_1}$:

Chi²/DoF --

R² 0.19796

Parameter ValueError

y0 348.11802 --
A14.51335E11 --
t1 1.9686 --

[2010/02/27 17:33 "/Graph1" (2455254)]

Polynomial Regression for Data1_UTS:

$$Y = A + B1*X + B2*X^2$$

Parameter	Value	Error
A	550198.15312	0
B1	-25012.75361	0
B2	284.46073	0

R-Square (COD)	SD	N	P
1	0	3	<0.0001